# Screening of Protein Kinases and Inhibitors Using Optical Sensors

**Dissertation**
der Mathematisch-Naturwissenschaftlichen Fakultät
der Eberhard Karls Universität Tübingen
zur Erlangung des Grades eines
Doktors der Naturwissenschaften
(Dr. rer. nat.)

vorgelegt von
Viola Wurster

Tübingen
2024

Gedruckt mit Genehmigung der Mathematisch-Naturwissenschaftlichen Fakultät der Eberhard Karls Universität Tübingen.

| | |
|---|---|
| Tag der mündlichen Qualifikation: | 19.07.2024 |
| Dekan: | Prof. Dr. Thilo Stehle |
| 1. BerichterstatterIn: | Prof. Dr. Carolin Huhn |
| 2. BerichterstatterIn: | Prof. Dr. Günter Gauglitz |

## Declaration in lieu of oath
## Eidesstattliche Erklärung

Ich erkläre hiermit, dass ich die zur Promotion eingereichte Arbeit mit dem Titel: "Screening of Protein Kinases and Inhibitors Using Optical Sensors" selbständig verfasst und nur die angegebenen Quellen und Hilfsmittel benutzt und wörtlich oder inhaltlich übernommene Stellen als solche gekennzeichnet habe. Ich erkläre, dass die Richtlinien zur Sicherung guter wissenschaftlicher Praxis der Universität Tübingen (Beschluss des Senats vom 25.5.2000) beachtet wurden. Ich versichere an Eides statt, dass diese Angaben wahr sind und dass ich nichts verschwiegen habe. Mir ist bekannt, dass die falsche Angabe einer Versicherung an Eides statt mit Freiheitsstrafe bis zu drei Jahren oder mit Geldstrafe bestraft wird.

Tübingen, den

Viola Wurster

## Acknowledgments

Als erstes bedanke ich mich bei Prof. Carolin Huhn, dass sie mir die Möglichkeit gegeben hat, mich im Projekt zu meiner Promotion zu entfalten. Ich danke für das Vertrauen, mich selbständig arbeiten zu lassen, die Unterstützung und den Input, wenn ich an Grenzen gestoßen bin und die viele Zeit des Korrigierens um mich auf allen wissenschaftlichen Ebenen auszubilden.

Vielen Dank an meine weiteren Betreuer Dr. Peter Fechner und Prof. Günther Proll, für jeden hilfreichen Tipp, das anaysierende Diskutieren, die Unterstützung vor allem bei den praktischen Arbeiten und für das Einbringen eurer Expertise im Gebiet der Biosensorik. Auch Prof. Günter Gauglitz danke ich für alle wissenschaflichen Ratschläge wenn ich mit meinem Latein am Ende war, sowie die spannenden Gespräche bei gemeinsamen Konferenzen.

Ich danke allen Mitarbeitern der Firma Merck, die an diesem Projekt beteiligt waren: allen voran Jens Baumgärtner und Dr. Matthias Frech, die mich mit Analysen und Informationsaustausch sehr stark unterstützt und mir die aufgereinigten Kinasen für meine Experimente zur Verfügung gestellt haben. Ich danke der Analytikabteilung der Firma Merck unter der Letigung von Dr. Michael Arlt für die finanzielle Unterstützung im Projekt zu meiner Dissertation.

Vielen Dank an Prof. Martina Marchetti-Deschmann und ihren Arbeitskreis, für die freundliche und unterstützende Aufnahme bei meinem kurzen Foschungsaufenthalt an der TU Wien. Vielen Dank für die Betreuung und vor allem das Vertrauen, mich so schnell mit dem MALDI-TOF alleine messen zu lassen.
Außerdem danke ich Prof. Natalia Ivleva von der TU München und Leon Biesterfeld vom AK Prof. Jannika Lauth (Uni Tübingen), für die Kooperation und die Raman- und ATP-IR-Messungen meiner Sensoren.

Vielen Dank an alle Mitarbeitenden im IPTC Sekretariat, im Glasladen, den Werkstätten und der Chemikalienausgabe, die die alltägliche Arbeit am Laufen halten und bei allen Problemen in diesen Bereichen unterstützend zur Seite stehen.

Lieber AK Huhn (Chicken Nuggets), ich danke euch für die schöne gemeinsame Zeit. Danke für die seelische und moralische Unterstützung, für die Zusammenarbeit in der Lehre, das viele Lachen und die Gespräche, die vom Laboralltag ablenken konnten. Vielen Dank auch an Monika Conrad für die schöne gemeinsame Zeit auf Konferenzen.

Danke auch an meine Praktikantinnen Erica Schmitt, Xian Xiao und Rebecca Pamies-Cuberos für die Mitarbeit in meinem Projekt und Rebecca für die spätere Zuarbeit als Hiwi.

Ich danke der gesamten Ebene 6 im Chemie-Bau der Uni Tübingen (AK Huhn, AK Gaulitz, AK Schwarzer, AK Fink), dass ihr so motiviert bei meinem Pausenexpress dabei wart. Danke euch allen für die interessanten und netten Gespräche zwischendruch.

Ein herzliches Dankeschön an meine Familie: Mama, Papa, Tina, Felix, ihr wart immer für mich da, habt mit mir Meilensteine gefeiert und mich in schwierigen Phasen unterstützt. Ohne euch an meiner Seite (oder meinen Ohren) wäre vieles für mich so nicht möglich gewesen.

# Author Contribution

**Erklärung nach §6 Abs. 2 der Promotionsordnung der Mathematisch-Naturwissenschaftlichen Fakultät der Universität Tübingen**

My work for this thesis was supported in the scientific idea, the laboratory work and data generation, the analysis and interpretation of these data and finally the writing process of this thesis by supervisors, consultants, colleagues and interns. Thus, a transparent disclosure of this author distribution is given here.

*Introduction, Overall Discussion and Summary, Outlook*
The introduction is a general review of the state-of-the-art for screening methods for protein kinases and inhibitors. Revision and input on further research topics was provided by Prof. Carolin Huhn, Dr. Peter Fechner and Prof. Günther Proll. Joint discussions enhanced the Section "Overall Discussion and Summary" and "Outlook".

*Results and Discussion*
Some practical work and data evaluation were conducted by my interns Erica Schmitt, Xian Xiao and Rebecca Pamies-Cuberos as part of their internships under my supervision. Erica Schmitt made preliminary test experiments of the binding inhibition assays, Xian Xiao assisted the change of the measurements systems from RIfS to 1-λ reflectometry and Rebecca Pamies-Cuberos was involved in most of the regeneration tests in RIfS. Sensor preparation for all sensors, which I investigated in RIfS to prepare the surface analysis investigations was done by Rebecca as well, as a student assistant.
For technical support and laboratory work I was supported by Dr. Peter Fechner.
MALDI-TOF-MS measurements were possible with the equipment in the laboratory of Prof. Martina Marchetti-Deschmann at the TU Wien. Together with her coworker Antonia Malissa, who supervised me during my two-week research travel to Austria, we discussed, analyzed and interpreted the MALDI results. All ATR-IR investigations were performed with he equipment of the Leibnitz Universität Hannover by Leon Biesterfeld, from the Eberhard Karls Universität Tübingen in the working group of Prof. Jannika Lauth. He supported the evaluation and interpretation of these data. The cooperation partner Prof. Nathalia Ivleva conducted all Raman experiments, including the evaluation and we, my supervisor Prof. Carolin Huhn and I, discussed all results together with her.

*Scientific Discussion*
During diverse meetings with the analytical department of Merck as cooperation partner, we exchanged scientifc expertise with all collaborators involved: Dr. Michael Arlt, Dr. Anja Goettsche, Dr. Sebastien Moniot, Sebastian Fuchs, Dr. Matthias Frech, Dr. Oliver Schadt, Jens Baumgärtner, Marc Krenkel and Yannik Schermer. Purified kinases were provided by Dr. Matthias Frech (Molecular Interaciton and Biophysics) and Martin Lehmann (Protein Crystallography). Data of the ingredients of the protein mix were provided by Jens Baumgärtner.
Prof. Günter Gauglitz supported the working processes as a mentor with his broad scientific expertise.
Dr. Peter Fechner and Prof. Günther Proll promoted this thesis by their scientific expertise especially with trouble shooting and supervision in the data generation, analysis and interpretation. The writing process of the thesis was supported by revisions from Dr. Peter Fechner.
Prof. Carolin Huhn was the project manager of the cooperation project with Merck. She also supervised my thesis, gave support in the scientific idea, in the analysis and interpretation and also revised the written thesis.

# Content

## Abbreviations

| | |
|---|---|
| ACN | acetonitrile |
| AI | artificial intelligence |
| AMD | amino dextran |
| ADP | adenosine diphosphate |
| ATP | adenosine triphosphate |
| ATR-IR | attenuated total reflection infrared spectroscopy |
| BLI | biolayer interferometry |
| bia | binding inhibition assay |
| BisX | bisindolylmaleimide X |
| BSA | bovine serum albumin |
| CE | capillary electrophoresis |
| CHAPS | 3-[(3-cholamidopropyl)dimethylamonio]-1-propanesulfonate |
| Da-PEG | diamino polyethylene glycol |
| DCM | dichloromethane |
| DMF | *N,N*-dimethylformamide |
| DMSO | dimethyl sulfoxide |
| DNA | deoxyribonucleic acid |
| DS | docking simulation |
| EDC | 1-ethyl-3-(3-dimethylaminopropyl)carbodiimide |
| EDTA | ethylenediaminetetraacetic acid |
| ELISA | enzyme-linked immunosorbent assay |
| FAK | focal adhesion kinase |
| GA | glutaric anhydride |
| GdmCl | guanidinium chloride |
| GOPTS | (*3*-glycidyloxypropyl)trimethoxy silane |
| ITC | isothermal titration calorimetry |
| ITO | indium tin oxide |
| LC | liquid chromatography |
| LOD | limit of detection |
| MALDI | matrix assisted laser desorption/ionization |
| MES | 2-(*N*-morpholino)ethanesulfonic acid |
| MS | mass spectrometry |
| MST | microscale thermophoresis |
| NHS | *N*-hydroxy succinimide |
| NP-STP | magnetic nanoparticles, with staurosporine immobilized on the surface |
| PBS | phosphate-buffered saline |
| PDB | protein data base |
| PDMS | polydimethylsiloxane |
| PEG | polyethylene glycol |
| PKA | cAMP-dependent protein kinase |
| PKB (AKT1) | protein kinase B (RAC(Rho family)-alpha serine/threonine-protein kinase) |
| RIfS | reflectometric interference spectroscopy |
| RNA | ribonucleic acid |
| ROI | region of interest |
| RSD | relative standard deviation |
| SA | sinapinic acid |

| | |
|---|---|
| SCORE | single color reflectrometry |
| SPR | surface plasmon resonance |
| STP | staurosporine |
| STP-Red | staurosporine with red fluorescence label |
| SYK | spleen tyrosine kinase |
| TFA | trifluoroacetic acid |
| TGFβ (ALK5) | transforming growth factor beta |
| TOF | time of flight |
| TRIS | tris(hydroxymethyl)aminomethane |
| TSA | thermals stability shift assay |
| UV-Vis | light with the wavelengths in the ultraviolet and visible region (200-800 nm) |

## Abstract

Many cell processes, such as cell growth and proliferation are regulated by active protein kinases. These enzymes act non-selectively, which may promote tumor growth in the presence of tumor cells. The activity of ATP-binding kinases, such as serine/threonine- or tyrosine-kinases, can be inhibited by small molecules occupying the ATP-binding pocket. Protein kinase inhibitors are thus interesting target molecules in pharmaceutical research.

Affinity and kinetics of the interactions between protein kinases and inhibitors are important parameters for drug development. Analytical methods providing these data ideally label-free and with a high time-resolution are sparse, limiting their application in screening methods.

The aim of this thesis is the development of a method that can characterize the interactions between protein kinases and possible inhibitors with the possibility to screen both, kinases and inhibitors.

Docking simulations and microscale thermophoresis (MST) were used to simulate and proof binding strengths between selected protein kinases and small molecules functioning as inhibitors. Binding energies were simulated with -12 to -6 kcal/mol in a good comparison to literature data for the inhibitor interaction. The binding affinities of the direct and competitive MST analyses differed, depending on the chosen pairs of protein kinases and inhibitors, but overall strong interactions as already indicated by the simulations were determined.

With the knowledge of suitable pairs of protein kinases and inhibitors, label-free and time-resolved optical biosensors were developed using reflectometric interference spectroscopy and 1-λ reflectometry for detection. Sensors were prepared by modifying the surface of glass transducers, including a biopolymer layer and a final linkage to an inhibitor molecule. Staurosporine (STP), a natural product and the most universal model kinase inhibitor, was used for the method development. Kinase-inhibitor interactions were monitored in the heterogeneous phase via direct assays and also in the homogeneous phase via binding inhibition assays with already approved drugs and other promising research inhibitors. Binding affinities as well as the binding kinetics were calculated, corroborating results from MST. Due to the surprisingly strong interactions between the protein kinases and inhibitors on the biosensors, preventing successful regeneration of the sensor surfaces, various regeneration protocols were tested and surface modifications were investigated. With surface analytical methods of matrix assisted laser desorption/ionization-mass spectrometry (MALDI-MS), attenuated total reflection infrared spectroscopy (ATR-IR) and Raman microscopy reasons for the strong interactions were searched for.

With the optimized method of 1-λ reflectometry and the use of array-based sensors, where different inhibitors were simultaneously immobilized in different spots on one sensor, successful screening of kinases and inhibitors was achieved.

The surface chemistry of the sensors was further transferred to magnetic nanoparticles, which allowed to extract kinases from solution for further analytic investigation.

# Zusammenfassung

Klassische Zellprozesse, wie zum Beispiel Zellwachstum und -proliferation werden von aktiven Proteinkinasen reguliert. Da diese Enzyme häufig nur mit geriner Selektivität arbeiten, unterstützen sie in Gegenwart von Tumorzellen auch das Tumorwachstum. Die Aktivität von ATP-bindenden Kinasen, wie zum Beispiel Serin/Threonin- oder Tyrosin-Kinasen, kann mit kleinen Moleküle, die kompetitiv die ATP-Bindungstasche besetzen, gehemmt werden. Daher sind Inhibitoren für Proteinkinasen sehr interessante Zielsubstanzen in der pharmazeutischen Forschung. Sehr wichtige Parameter für die Medikamentenentwicklung sind die Affinität und die Kinetik der Wechselwirkungen zwischen Proteinkinasen und Inhibitoren. Analytische Methoden, die diese Daten markierungsfrei und mit hoher zeitlicher Auflösung bereitstellen und zusätzlich ein Screening ermöglichen, sind sehr selten.
Das Ziel dieser Arbeit ist die Entwicklung einer analytischen Methode, die die Wechselwirkungen zwischen Proteinkinasen und möglichen Inhibitoren charakterisiert und zudem ein Screening sowohl von Kinasen als auch von Inhibitoren ermöglicht.
Mittels Docking Simulationen und der Thermophorese auf Mikroebene (MST) wurde getestet, ob die Proteinkinasen und kleinen Moleküle als Modell-Inhibitoren, die für diese Arbeite ausgewählt wurden, ausreichende Wechselwirkungen erwarten lassen. Mit den Simulationen wurden Bindungsenergien im Bereich von -12 bis -6 kcal/mol simuliert, die eine gute Übereinstimmung mit Literaturwerten zeigen. Die Bindungsaffinitäten der direkten und kompetitiven MST Messungen waren hoch, unterschieden sich aber deutlich je nach Paarung von Proteinkinase mit Inhibitor.
Unter Verwendung der Reflektometrischen Interferenzspektroskopie und der 1-λ Reflektometrie wurden markierungsfreie und zeitaufgelöste optische Biosensoren entwickelt. Zur Herstellung der Sensoren wurde die Oberfläche der Glastransducer modifiziert, wofür eine Schicht Biopolymer aufgebracht und abschließend Inhibitormoleküle an die Sensoroberfläche gebunden wurden. Die Methodenentwicklung wurde mit dem Naturprodukt Staurosporin (STP) durchgeführt, dem universell bekanntesten Kinaseninhibitor, der häufig als Modell-Inhibitor verwendet wird. Die Wechselwirkungen wurden in heterogener Phase mit einem direkten Assay und in homogener Phase mit einem Bindungshemmtest mit bereits zugelassenen Medikamenten und anderen vielversprechenden Forschungs-Inhibitoren verfolgt. Bindungsaffinitäten und Bindungskinetiken wurden für verschiedene Paare von Proteinkinasen und Inhibitoren bestimmt. Trends der Bindungsaffinitäten, die mit den Simulationen und MST bestimmt wurden, konnten mit den Ergebnissen der Sensormessungen bestätigt werden. Aufgrund von unerwartet starken Wechselwirkungen zwischen den Proteinkinasen und Inhibitoren auf den Sensoren, welche eine erfolgreiche Regeneration verhinderten, wurden verschiedene Regenerationsprotokolle getestet und weitere Oberflächenmodifikationen der Sensoren zur Optimierung eingeführt. Der Ursprung der starken Wechselwirkungen wurde mit Methoden zur Oberflächenanalytik wie matrix assisted laser desorption/ionization-Massenspektrometrie (MALDI-MS), attenuated total reflection-Infrarotspektroskopie (ATR-IR) und Raman Mikroskopie untersucht.
Mit der optimierten Methode der 1-λ Reflektometrie und unter Verwendung von array-basierten

Sensoren, auf denen verschiedene Inhibitoren gleichzeitig immobilisiert wurden, konnte ein erfolgreiches Screening von Kinasen und Inhibitoren erreicht werden.
Die entwickelte Oberflächenchemie der Sensoren wurde anschließend erfolgreich auf magnetische Nanopartikel übertragen, die eine Extraktion von Kinasen aus Lösungen für weitere Analytik ermöglichen.

"In the presence of staurosporine arose an idea: If marine bacteria can synthesize a drug that inhibits kinases non-specifically, then undoubtedly a team of chemists can produce a drug, that specifically impacts certain kinases within cells."

paraphrased from
The Emporer of all Maladies - A Biography of Cancer
Siddharta Mukherjee

# 1 Motivation

In the latest "Cancer statistics", cancer is not only found to be the second most important cause of death worldwide, but also as "the leading cause [of death] among people younger than 85 years" [1].
With the FDA having approved imatinib 2001 as anti-tumor drug, inhibiting the kinase ABL, the investigations of the interactions between protein kinases and small molecules as possible inhibitors are intensified [2]. Protein kinases promote cell processes by phosphorylation of enzymes using ATP. This process is often non-selective and thus, healthy cells and e.g. tumor cells are not discriminated. Generating information on the inhibition of these enzymes by small molecules is an analytical challenge for pharmaceutical research.
Monitoring these interactions is possible with various methods, which, however, provide different information: e.g. data on binding affinity and kinetics, specificity and selectivity of inhibitors towards kinases. Not all of the available methods are applicable directly to biological samples and only a few are high throughput methods. Especially the information on binding kinetics is important in pharmaceutical research, but the most common analytical methods cannot provide it. Furthermore, screening is mostly applicable for one binding partner only. With that, the major limitations are the information on the binding kinetics and the possibility to provide a screening for both, protein kinases and inhibitors with one method.
The most promising methods to close this gap are optical biosensors, where the specific interaction between protein kinases and small molecules has already been studied with surface plasmon resonance, providing kinetic data. Optical bionsensors based on the interference of reflected light have not yet been implemented for monitoring specific interactions between protein kinases and inhibitors, but seem highly promising, given their application in other biological systems [3–5].
In order to develop this methodology for kinase research towards a comprehensive strategy, biosensor assays with reflectometric interference spectroscopy (RIfS) and 1-λ reflectometry are chosen in this thesis. The thesis focuses on different ATP-dependent protein kinases interacting with the ATP-competitive staurosporine (STP) as a non-specific inhibitor, and further promising inhibitors, such as imatinib and STP-like molecules. Kinetic data of the interactions are evaluated. This forms the basis to use 1-λ reflectometry in order to implement a method that is able to screen both, protein kinases and inhibitors.

"With a faceless, meaningless surface, a protein is generally not "druggable"; flat poker face topologies make poor drug targets. If on the other hand, the protein's surface is riddled with deep grooves and pockets, it is often attractive to binding molecules - and thus a potentially responsive target."

paraphrased from
The Emporer of all Maladies - A Biography of Cancer
Siddharta Mukherjee

# 2 Introduction

The number of patients diagnosed with cancer grows every year, making it to one of the recently most deadly diseases. Each year, millions of deaths can be attributed to cancer. While women mostly suffer from breast cancer, prostate cancer is prevalent for males [6]. Besides reducing cancer elicitors, the development of new treatment strategies has led to an intense decline of cancer mortality [7]. To further expand this development, research on diagnostic methods for the onset of cancer detection as well as new drugs needs to be extended. A promoter for cancer formation is the non-selective interaction of protein kinases with cancer-affected cells. In general, kinases regulate cell growth, proliferation, differentiation and further vital cell processes. Due to their lack of selectivity, all these cell processes are also promoted in tumor cells [6]. Therefore, protein kinases, coded by 2.5% of the human genome, are some of the most interesting drug targets [2, 8]. For enzymes regulated by ATP, such as serine/-threonine or tyrosine kinases, inhibitors, competitive to ATP, are highly interesting drugs. Many studies show, that small molecules, containing a quinazoline ring, fit well into the ATP-binding site [9].

### 2.0.1 Inhibitors as Drug Candidates

Pharmaceutical research on ATP-competitive inhibitors focuses on selective molecular recognition in specific protein-ligand complexes with the goal to find a specific inhibitor for each target protein kinase [10, 11]. As inhibitors can regulate enzymatic reactions in different processes, this article will review the competitive interactions in the ATP-binding site, ignoring non-competitive (allosteric) as well as uncompetitive inhibition [12]. Generally, for pharmaceutical research on ATP-competitive inhibitors 1:1 interactions are assumed [13, 14]. The inhibitors presented in the literature are mostly small molecules with a structure optimized to be taken up in the hydrophobic back pocket of the ATP-binding site in its active state [15, 16]. To be applicable as a drug, the inhibitor has to replace at least 90% of the ATP bound by the protein kinase [17].

The gold standard for drug design is the small molecule staurosporine, which interacts with many protein kinases in a 1:1 complex, providing a model inhibitor for method development and monitoring in assays [14]. Staurosporine is a microbial alkaloid discovered in 1977 to be a highly potent inhibitor for serine-/threonine kinases as well as for tyrosine kinases. It is competitive to ATP but not specific regarding different protein kinases [18–22]. The high cross-reactivity and the resultant cytotoxicity of staurosporine are the main reasons for this promising small molecule to be only deployed in laboratory experiments [20, 23]. Many staurosporine analogues show much higher specificity to defined protein kinases [23, 24]. The fact, that staurosporine, being a much larger molecule than ATP, can enter the ATP-binding pocket in the protein kinases, demonstrate a significant flexibility in the protein structure and thus a wide structured variety in suitable inhibitor molecules [25].

In 2001, the U.S. Food and Drug Administration approved the first kinase inhibitor as drug: imatinib, known as ‘Gleevec’ and ‘Glivec’ [26]. For nearly all types of chronic myeloid leukemia

it is a highly successful drug, demonstrating that even after 20 years of research since the approval of imatinib, the discipline has further possibility to grow [2, 6]. In the work of Cohen et. al. and Lorenz et. al., a chronological overview over the development of ATP-competitive inhibitors from the first discovery to clinical application is represented [26, 27]. Another detailed overview over inhibitors in clinical trial, starting with fasudil approved as a drug in 1995, albeit not for kinase inhibition, was presented by Attwood et al. They discussed, that these drugs not only have effects in cancer treatment but can also be used as drug for other diseases, such as myelofibrosis, dermatitis, rheumatoid arthritis and other immune diseases [28]. Currently, over 70 compounds are FDA approved as pharmaceuticals, globally over 100 protein kinase inhibitors are registered as drugs [28, 29].

### 2.0.2 Need for Screening Methods

Given the diverse types of possible inhibitors and the large variety of kinases as possible targets, efficient screening methods are required to identify drug candidates or relevant kinases in cancer research [30]. The primary goal of analysis methods is the identification of kinases interacting with a specific inhibitor, and therefore to find one suitable and specific inhibitor for one target kinase. Kinase as well as inhibitor screening can identify pharmaceutically interesting compounds in a rapid and effective way [31]. Whereas inhibitor screening provides information on which the inhibitor is suitable for the considered target kinase, kinase screening provides information about the specificity of the possible drug. In addition, screening can unravel susceptibility in clusters and kinase families towards specific inhibitor structures and study cross-reactivity. The best screening methods also provide thermodynamic and kinetic data of the specific inhibition interaction to verify the applicability of the small molecule as intended drug.
An example is described in the review of Gao et al. where the findings in the overview table over non-specific tyrosine kinase screening assays clearly show, that some inhibitors are found to inhibit different kinases, what implies that inhibitors are not absolutely selective and therefore, a kinase screening is as important as an inhibitor screening [30]. Most studies focus only on one specific inhibitor-kinase pair, making it difficult to deduce general or widely applicable information. For a broader assessment of kinase-inhibitor interactions and to better understand cross-reactivities, screening methods have to be applied [9].
The requirement for good screening methods are:

- low sample consumption, low costs
- sensitivity in concentration regions reproducing biological application
- preferably a label-free method to mitigate working steps, contamination and error sources in order to prevent influences on the kinase-inhibitor interaction
- a qualitative and quantitative method which provides data on the binding affinity and binding kinetics (time-resolved detection)

- possibility for high throughput screening to save time
- possibility to be applied also in matrices such as cell lysates and cells

This introduction summarizes and presents methods providing important data regarding the inhibition of protein kinases and thus, assays detecting interactions between protein kinases and small molecules. It is intended to demonstrate the large variety of strategies instead of a detailed description of every single assay. Detailed reviews of specific methods can be found in the literature [30, 32, 33].
Due to highly promising features, a focus is set on optical biosensors in this work. While electrochemical sensors were reviewed by Fathi et al. in 2022, classical methods such as radiometric methods and ELISA, as well as some mass spectrometric and electrophoretic applications, were summarized by Gao et al., highly focusing on protein activity [30, 32]. Considering the inhibition of kinases, detailed information on less familiar but highly promising assays are given in our work. A summary on assays covered in this work is given in Table 2.1.

## 2.1 Methods

### 2.1.1 Basic Considerations

Research on protein kinase interactions with small molecules is conducted with a wide spectrum of analytical methods. Most methods, from radiometric over various luminescence methods to separation techniques combined with mass spectrometry, require either the labelling of one of the binding partners or another compound responsible for the detected signal, where then the binding between protein kinases and inhibitors is only recorded indirectly. This also holds true for one of the most important assays: ELISA. Labelling has the major drawback of additional operation steps, which can cause contamination and error sources, higher costs and workload and longer experimental times. It also may change the molecular structure or conformation of the inhibitor or protein or even the protein folding with regard to the tertiary and quaternary structure. This might interrupt or alter the binding mode, so that the binding characteristics of unlabeled compounds relevant in further clinical trials may not be described accurately. Anyway, labeling mostly improves the sensitivity of a method. In Figure 2.1 an overview over the most important methods known for detecting protein kinase interaction with inhibitors is given. The methods are divided into labeled and label-free methods.
Further fundamental aspects regarding the quality of the analytical method is the performance in the homogeneous or heterogeneous phase. Assays in the homogeneous phase demonstrate the interactions similar to that in the pharmaceutical application. In heterogeneous assays, one of the binding partners is linked to a surface, which is comparable to a labeling, due to changes in the molecular structure. In the course of this review it will become apparent, that heterogeneous methods generate kinetic data as a huge advantage. In addition, many heterogenous assays can be converted into homogenous assays. In Figure 1, these assays are marked with half a colored

filling.
In order to save time during the experiments, high throughput methods are of interest, not only in drug development. Besides, information of the system beyond the interaction between protein kinases and inhibitors, such as the identification of the binding partners, is a supplementary advantage. Methods coupled to a mass spectrometric investigation can provide such data.

The fact, that many kinases show similarities in their binding pockets and also prospective inhibitors often contain similar structure elements, data on the specificity of the kinase-inhibitor-pairing is highly important [34]. At best, an inhibitor only interacts with one specific protein kinase with strongly elevated binding constants [35]. This specificity is determined by the affinity of the particular inhibitor towards different kinases. It is an extremely important parameter for a drug candidate. The sum of the interaction energies (van-der-Waals energies, electrostatic energies between protein binding pocket and ligand as well as to the solvent) quantifies the binding strength and defines the binding affinity [36, 37]. Both enthalpic and entropic effects are relevant [10]. The binding affinity is determined by the association/affinity constant $K_a$ [$M^{-1}$] or the dissociation constant $K_d = \frac{1}{K_a}$ [M].
For comparison of the inhibition of enzymes, many studies use the $IC_{50}$ value: the concentration of the inhibitor at half the maximal inhibition. In contrast to the constants describing the affinity, $K_a$ and $K_d$, in competitive assays the $IC_{50}$ value is influenced by the ATP concentration used in the particular assay [38].
In addition to the binding affinity, kinetic data is important for understanding the reaction dynamics of a drug candidate with its target. Affinity and kinetics, defined by the rate constants for association and dissociation $k_a$ [$M^{-1}\,s^{-1}$] and $k_d$ [$s^{-1}$], are connected via the relation $K_d = \frac{k_d}{k_a}$ . For protein-ligand pairs with similar binding affinities, the kinetic data is found to differ by a few orders of magnitude [39].
Dissociation constants $K_d$ were reported in a region of of $10^{-2}$-$10^{-12}$ M, depending on the kinase or inhibitor of each study [10, 40]. Association rate constants of a kinase interacting with an inhibitor are often about $10^8\,M^{-1}\,s^{-1}$, increasing with larger proteins [17]. Not all developed assays give quantitative information as output, especially some radioactive and fluorescence-based methods cannot provide affinity or kinetic data.

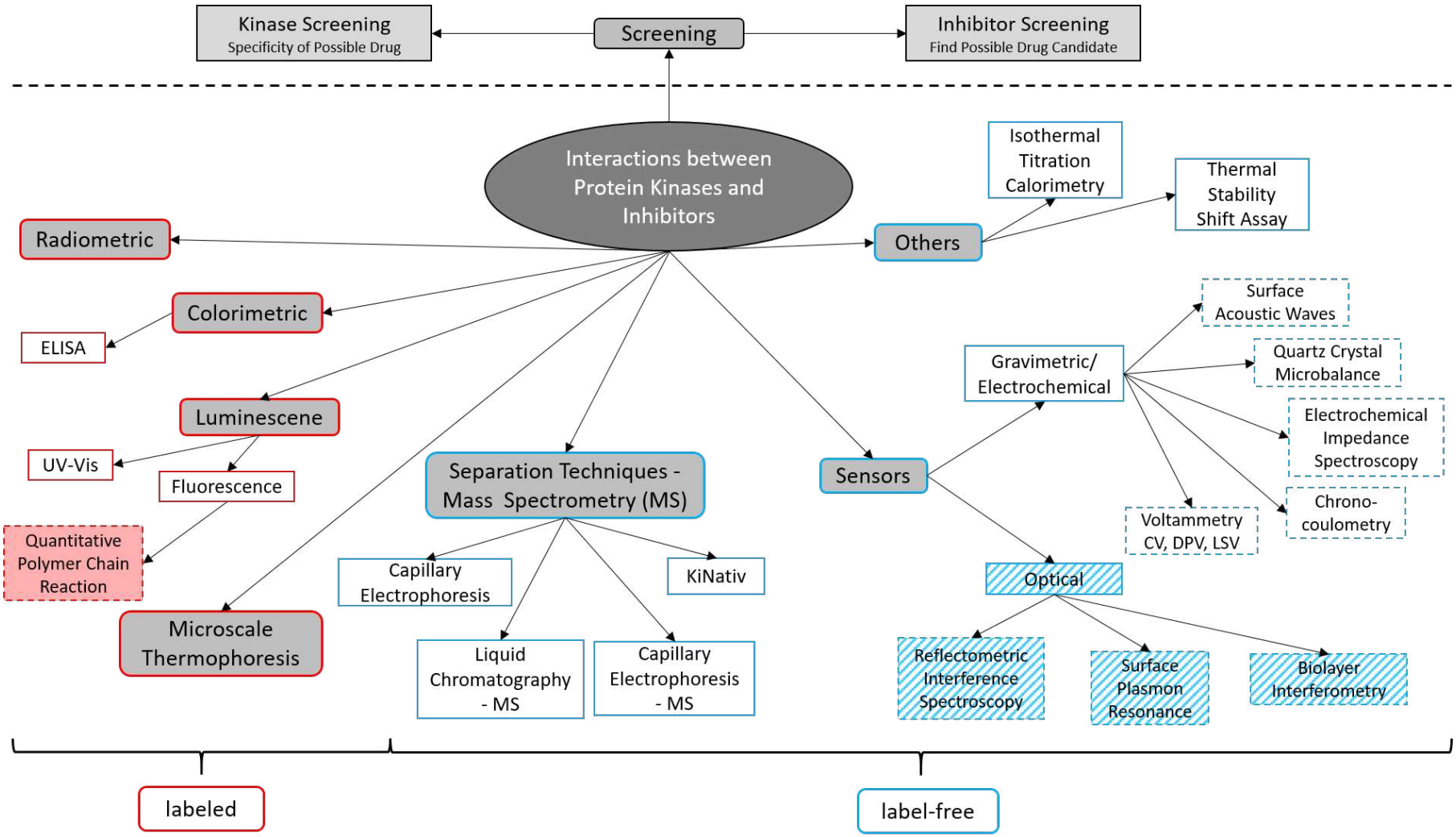


**Figure 2.1:** Graphical overview of methods to detect protein kinase interactions with inhibitors. The strongest separation is by the characteristics of labeled vs. label-free methods, marked with red (labeled) and blue (label-free) frame. Assays performed in homogeneous phase are without colored filling, assays performed in heterogeneous phase are marked with colored filling (red or blue). Because assays on optical sensors are mostly in heterogeneous phase, the interactions in the homogeneous phase can also be detected, which is marked with half a blue filling.

**Table 2.1:** Comparison of method requirements for the detection of protein kinase inhibition. As data on the kinetic behavior of the interaction between protein kinase and inhibitor are only given for optical biosensors (surface plasmone resonance, reflectometric interference spectroscopy, biolayer interferometry) and ITC and data on the identification of the kinases is only given by mass spectrometric (MS) methods, columns for these characteristics are not given explicitly.

| Method | Labeling | Screening | HTS | Cell-based | Binding Affinity | References |
|---|---|---|---|---|---|---|
| **Simulations** | | | | | | |
| Docking Simulation | - | kinases and inhibitors | yes | - | - | [41–43] |
| **Radiometric** | | | | | | |
| Radiometric | yes | kinases or inhibitors | no | no | depending on assay | [20, 38, 44–46] |
| **Luminescence** | | | | | | |
| UV-Vis, Nanoparticles | yes | inhibitors | yes | no | yes | [47] |
| Fluorescence | mostly | kinases (+ inhibitors) | yes | (yes) | (yes) | [40, 48–50] |
| Quantitative Polymer Chain Reaction | yes | inhibitors | no | no | yes | [22, 51] |
| Colorimetric, ELISA | yes | inhibitors | (yes) | no | yes | [52–54] |
| **Separation Techniques - Mass Spectrometry (MS)** | | | | | | |
| Capillary Electrophoresis | no | kinases + inhibitors | yes | no | yes | [55–57] |
| Capillary Electrophoresis-Light Induced Fluorescence | (yes) | kinases + inhibitors | yes | yes | yes | [58, 59] |
| Chromatography-MS | no | kinases | yes | no | yes | [13, 60] |
| Liquid Chromatography-MS with Kinobeads | yes | kinases | no | yes | no | [61] |
| Liquid Chromatograph-MS/MS with Kinobeads | no | inhibitors | no | yes | yes | [34] |
| Frontal Affinity Chromatography-Liquid Chromatography-MS | yes | inhibitors | yes | no | yes | [62] |
| Matrix Assisted Laser Desorption Ionization-MS | no | inhibitors | yes | no | no | [63] |
| Matrix Assisted Laser Desorption Ionization-Time of Flight-MS | yes | kinases | yes | no | no | [64] |

| Method | Labeling | Screening | HTS | Cell-based | Binding Affinity | References |
|---|---|---|---|---|---|---|
| KiNativ | yes | kinases + inhibitors | yes | yes | yes | [65, 66] |
| **Microscale Thermophoresis** | | | | | | |
| Microscale Thermophoresis | no | kinases + inhibitors (depending on assay and labeling) | no | cell lysate | yes | [67–72] |
| **Sensors** | | | | | | |
| Chronocoulometry, Electrochemical Impedance Spectroscopy | no | inhibitors | no | no | yes | [73] |
| Electrochemical Sensor | no | kinases + inhibitors | no | no | yes | [74–78] |
| Surface Acoustic Waves | no | inhibitors | no | yes | no | [79, 80] |
| Surface Plasmone Resonance | no | kinases + inhibitors (no kinase screening when bound to sensor surface) | yes | yes | yes | [81–84] |
| Reflectometric Interference Spectroscopy (Single Color Reflectometry) | no | kinases + inhibitors | yes | yes | yes | in current research, in this thesis |
| Biolayer Interferometry | no | kinases + inhibitors | yes | yes | yes | [85–88] |
| **Other Methods** | | | | | | |
| Thermal Stability Shift Assay | no | kinases + inhibitors (depending on assay) | yes | yes | no | [9, 89–92] |
| Isothermal Titration Calorimetry | no | no | no | yes | yes | [93–95] |

### 2.1.2 Digital Libraries, Simulations

The creation of a new drug often lasts over 14 years on average with costs up to 1 billion USD, requiring pre-screening methods and ideally an a-priori estimation of the types and strengths of kinase-inhibitor interactions [96, 97]. Docking simulation experiments convince with low costs, fast performance, no labelling or synthesis of molecules needed and the availability of the energetic data [98]. Due to the fact, that proteins and ligands have many degrees of freedom, calculating all their potential interaction sites is extremely complex. Structure-based drug design can generate a selection of protein-ligand pairings theoretically working well and aid in identifying lead structures, shortening the pharmaceutical development and its costs [99]. With prior docking simulation experiments, the number of inhibitors selected for further experimental screening can be drastically reduced [98]. Therefore, computational assistance is an important step for fast results in drug development also allowing high throughput [100].
However, despite progress in modeling, disadvantages still appear. A large number of false-positive calculated kinase-inhibitor pairs is a huge issue to be worked on. Binding efficiencies may be overestimated necessitating to reduce the number of hits in subsequent screening [98]. Besides, docking simulations rely on the quality of molecular models from the libraries and software and are highly dependent on the experience of the operator [101]. Databases of protein structures are based on crystallographic data, which may not well reflect the protein structure in solution. The software performance not only determines the computation time but also the accuracy of the simulated data, e.g. the charge of the molecules, the structural flexibility or the dimensions of the hydration shell [99, 102].

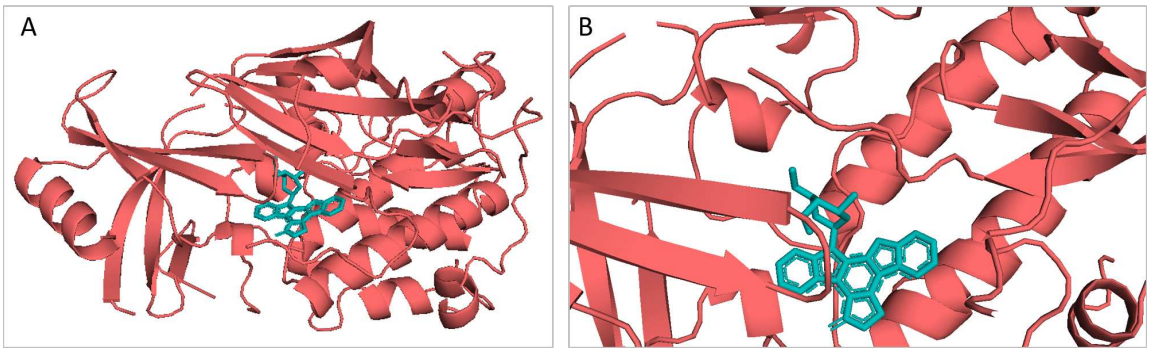


**Figure 2.2:** Docking Simulation of the protein kinase B (AKT1) with staurosporine inside the ATP-binding pocket of the kinase via AutodockTools and Vina. The kinase structure is from the open access Protein Data Base, the staurosporine structure is drawn via ChemSketch. The binding energy was simulated to -12.4 kcal/mol. A: Image of the whole protein. B: Zoomed in [42].

In the last decade, artificial intelligence (AI) is increasingly implemented in docking simulations. An example is Vina scoring, which still uses algorithms such as Monte Carlo search, as an application of AI [103]. Because protein conformation can be predicted from the amino acid sequence, access to an extended field of protein structures, which are not yet determined experimentally, has been created [104]. In order to reduce false positive hits and increase the simulation accuracy, AI helped to combine information of different screening [105].

Furthermore, intelligent systems for result combination of different screening methods are applied, in order to reduce false-positive hits and increase the simulation accuracy [105]. A short future perspective is given in the discussion of this work.

## 2.2 Labeled Methods

As already described, labeling at the kinase or inhibitor structure alters the binding behavior. Methods where labeling also occurs on another compound responsible for the detection, are common. Here, the binding behavior of kinases with inhibitors is unaffected, however the detection requires an additional process and the interactions between protein kinases and inhibitors are monitored indirectly. Given that, every labeling increase time and costs. All methods including a labeling, no matter on which molecule, are defined as labeled methods in this review, representing the summarized drawbacks of any labeling.

### 2.2.1 Radiometric- and Luminescence-based Methods

Due to the fact, that most radiometric- and fluorescence-based methods do not provide a label-free analysis nor screening possibilities, they are only discussed shortly in this work. Often defined as the "gold standard", radiometric methods include a $^{32}$P- or $^{33}$P-labeled ATP, a labeling not directly on one of the binding partners (kinases or inhibitors), but generating radiometric waste. The radioactivity of kinases after phosphorylation by radio-labeled ATP is evaluated. Inhibitor interactions can be detected in a competitive manner to the phosphorylation and binding affinities can be calculated only to some extent [34, 38, 51].
Also, quantitative polymer chain reaction methods give quantitative output of competitive binding assays, operating in real-time. DNA-tagged protein kinases interact with a recognition element on a surface, where a free inhibitor in solution releases the kinases into solution, by interacting with the kinases, and the polymer chain reaction gives quantitative results via a fluorescence detection that depends on the amount of produced DNA [22, 51].
Another commonly applied method is the colorimetric based enzyme-linked immunosorbent assay (ELISA). The detection of the interaction between protein kinases and inhibitors requires an adsorbance on the wells, which catches the protein kinases, plus an antibody, specifically binding to the protein kinase and linked to an enzyme, which emits light during the detection reaction. Different applications evaluate $IC_{50}$ values via titration experiments, that are comparable to radiometric and cellular assays. However, ELISA requires several further compounds until a detection of the binding between protein kinases and small molecules is possible, and the screening of inhibitors needs a lot of preparation time [52–54].
In the field of luminescence assays, several methods can be found in the literature. Due to the fluorescence of tryptophan, fluorescence as analysis method for kinases can well be applied, however, higher sensitivity can be achieved by fluorescence labeling of the proteins. These assays often give the possibility to a high throughput screening in the homogeneous phase, for

instance with assistance of phosphor-specific antibodies or substrates, which change their fluorescence upon phosphorylation, providing binding affinity data [40, 49]. With the ADP-Glo technology, generally a luminescence-based assay, kinase activity generating ADP is monitored by the back-conversion of ADP to ATP which induces the luminescence of the luciferase reaction. This technique measures inhibition by the absence of the luminescence [50]. Fluorescence polarization is a special method, which is used in cell-based binding assays or in the cell lysate, combined with kinobeads, where a kinase recognition element is coupled to beads, fishing kinases from aqueous solution. This method can be further connected to mass spectrometry (MS) to enable quantification [106]. Further luminescence methods are not discussed in this work, as a detailed review is given by Wang et al. [33].

### Microscale Thermophoresis

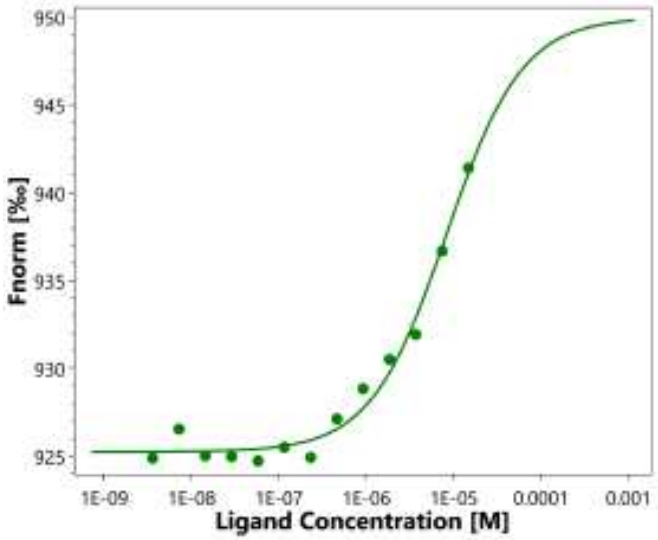


**Figure 2.3:** Dose-response curve of a microscale thermophoresis experiment with fluorescently labeled staurosporine in complex with focal adhesion kinase (40 nM) in competition with titrated bisindolylmaleimide X and an evaluated $K_d$ value of 8.2 µM. The experiments were performed with the Monolith NT.115 device and MO.Control Software by nanotemper.

A novel technique, early from this century, to investigate the interaction between proteins and small molecules is microscale thermophoresis (MST). It convinces with an easy handling, fast and highly sensitive readout while low sample and reagent volumes are required [71, 107, 108]. While some publications classify the method as label- and preparation free, most reliable results can only be observed if one of the binding partners is labeled or has a strong autofluorescence, with which artifacts can be prevented [70, 109]. MST monitors changes in the parameters size, charge and hydration shell upon the interaction of the binding partners, one of them fluorescently detectable. At least one of these parameters changes due to the interaction of proteins, RNAs or aptamers with small molecules such as ATP, ligand-induced aggregation and protein dimerization or denaturation, even in biological liquids [67–69, 71, 109]. With MST, a precise evaluation of the dissociation constant is possible [71]. As MST is a method completely

conducted in the homogeneous phase, it can be complementary seen to surface-based methods, such as those using sensors, as described later.

## 2.3 Label-free Methods

### 2.3.1 Separation Techniques and Mass Spectrometry

Separation methods are often used to study kinase inhibitor interactions [55, 58, 59]. For these methods, changes in the electrophoretic mobility or the interaction with a chromatographic column, by concentration changes of the kinases and inhibitors as well as formation of the kinase-inhibitor-complex, are required. Depending on the detection method, peak area or height provide a quantification, affinity data is evaluated via titration experiments [55–59].
Capillary electrophoresis (CE) was often combined with laser induced fluorescence, providing binding affinity and $IC_{50}$ values, with the disadvantage of a protein labeling, which assured the fluorescence detection [58, 59]. Other CE-based enzyme assays are executed with the capillary in the function of a nanoreactor. Products of the enzyme reaction are produced directly in the capillary, where thereupon the separation via the differences in the electrophoretic mobilities are conducted and the reactants and products are detected by UV-detection [55–57].
Separation techniques coupled with mass spectrometry (MS) and MS/MS can identify kinases, kinase fragments, inhibitors or even kinase-inhibitor-complexes, depending on the energy of the ionization process. A general overview over liquid chromatography or frontal affinity chromatography coupled with MS to identify proteins and their targets as biopharmaceuticals are given in the work of I. van der Broek et al, and J. Slon-Usaciewicz et al [60, 110]. A special LC-MS method is called KiNativ and discussed further.
Mass spectrometry as stand-alone method is widely used, especially Matrix Assisted Laser Desorption/Ionization (MALDI) combined with a Time Of Flight analyzer (TOF). With very small amounts of sample, down to subfemtomols, the kinase-inhibitor complex formation can be shown due to an unlimited mass range, including protein as well as small molecule detection at the same time. While the affinity can also be calculated via titration experiments, some assays need internal standards for a qualitative and quantitative analysis [63, 111–114]. Furthermore, MALDI methods provide the advantage of sampling cell-lysates and cells. Both, direct binding assays (directly detecting the interaction between kinase and small molecule) as well as competitive assays (detecting the interaction between kinase and small molecule in the presence of another molecule competing for the proteins interaction site) are found in the literature, mostly generating affinity-based data. A favored MS analysis is the heterogeneous assay via kinobeads, to which kinase inhibitors are coupled and enzymes in demand are interacting to. The kinases are identified as full proteins or after a digestion as peptide analysis where the peptide sequences, which are phosphorylated, were identified. These assays can also be conducted in a competitive manner, when kinobeads and ATP or other inhibitors compete against the interaction sited of the kinases [8, 61, 115, 116]. For MS applications care has to be taken, because the ionization process can destroy the binding between the inhibitor and the enzyme,

hindering the detection of the binding [99].
As aforementioned, the LC-MS/MS method called KiNativ is highly successful in identification and quantification of protein kinases. The sampling of biological samples like cells and tissues is a great benefit of the MS-based analysis. While ATP, bound to a recognition element such as biotin or a fluorophore, interacts with the ATP-binding site of the protein, the acyl phosphate binds selectively to a lysin of the protein. The binding takes place in the ATP-binding pocket and after ATP releases the binding site, the protein is biotin- or fluorophore-labeled. In presence of inhibitors, less ATP molecules can find free binding sites resulting in a decreased labeling. The labeling in this method is not interrupting the kinase inhibitor interaction, while it takes place after the inhibition. With the KiNativ method, several inhibitors were observed, such as STP, imatinib, geftinib, dasatinib and others. Out of a set of 10 human cancer cell lines, 74 protein kinases were identified, already. With its high sensitivity, even the precise site of labeling at the protein can be told and furthermore, $IC_{50}$-values are calculated with the KiNativ method [65, 66].

### 2.3.2 Sensors

In drug discovery, sensors are in huge research in the last decades. Consisting of a transducer system, where a recognition structure is linked to as sensing element and an electronical readout, the binding of the compounds of interest, towards the recognition element is detected. Therefore, one of the greatest advantages of sensors is the independence of any reference system [99]. Using a biosensor, the bio-sensitive element can identify a wide range of biomolecules with high selectivity and sensitivity, depending on the key-lock principle of many strong biomolecular interactions [117–119]. Direct detection of the kinase-inhibitor interactions requires one of the binding partners as sensing element linked to the transducer and indirect detection is via the phosphorylation of a phosphor-specific peptide structure on the transducer. While electrochemical and gravimetrical methods predominantly use the indirect detection, a direct observation of the interactions between protein kinases and inhibitors are given by the optical sensors. Many sensor assays can be conducted in complex matrices, such as biological media including cell cultures or cultures of microorganisms, without prior purification [36, 117, 120, 121].

**Gravimetric and Electochemical Sensors**
Gravimetric and electrochemical sensors provide label-free and sensitive assays. Due to the similar assays of gravimetric and electrochemical methods, quartz crystal microbalance and surface acoustic wave as the most common gravimetric methods, can be discussed collectively with chronocoulometry, electrochemical impedance spectroscopy, or voltammetric applications [79, 80, 122]. For the detection of kinase-inhibitor interactions, all methods use an immobilization of a peptide recognition element on gold nanoparticles, a gold electrode or a graphene system [73, 77, 78]. Information on the activity and inhibition of a kinase in presence of ATP is given via the detection of the phosphorylation of the peptide structure on the sensing element, which is achieved via the phosphorylation of the protein kinase [74, 75]. Inhibitor screening

by titration experiments and $IC_{50}$-calculation is given, as well. It was found, that this data is comparable to the results of radiometric assays, all in the same order of magnitude [76]. A further benefit of the electrochemical methods is the reusability of the sensor surface and the possibility of quantitative analysis in the cell lysate [78–80]. More detailed information on electrochemical biosensors regarding protein kinase activity are given by the review of Fathi et al. [32].

**Optical Sensors**

Biosensors are often applied as optical biosensors [99]. The detection is based on absorbance, reflectance, interference, fluorescence or polarization. The methods discussed in this work base on the reflection of a light beam, that is irradiated to a transducer, and changes specific principles in the reflected light. An advantage of optical biosensors is, that direct, label-free methods can be used, which provide a high sensitivity and to monitor in real-time. The latter aspect gives rise to a kinetic output allowing to calculate rate constants required for defining the binding processes. Thus, optical biosensors can provide valuable and realistic information on thermodynamic and kinetic values which are proven as good prognosis for the efficacy of clinical applications [36, 39, 117, 120, 121, 123–126]. Furthermore, the lack of time-consuming preparation steps combined with a high cost-effectiveness of the assays it selves, simplicity of operation and speed of analysis has reached increase in their popularity for biochemical investigations, especially in drug discovery projects. A further benefit of biosensors is the possibility to conduct the assays also in complex matrices, such as cell cultures or lysates, without the need for purification steps [120]. Another great benefit of the sensors is the possibility for automation giving rise to a higher throughput [99].

While the most important part of optical biosensors is a transducer where a recognition element is immobilized and the binding process of the dissolved analyte is detected, a major drawback is this phase boundary. Therefore, in the association phase a diffusion of the analyte to the surface is required. Depending on the association rate constant, a mass transport limitation needs to be considered when it comes to kinetic evaluation. If the association is much faster than $10^6$ $M^{-1}s^{-1}$, precise determination of the $k_a$ value becomes difficult [11, 36]. Thus, which binding partner is immobilized on the transducer surface depends on the question of the study, considering the influence of the diffusion by different sizes of the analyte molecules: small molecule vs. protein [123, 127]. Both options evolves some drawbacks: If the inhibitor as small molecule is bound to the sensor surface, steric hindrance during the association of the protein must be prevented, requiring a certain distance to the surface polymer. This can be reached by coupling the inhibitor to the transducer via an indirect immobilization e.g. with a streptavidin-biotin sandwich [128]. In order to reduce the influences of the diffusion to the heterogeneous phase, the protein kinase can be immobilized. This however comes with the risk to alter the protein structure influencing the interaction with the inhibitor, compared to complex formation in solution, during the measurement [94]. Immobilizing the protein on the surface limits the regeneration possibilities, as care has to be taken not to damage the protein. Assay precision might be lower as the covalent bond formation between the kinases and the

surface may proceed at different sites of the protein (e.g. primary amines), which evolves a low surface homogeneity [81]. Independent of the molecules immobilized, the sensor surface must be optimized to prevent nonspecific interactions, especially in samples with high matrix load [119].

Among biosensors, surface plasmon resonance (SPR) is most often applied in pharmaceutical studies. A sample interacting with the recognition element on the transducer, which includes a gold layer for SPR, changes the refractive index and with that the evanescence wave in the reflected light beam. Therefore, changes of the thickness of layers attached to the sensor are calculated and the response is proportional to the molecular mass and concentration of the analyte [17, 81]. In most SPR applications, the protein kinase is immobilized on the transducer and interactions of the small molecules, such as inhibitors, with these immobilized proteins are detected. Many different assays were discussed in the literature, e.g. binding assays for over 40 protein kinases are described or kinase screening applications on arrays with enzymes such as PKA, EGFR and PKC inhibited with H89 (an STP-similar small molecule) [82, 83]. Intracellular signal transduction was monitored with SPR, where calcium levels are dependent on specific receptors at calcium-affecting proteins, scaled down to a single cell level. SPR was able to investigate the suppression of this transduction by STP [121]. Nordin et al. used SPR to show discrimination of kinases being active (phosphorylated) or inactive: active and inactive kinases were simultaneously immobilized on one transducer, forming an array-based sensor and samples (inhibitors and ATP) were investigated, showing that the inhibitor similarly binds both kinase forms [39]. Successful assays used only the catalytic subunit of kinases, inhibited e.g. by imatinib [81]. If a good regeneration of the sensor surface is reached, high throughput screening is possible and over 1000 samples can be measured on one single sensor [129].

Reflectometric interference spectroscopy (RIfS) is similar to SPR but uses different principles for detection: Changes in the interference spectra of the reflected light on a glass sensor upon changes in the physical thickness and the refractive index on the sensor surface, combined as optical thickness [124]. While RIfS detection includes the change of the physical thickness on the sensor, the smaller binding partner is immobilized on the transducer and the interactions with the larger analyte is investigated. Compared to SPR, the use of simple glass transducers avoids the need for gold coatings and RIfS is less sensitive to temperature fluctuations.
In general, RIfS is applicable to observe biomolecular interactions in pharmacological and physiological context [130]. A lot of studies regarding thrombin activity and inhibition can be found as example for pharmaceutical screening of biological compounds in binding inhibition assays [3, 4].
RIfS studies on interactions of protein kinases with inhibitors cannot yet been found, even if this sensor method provides the possibility to also detect the interactions in the homogeneous phase. This is possible when performing a binding inhibition assay, where the protein kinase as analyte is inhibited by a small molecule and this formed complex is then used as analyte on the sensor. Hence, the drawback of the phase boundary, which is comparable to a labeling, can be eliminated.

An enhancement of RIfS is the single color reflectometry (SCORE) also named 1-λ reflectometry. Here, a monochromatic light is used for irradiation, combining all benefits of RIfS but with a compact instrumentation, which is even portable. Using a single wavelength lowers the demands for high-end spectrometers. Adding a camera for monitoring the whole surface of the transducer, sensor arrays are accusable. Via spotting to create sensor arrays, different recognition elements can be immobilized on the surface simultaneously to implement a screening technique [5, 131]. SCORE was also proven to show good results in testing biomolecular interactions in complex matrices, e.g. the quantification of anti-salmonella in serum [5]. As for RIfS, investigations on protein kinase inhibition with SCORE are not published yet.
An advancement of RIfS was made by biolayer interferometry in the last 20 years. The difference to RIfS and the main benefit of this method is the use of an optical fiber glass bundle as sensor. The surface modification of RIfS is transferred to the end of the glass bundle, which is then immersed into the analyte solution and transporting the light and its reflection. With this, the limitations by microfluidic devices and the dependency of the kinetic data on the diffusion is avoided [85, 132]. With BLI, not only antibody-antigen interactions [133] and also inhibitor interactions with kinases [88] were investigated, but also virus-like particles and whole influence virus [87, 134, 135]. Using 96-well plates, a higher throughput can be achieved. Biological samples such as living cells were directly accessible as well [85].
The publication record for BLI shows a steep increase in the recent years: for 2013 only 240 publications can be found, ten years later in 2023, 2150 studies were published (google scholar, 2024-03-06). The interest in BLI increases, regarding its benefits. Comparing these publication records to the ratio of RIfS, show inversed information: in the 2010s, for RIfS approximately 8800 papers were published, for the BLI only 5100. In the early 2020s, more studies for BLI are found: 8000 towards 5100 for RIfS.

### 2.3.3 Other Methods

Isothermal Titration Calorimetry (ITC) is a further label-free method, which reveals heat change of a solution upon binding events when analytes are titrated in a measurement cell vs a reference cell, including biological and physiological samples. ITC draws conclusion to several binding characteristics such as affinity, stoichiometry, entropy and enthalpy of the binding and kinetic data e.g. for enzyme inhibition with small molecules [93–95]. The serious drawback of ITC is the relatively large amount of sample required and that high throughput applications cannot be realized [93].
A label-free low-cost method, which monitors the thermal denaturation of proteins dependent on the affinity to other molecules by fluorescence detection, is the thermal stability shift assay (TSA). The method shows good performances in cellular formats and tissues and was applied in high throughput applications [89, 90], but not yet found to be applied for protein kinases interacting with small molecules. For example, inhibitors interacting with STAT proteins were described in cell lysates and intact cancer cells [92]. Neither kinetic data nor binding affinities are part of the TSA output, it only detects thermal shifts, while it requires another method

for quantification of the investigated proteins to correlate the temperature date to affinity date with e.g. a western blot, ITC or other affinity detecting methods [9, 89, 91].

"Science doesn't give a shit. Science is reliable in its variability. Science does whatever the fuck it wants. God, I love science."

Love on the Brain

Ali Hazelwood

# 3 Experimental Section

## 3.1 Chemicals

**Table 3.1:** Overview over all the chemicals used.

| **Chemicals** | **Manufacturer** |
|---|---|
| acetone | Merck, Darmstadt-D |
| acetonitrile (ACN) (99 +%) | Sigma Aldrich, Steinheim-D |
| amino dextran (AMD) 50 % functionalization (100 kDa) | Innovent, Jena-D |
| adenosine 5'-triphosphate disodium salt (ATP) (99 +%) | Sigma Aldrich, Steinheim-D |
| 2-(1H-benzotriazole-1yl)-1,1,3,3-tetramethylamonium tetrafluoroborate (98 +%) | Sigma Aldrich, Steinheim-D |
| biotin (99 +%) | Sigma Aldich, Steinheim-D |
| bovine serum albumin (BSA) (lyophilized powder, 96 +%) | Sigma Aldrich, Steinheim-D |
| diaminopolyethylene glycol (Da-PEG) (2 kDa) | Rapp Polymere, Tübingen-D |
| dichloromethane, anhydrous (DCM) (99.8 +%) | Sigma Aldrich, Steinheim-D |
| diisopropylcarbodiimide (DIC (98 +%)) | Fluka, Buchs-CH |
| *N,N*-dimethylformamide (DMF) ($H_2O \leq 0.1$ %, 99.8 +%) | Sigma Aldrich, Steinheim-D |
| dimethyl sulfoxide (DMSO) (99.5 +%) | Sigma Aldrich, Steinheim-D |
| 1-ethyl-3-(3-dimethylaminopropyl)cabodiimide (EDC) | Sigma Aldrich, Steinheim-D |
| glutaric anhydride (GA) (95 %) | Fluka, Buchs-CH |
| (*3*-glycidyloxypropyl) trimethoxysilane (GOPTS) (98 +%) | Sigma Aldrich, Steinheim-D |
| hydroxybenzotriazole (97 +%) | Sigma Aldrich, Steinheim-D |
| hydrogen peroxide ($H_2O_2$) (30% w/w) | Sigma Aldrich, Steinheim-D |
| magnesium chloride ($MgCl_2$) (buffer kit, 1 M) | ThermoFisher Scientific, Vilnius-L |
| 2-morpholine-4-yl ethanesulfonic acid (EDC) | Sigma Aldrich, Steinheim-D |
| nanomag-CLD, magnetic nano particles 500 nm, PEG-COOH | micromod Partikeltechnologie, Rostock-D |
| sodium chloride (NaCl) (99.8 +%) | Sigma Aldrich, Steinheim-D |
| *N*-hydroxy succinimide (NHS) (98 +%) | Sigma Aldrich, Steinheim-D |
| *N,N*-diisopropylethylamine (99 +%) | Sigma Aldrich, Steinheim-D |
| polydimethylsiloxane (PDMS), Wacker Silikon ELASTOSIL RT607 (A+B) | Reiff, Reutlingen-D |
| polyethylene glycol 2000 (PEG) (2 kDa) | Alfa Aesar, Karlsruhe-D |
| potassium dihydrogen phosphate ($KH_2PO_4$) | Sigma Aldrich, Steinheim-D |
| potassium hydroxide (KOH) (85 +%) | Sigma Aldrich, Steinheim-D |
| sinapinic acid (SA) (98 +%) | Sigma Aldrich, Steinheim-D |
| sulfuric acid ($H_2SO_4$) (95 +%) | VWR International LLC, Rosny-sous-Bois-F |
| SuperBlock Blocking Buffer in PBS | Sigma Aldrich, Steinheim-D |
| tris(hydroxymethyl)aminomethane (TRIS) (99.9 +%) | Sigma Aldrich, Steinheim-D |
| trifluoroacetic acid (TFA) (99 +%) | Sigma Aldrich, Steinheim-D |

**Table 3.2:** Overview over all the protein kinases used. *Protein kinase A was found to include different other proteins by Jens Baumgärtner from Merck, Darmstadt. Therefore, it is named protein mix in this thesis.

| **Protein Kinase** | **Manufacturer** |
|---|---|
| focal adhesion kinase, fragment 410-689 (FAK) | provided by Merck, Darmstadt-D |
| protein kinase B, fragment 144-445 (PKB, AKT1) | provided by Merck, Darmstadt-D |
| protein mix*, protein kinase A from bovine heart (PKA) (lyophilized powder) | Sigma Aldrich, Steinheim-D |
| spleen tyrosine kinase, fragment 356-635 (SYK) | provided by Merck, Darmstadt-D |
| transforming growth factor beta, fragment 200-503 (TGF$\beta$, ALK5) | provided by Merck, Darmstadt-D |

**Table 3.3:** Overview over all the inhibitors used.

| **Inhibitor** | **Manufacturer** |
|---|---|
| dasatinib | Sigma Aldrich, Steinheim-D |
| fasudil | Sigma Aldrich, Steinheim-D |
| fragment1 | provided by Merck, Darmstadt-D |
| fragment2 | provided by Merck, Darmstadt-D |
| imatinib | Sigma Aldrich, Steinheim-D |
| bisindolylmaleimide X (BisX) | Iris Biotech GmbH, Marktredwitz-D |
| staurosporine (STP) (99 +%) | Alfa Aesar, ThermoFisher, Kandel-D |
| staurosporine-Red (STP-Red) | Perkin Elmer, Massachusetts-USA |

**Table 3.4:** Overview over all solutions required in protocols.

| **Solution** | **Ingredients** |
|---|---|
| KOH | 6 M in milliQ $H_2O$ |
| MES buffer | MES 0.5 M, milliQ water, pH 6.3 (with $Na_2CO_3$ 2.5 M) |
| PBS buffer | NaCl 0.15 M, $KH_2PO_4$ 10 mM, milliQ water, pH 7.4 |
| piranha etch | $H_2SO_4$ (concentrated), aqueous $H_2O_2$ (30 %), 3:2 |
| SA7 | 7 mg/mL sinapinic acid in 30% ACN and 70% TFA (0.1%) |
| TRIS buffer | 2.42 g TRIS, 10 mL $MgCl_2$ buffer kit 1 M, milliQ water, pH 7.4, titration with KOH or HCl, total volume 1 L |

**Table 3.5:** Overview over all chemicals for regeneration solutions.

| **Regeneration Media** | **Manufacturer** |
|---|---|
| acetic acid (99 +%) | Sigma Aldrich, Steinheim-D |
| acetonitrile (99.8 %) | Sigma Aldrich, Steinheim-D |
| 1-butanol (99.9 %) | Sigma Aldrich, Steinheim-D |
| CHAPS deterent | Thermo Fisher Scientific, Massachusetts-USA |
| ethanole (EtOH) (96 %) | VWR chemicals, Leuven-B |
| ethanolamine (98 +%) | Sigma Aldrich, Steinheim-D |
| formamide (99 +%) | Sigma Aldrich, Steinheim-D |
| formic acid (95 +%) | Sigma Aldrich, Steinheim-D |
| glycine Reagent Plus$^{TM}$ (99 +%) | Sigma Aldrich, Steinheim-D |
| guanidinium chloride (GdmCl) (99 +%) | Sigma Aldrich, Steinheim-D |
| magnesium dichloride ($MgCl_2$) | Sigma Aldrich, Steinheim-D |
| malonic acid (99 %) | Sigma Aldrich, Steinheim-D |
| trypsin-EDTA (0.05 %) | Gibco, Paisley-UK |
| oxalic acid (98 %) | Sigma Aldrich, Steinheim-D |
| phosphoric acid ($H_3PO_4$) (85 %) | Sigma Aldrich, Steinheim-D |
| piperazine (99 %) | Sigma Aldrich, Steinheim-D |
| polysorbate 20 (Tween20) | Thermo Fisher Scientific, Massachusetts-USA |
| polysorbate 80 (Tween80) | Thermo Fisher Scientific, Massachusetts-USA |
| potassium thiocyanate (KSCN) (96 %) | Sigma Aldrich, Steinheim-D |
| sodium EDTA solution ($Na_2-$EDTA) (99 +%) | Fluka, Buchs-CH |
| sodium acetate (NaOAc) (99 %) | Sigma Aldrich, Steinheim-D |
| sodium dodecyl sulfate solution (SDS) (20 % in $H_2O$) | Sigma Aldrich, Steinheim-D |
| sodium phosphate ($Na_3PO_4$) (96 %) | Sigma Aldrich, Steinheim-D |
| Triton X-100 | Thermo Fisher Scientific, Massachusetts-USA |
| urea | Sigma Aldrich, Steinheim-D |
| zwittergent 3-12 | Sigma Aldrich, Steinheim-D |

**Table 3.6:** General equipment and software.

| | |
|---|---|
| origin 9.7.0.188 | Origin 2020, OriginLab, Massachusetts-USA |
| pH meter | inoLab pH 7110, Xylem Analytics Germany, WTW, Weinheim-D |
| milliQ water processor | Purelab Classic ultrapure water processor, ELGA LabWater Veolia Water Technologies, Celle-D |
| ultrasonic bath | Sonorex Super 10 P, Bandelin electronic, Berlin-D |
| vibrating table | Thermomixer compact, Eppendorf, Hamburg-D |

## 3.2 Methods and Equipment

### 3.2.1 Docking Simulation

**Table 3.7:** Software used for the docking simulations.

| | |
|---|---|
| AutoDock 1.5.6 | Scripps Research, La Jolla-C |
| AutoDock Vina 1.5.6 | Scripps Research, La Jolla-C |
| ChemSketch, freeware version | ACD/Labs, Toronto-C |
| Protein Data Base (PDB) | wwPDB Foundation, open access database |
| PyMOL 3.0 | DeLano Sicentific LLC, Schrädinger Inc. |

Drug design is mostly aided by computational simulations of the interactions between receptor and ligand. In order to predict preferred binding orientations with docking simulations, the ligand (inhibitor, drug) is simulated in its fitting into the receptor structure (protein) to form a complex. Free binding energies are calculated, as well as the stability of the complex [102]. Two important open source programs for these simulations are AutoDock and AutoDock Vina. These AutoDock tools simulate the semi-empirical free energy force field of the protein, in combination with the ligand, torsional degrees of freedom, while bond angles and lengths are held constant [136, 137].
During the simulation process, enthalpic contributions are evaluated, such as dispersion and repulsion, hydrogen bonding as well as entropic contributions like changes in conformational mobility and solvation [136]. The evaluation provides the energy contribution of the protein and ligand in their unbound state and in their bound state as complex. Additionally, the energy contribution for the intramolecular interactions transitions in the bound state are calculated separately for each molecule. Three pair-wise summands (intramolecular energies $V$ for the bound and unbound stat of ligand L, protein P and complex) plus the entropy loss due to the complex formation of the two molecules $\Delta S_{conf}$ are required for the calculation of the free binding energy $\Delta G$, see Equation 1 [136].

$$\Delta G = (V_{bound}^{L-L} - V_{unbound}^{L-L}) + (V_{bound}^{P-P} - V_{unbound}^{P-P}) + (V_{bound}^{P-L} - V_{unbound}^{P-L} + \Delta S_{conf}) \quad (1)$$

Each summand evaluates the particular forces of dispersion and repulsion, hydrogen bonding as well as electrostatic forces and desolvation [136].
The output of the docking computation are the simulated free binding energies in kcal/mol as well as the specific position and orientation of the ligand in the binding pocket of the protein or at the protein surface [42].

Docking simulations are conducted with the open source programs AutoDock, AutoDock Vina, ChemSketch and PyMOL. The 3-D structures of the proteins are searched in the Protein Data Bank PDB (Worldwide Protein Data Bank) and saved as pdb-files. This file is opened in

PyMOL, the defined amino acid sequence without water molecules are extracted and saved as new pdb-file. The new pdb-file is opened with AutoDock. Hydrogens are edited from the molecule and the Gasteiger charges computed separately. This protein structure is saved as a pdbqt-file, the extended version of a pdb-file [42]. Now the ligand is drawn with ChemSketch, saved as pdb-file and opened with AutoDock. For ligands, hydrogens and charges are adapted automatically and the structure must only be saved as pdbqt-format. As the last preparation step, the Grid Box is defined as the part of the protein used to search for interactions between the molecules. The docking simulations are performed with two different Grid Boxes, one included the whole protein, the other only used the ATP-binding site. In order to reduce calculation times, the protein structure is treated as rigid, flexibility is only allowed for the ligand. Position and size of the Grid Box are added to the txt-file as configuration protocol, as shown in Figure 3.1.

```
receptor = rec.pdbqt
ligand = lig.pdbqt
center_x = 5
center_y = 5
center_z = 5
size_x = 20
size_y = 20
size_z = 20
out = out-rec.pdbqt
log = results.txt
```

**Figure 3.1:** Configuration protocol for the docking simulation. The pdbqt-files of the receptor (protein) and ligand (inhibitor) are defined, as well as the position of the Grid Box (here exemplarily defined as 5) and its extension along the axis (here exemplarily defined as 20). As output, a pdbqt-file with the structures of the ligand and a txt-file with the computed free binding energies is obtained.

After computing, the output is saved as txt-file where the binding energies are defined in kcal/mol. Furthermore, a pdbqt-file is saved, including the nine ligand positions with the highest free binding energies and their orientations at the protein structure. If the output pdbqt-file is opend in PyMOL, together with the protein structure, all nine interactions are displayed (see Section 4.1).

### 3.2.2 Microscale Thermophoresis

**Table 3.8:** Hard- and software used for the MST investigations.

| | |
|---|---|
| Monolith NT.115 | Nanotemper Technologies, München-D |
| Monolith NT.115 Capillaries | Nanotemper Technologies, München-D |
| MO.Control Software | Nanotemper Technologies, München-D |

Characterization and quantification of interactions between proteins and ligands or proteins and proteins in solution is possible by thermophoresis [67]. Microscale thermophoresis (MST) is a method to determine thermodynamic parameters by the detection of changes in charge,

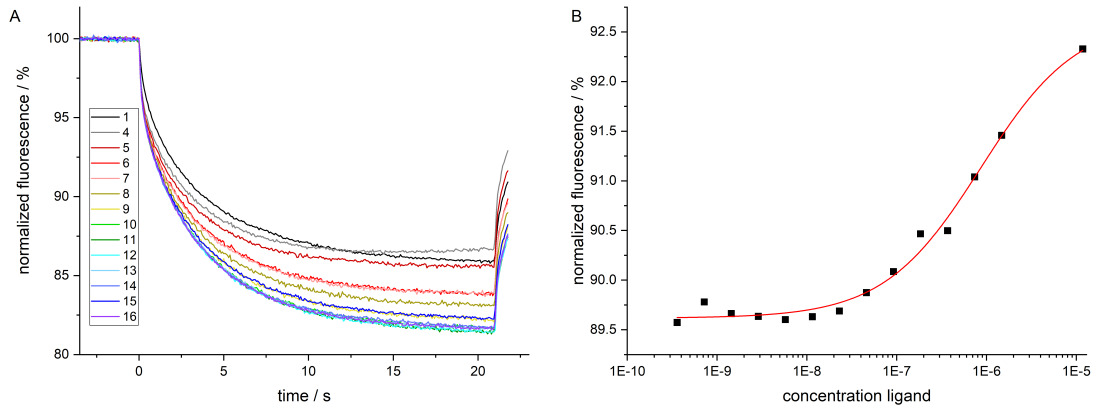


**Figure 3.2:** A: Fluorescence signal of a titration experiment measured with MST. At time 0 s the IR-laser is switched on leading to a local change in temperature. The change in the fluorescence intensity by molecular movement out of the hot region is recorded. In this example, decreasing amounts of ligands (1-16) bound to the protein decelerates the movement, resulting in a decrease of the fluorescence decline from black over red, yellow and green to blue and violet curves. B: Sigmoidal dependency of an MST fluorescence signal obtained when plotting the normalized fluorescence at a specific time against the logarithmic concentration of the ligand. In this example, the change in fluorescence increases with higher concentration of the ligand.

size or the hydration shell of proteins or ligands, depending on their movement in a microscopic temperature gradient [70, 107, 108]. The theoretical basis for the thermophoresis is the Ludwig-Soret effect describing the thermal diffusion induced by a temperature gradient. In a fluorescence microscope, a laser radiates IR-light to a capillary filled with sample solution, heating the sample with high precision. The temperature gradient of 2-6 K, created in the capillary, induces a diffusion of the molecules. The resulting motion is based on the interaction of the heat flow and the mass flow. Owing to the change in temperature ($\Delta_T$), different molecules leave the region of elevated temperature at a different speed [108]. The concentrations of the biomolecules in the hot and cold region ($c_{hot}$, $c_{cold}$) change exponentially with the Soret Coefficient ($S_T$) as exponent, see Equation 2 [70].

$$\frac{c_{hot}}{c_{cold}} = e^{-S_T \cdot \Delta_T} \tag{2}$$

The motion of molecules of the thermophoresis is followed via fluorescence signal, necessitating one of the binding partners to be fluorescently labeled.

For an MST experiment, 16 capillaries are filled with sample, where the non-labeled binding partner is titrated. Excitation for fluorescence is achieved by stimulating the fluorescence with an LED in blue, green or red, dependent on the labeling. Each capillary is checked for its fluorescence quality compared to the fluorescence in the other capillaries, and a baseline is set. The IR-laser is then switched on with a wavelength of 1480 nm. The thermophoresis is observed by detecting the fluorescence decrease in the hot region in the capillary. By turning off the laser, the molecules return to the normal distribution by back diffusion and mass transport.

In a titration experiment, the concentration of the titrated ligand is step-wise reduced by a factor of two, while the fluorescence intensities are recorded, see Figure 3.2 A. Differences in the fluorescence intensities are displayed depending on the logarithmic concentration, which shows a sigmoidal dependency of the fluorescence intensity during an MST experiment, see Figure 3.2 B.
MST measurements are performed with Monolith NT.115 and automatically evaluated by the MO.Control Software. For all additional evaluations the software origin is used.
Monolith NT.115 can perform serial dilutions for 16 fractions. Following the instructions for mixing the solutions, Monolith Capillaries are filled and inserted into the device for MST.

### 3.2.3 Sensor Measurements: Surface Modification

**Table 3.9:** Hard- and software used for the surface modification of the transducer.

| | |
|---|---|
| interference glass D263 borosilicate glass | transducer, coated with 10 nm $Ta_2O_5$ and 330 nm $SiO_2$, Schott, Mainz-D |
| MicroGrid II | spotter, BioRobotics Inc., Massachusetts-USA |
| TAS Application Suite | spotter software, BioRobotics Inc., Massachusetts-USA |
| Xtend$^{TM}$ Capillary Microarray Pins | capillaries, 130 µm diameter, LabNEXT, Wolfville-CAN |

The commercial transducers for sensor investigations are composed of several layers. The glass substrate used as base is coated with a $Ta_2O_5$ layer of 10 nm followed by a 330 nm thick $SiO_2$ layer. This silica layer is modified to either prevent non-specific interactions in further sensor investigations and to covalently bind the inhibitor to the transducer surface. Detailed information on each surface modification step for RIfS and 1-λ transducers is summarized in Table 3.10 and in Figure 3.3.

**Table 3.10:** Detailed information of chemicals and solutions used for each surface modification step for RIfS and 1-λ transducers.

| **Surface Modification Step** | **Substance** | **Transducer** | |
|---|---|---|---|
| | | **RIfS** | **1-λ** |
| Silanization | GOPTS | 10 µL | 100 µL |
| Immobilization of Biopolymer | AMD in milliQ water 7 g/mL<br>PEG in DCM 4 mg/mL | 10 µL<br>20 µL | 100 µL |
| Binding of Biotin | TBTU 0.95 g/mL + HOBT 0.45 g/mL + Biotin 0.7 g/mL in DIPEA | 5 µL | |
| Refunctionalization | GA in DMF 2 g/mL | 10 µL | 100 µL |
| Activation via Active-ester | NHS 0.15 g/mL + DIC 0.23 mL/mL in DMF | 10 µL | 100 µL |
| Binding of Inhibitors | inhibitor in DMSO 1 mg/mL | 5 µL | manual: 0.03 µL<br>spotter: 1 nL |

**Activation**

The transducers are cleaned with a 30-second incubation of 6 M KOH solution and washed with milliQ water. For activation, the transducers are incubated with fresh piranha etch (30% aqueous hydrogen peroxide with concentrated sulfuric acid in a volume-ratio of 2:3) for 15 min in an ultrasonic bath. The activated transducers are washed with milliQ water and dried under a stream of nitrogen. Due to the surface's sensitivity to humidity, the activated transducers need to be silanized immediately.

**Silanization**

Activated transducers are silanized in a sandwich technique with *3*-glycidyl-oxypropyl)-trimethoxy silane (GOPTS), see Figure 3.3 'Silanization'. GOPTS is placed between the activated surfaces of two transducers (sandwich technique) and incubated for one hour in a dry chamber at ambient temperature. The silanized transducers are washed with water-free acetone, dried under a stream of nitrogen and further processed immediately.

**Immobilization of Biopolymer**

The biopolymer aminodextrane (AMD) is immobilized on the silanized transducer by a sandwich technique in a water vapor chamber over night at ambient temperature, see Figure 3.3 'Immobilization of Biopolymer'.
Alternatively, polyetyhlene glycol (PEG) as biopolymer is dissolved in dichloromethane (DCM), dropped onto each silanized transducer surface and incubated at 70°C over night.
Every immobilization process is finalized by washing with milliQ water and drying the surface under a stream of nitrogen.
Transducers immobilized with biopolymer can be stored at 4°C for several weeks.

**Binding of Biotin**

Biotin is linked directly to the amino-function of the AMD on the transducer surface. A solution of 2-(1H-benzotriazole-1yl)-1,1,3,3-tetramethylammonium tetrafluoroborate, hydroxybenzotriazole and biotin in *N,N*-diisopropylethylamine is incubated with the sandwich technique in a chamber saturated with vapor of dimethyl formamide (DMF) at ambient temperature over night. The transducers are cleaned with DMF and milliQ water and dried under a stream of nitrogen. Biotin-modified transducers can be stored at 4°C up to several weeks until use.

**Refunctionalization**

Binding an inhibitor to the transducer surface requires a refunctionalization of the amino-function of the biopolymer, see Figure 3.3 'Refunctionalization'. For this, glutaric anhydride (GA) is incubated with the sandwich technique for six hours in a chamber saturated with vapor of DMF at ambient temperature. After cleaning with DMF and milliQ water and drying under a stream of nitrogen, the transducers can be stored at 4°C for several weeks.

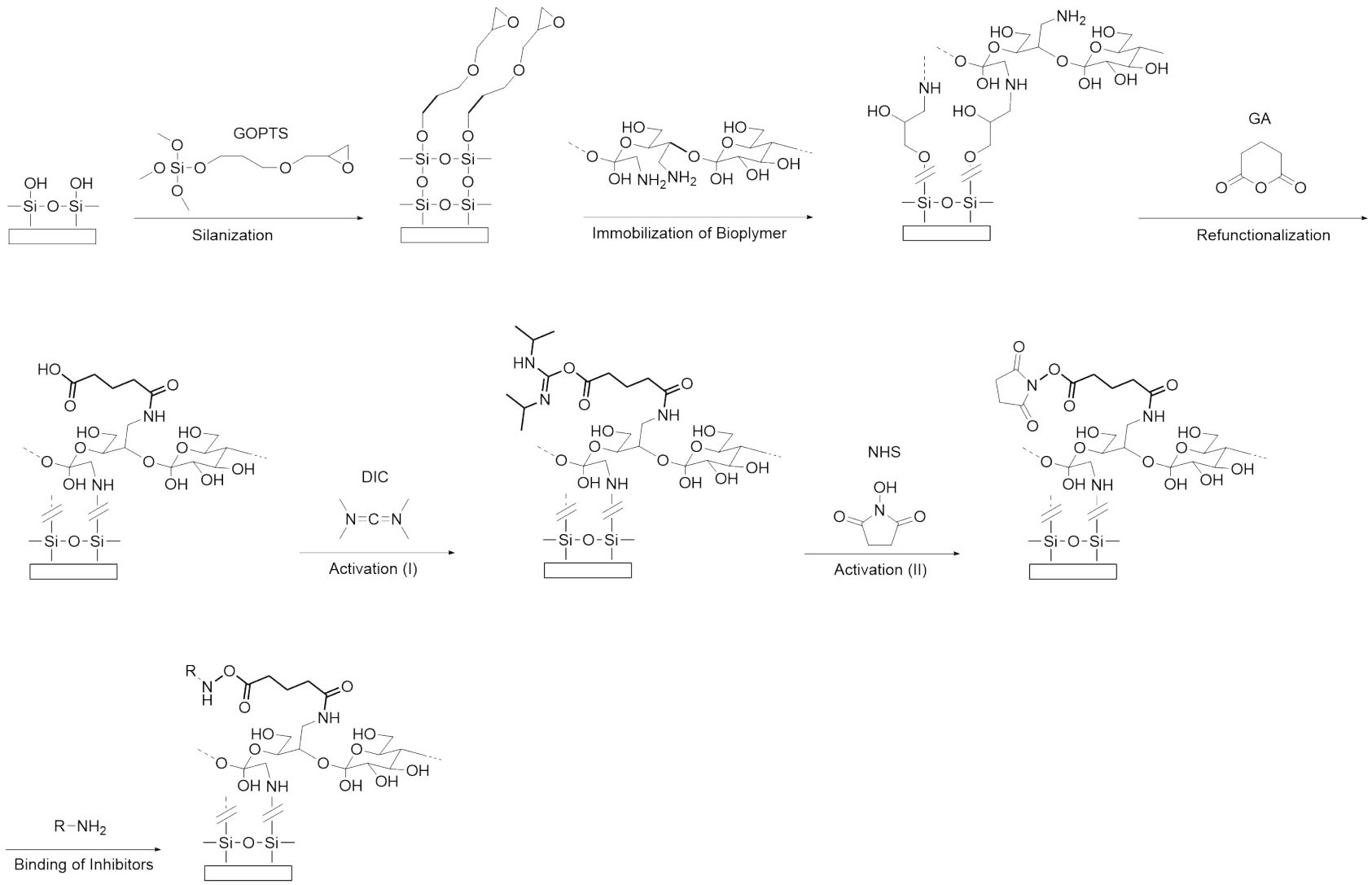


**Figure 3.3:** Chemical reaction steps for the surface modification of the transducers for RIfS and 1-λ reflectometry.

**Activation via Active-ester**

The refunctionalized transducer surface is activated in a sandwich by a mixture of *N*-hydroxy succinimide (NHS) and diisopropylcarbodiimide (DIC) in DMF, see Figure 3.3 'Activation (I) and (II)'. After incubation for four hours in a DMF vapor chamber at ambient temperature, the transducers are cleaned with water-free acetone and dried under a stream of nitrogen. The activated surface is instable and requires a prompt further processing.

**Binding of Inhibitors**

The activated transducer surface is now ready to bind inhibitors via their amino group see Figure 3.3 'Binding of Inhibitor'. Structures of all used inhibitors are displayed in Figure 3.4. The activated surfaces of the RIfS transducers are covered with a solution of the inhibitor in dimethyl sulfoxide (DMSO). The binding process is conducted in a DMSO vapor chamber while excluding exposure by UV-light for one hour at ambient temperature and afterwards at 4°C over night. Final RIfS transducers are washed with milliQ water, dried under a stream of nitrogen and stored at 4°C for up to several weeks until use.

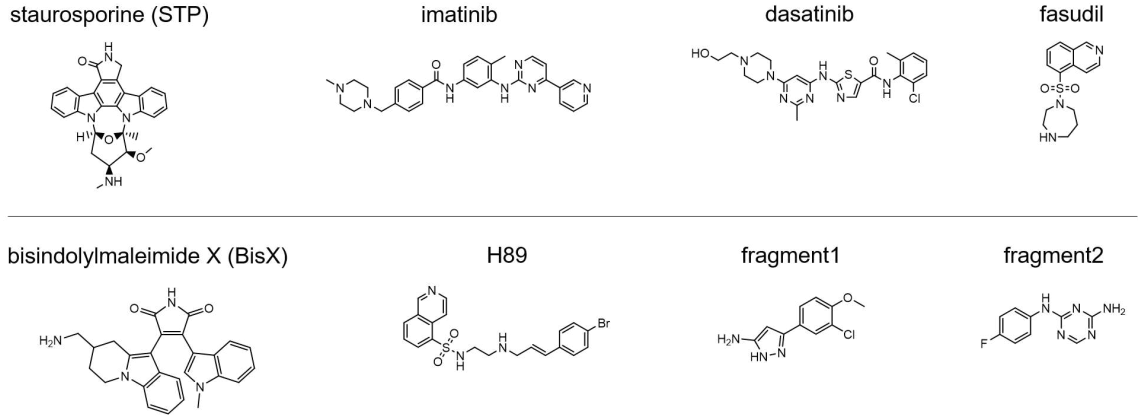


**Figure 3.4:** Molecular structures of all in inhibitors selected for this work.

Spotting experiments are performed with 1-λ reflectometry. In contrast to the method described for 'Binding of Inhibitors', not the whole activated surface is covered with inhibitor for further binding. Spotting leaves parts of the activated surface free of inhibitors and thus allows several small spots to be placed on the surface whereas inhibitor-free regions of the transducer surface is open for signal referencing, described in Section 4.3.4. For screening applications, binding of inhibitors to activated 1-λ transducers are conducted in two ways:

1. Manual spotting by hand (pipetting): A solution of inhibitor in DMSO is applied in up to five individual droplets onto the measurement region of the activated surface of the transducer. Each droplet may contain a different inhibitor. The binding reaction takes place in a DMSO vapor chamber under exclusion of UV-light for one hour at ambient temperature and afterwards at 4°C over night. The transducers are then washed with milliQ water and dried under a stream of nitrogen. They can be stored at 4°C for several weeks until use.

2. Automatic spotting via spotter: Small droplets of inhibitor in DMSO are applied to the activated transducer surface via the ceramic pin of the spotter. After drying, the process is repeated twice to increase the surface covering of inhibitor. Transducers spotted automatically are called arrays-based and stored at 4°C without further cleaning, until use.

In Fig. 3.5, the different spot sizes dependent on the spotting methods are visible.

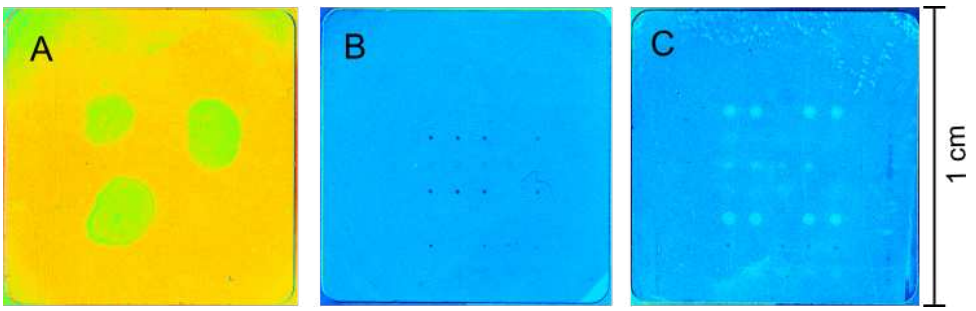


**Figure 3.5:** Difference images of transducer surfaces after association of kinases showing differences in spot size on 1-λ transducer depending on the spotting method for the inhibitor. A: manual spotting by hand. B and C: automatic spotting using a spotter with differently defined spot sizes by the software.

### 3.2.4 Sensor Measurements: RIfS and 1-λ reflectometry

Sensor measurements are performed with systems constructed in-house, seen in the schematic description in Figure 3.6. The utilized hard- and software are defined in Table 3.11.

**Table 3.11:** Hard- and software used for the sensor measurements.

| | |
|---|---|
| CCD camera, pco.camera (Typ 1600) | Excelitas Technoloiges Corp., Waltham, Massachusetts-USA |
| IFZ | evaluation of the interference spectra from Measure, in-house software by the working group of Prof. Gauglitz, Eberhard Karls Universität Tübingen-D |
| ImageJ | U.S. National Instituites of Health, Bethesda, Maryland-USA |
| Measure | measurements of interference spectra in RIfS, control of the autosampler, in-house software by the working group of Prof. Gauglitz, Eberhard Karls Universität Tübingen-D |
| outlet | Hamilton-6-way-outlet, Microlab MVP, Hamilton Company, Reno Nevada-USA |
| pco.camware | Excelitas Technologies Corp., Waltham, Massachussetts-USA |
| pump | Hamilton injection fluidics, Microlab 500 series, double injection dispenser (2 x 100 µL), Hamilton Company, Reno Nevada-USA |
| ROTOFIX 46H | centrifuge for producing the flow cell, Hettich, Tuttlingen-D |
| spectrometer | diode-array spectrophotometer, SPEKOL 1100, Analytik Jena, Jena-D |

### Measuring Setups

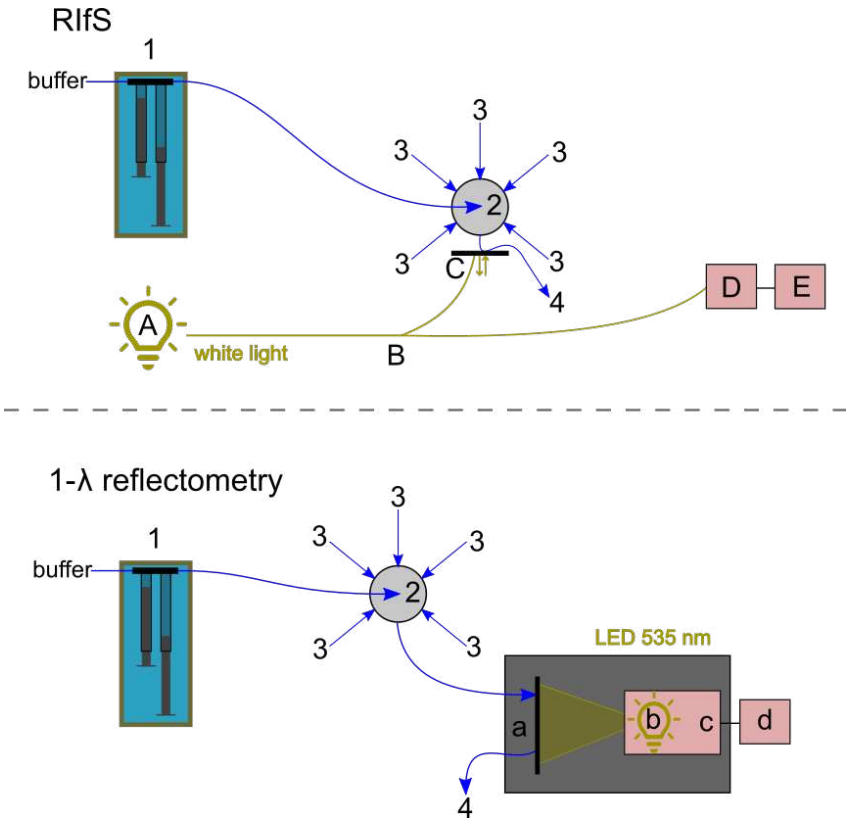


**Figure 3.6:** Schematic description of the measuring setup of RIfS and 1-λ reflectometry. The general setup is similar for both applications: 1 - pump system, 2 - valve, 3 - inlet for different samples, 4 - waste. RIfS: A - light source (halogen lamp), B - y-shaped optical fiber, C - flow cell with transducer, D - spectrometer, E - computer with software. 1-λ reflectometry: a - flow cell with transducer, b & c - light source (535 nm) and CCD camera, d - computer with software. In 1-λ reflectometry, flow cell, light source and camera are inside a dark box.

In both setups in Figure 3.6, samples are injected via the outlet. An autosampler connected to a pump system regulates the flow speed of the samples over the sensor. In RIfS measurements, white light from a halogen lamp, guided via an optical fiber in y-shape, irradiates the back of the transducer, see Figure 3.6. One half of the reflected light is guided to the spectrometer, the other half back to the light source.

Besides the difference in the size of the transducers for RIfS and 1-λ reflectometry, compare Figures 3.8 B, 1-λ reflectometry uses green light at a wavelength of 535 nm for irradiation. As shown in Figure 3.6, the green light is irradiated to the back of the non-reflecting transducer that is installed in a self-constructed flow channel, see Figure 3.8 A. The reflected light is detected with the CCD camera. The intensity changes of the recorded images are evaluated with ImageJ.

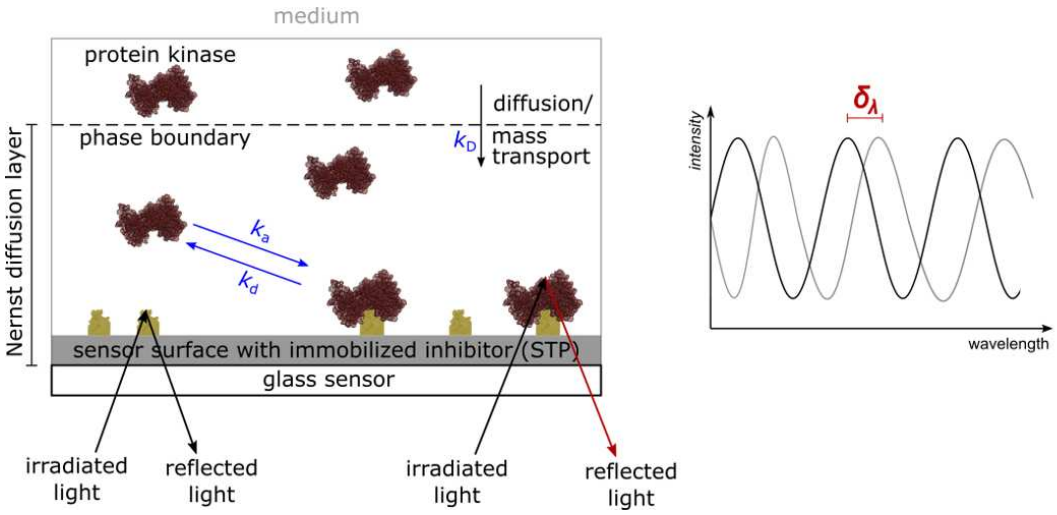


**Figure 3.7:** Schematic description of a direct assay on a sensor, where inhibitor is immobilized on the transducer surface. Protein kinase, which is flushed over the sensor, interacts with the inhibitor on the transducer, increasing the upper layer of the transducer. Thereby, the reflection point of the irradiated light changes, which changes the constructive interference spectrum. The resulting binding curve is displayed in Figure 3.9.

The flow cell for 1-λ reflectometry is produced in-house using a form which can be placed in the centrifuge. Silicone Elastosil RT 607 A and B are mixed at a ratio of 9:1 (g:g), and the mixture is stirred for 5-10 minutes. Then, the mixture is poured into the form and centrifuged for 15 minutes at 1500 rpm to remove remaining air bubbles. The mixture in the form is heated to 70°C for 75 minutes. After releasing the flow cell from the form, it is washed three times for 5 minutes with water-free acetone and baked at 70°C over night.

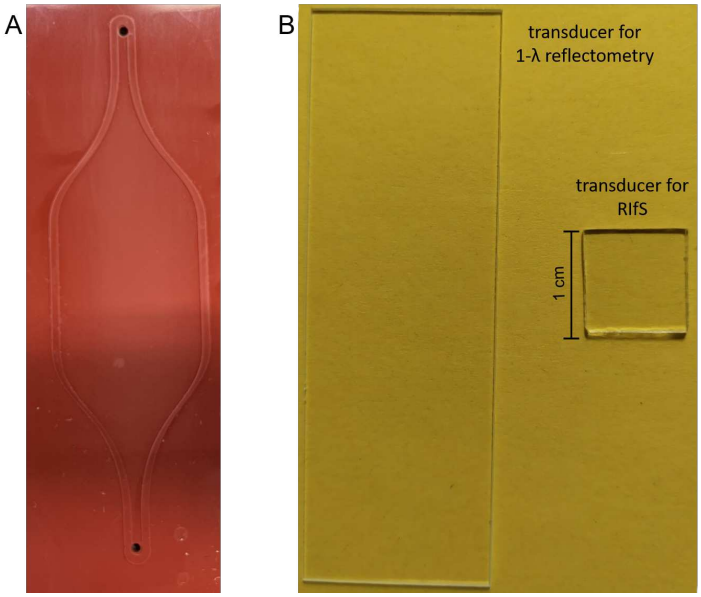


**Figure 3.8:** A: Silicon flow cell for 1-λ reflectometry measurements. B: Picture of the transducers for 1-λ reflectometry and the smaller RIfS transducer.

### 3.2.5 Sensor Measurements: Biochemical Assays and Regeneration

A short overview over the sensor measurements with an exemplary binding curve is provided in Figure 3.9. The sensor measurements start with a flow of buffer over the sensor to record a spectral baseline, followed by flushing with a blocking solution to saturate non-specific binding sites on the transducer. During the association phase, kinases as sample are flushed over the sensor surface, interacting with the inhibitors bound to the transducer, which causes an increase in the layer thickness. A following flow of buffer defines the dissociation phase, evolving an equilibrium between association and dissociation of the kinases on the sensor. The sample is regenerated from the transducer surface by flushing a regeneration medium through the system. After the regeneration, buffer is flushed over the transducer again, and the sensor signal ideally returns to the original baseline, indicating a complete regeneration. By flushing solutions such as plain buffers or protein mixtures over the transducer surface without any specific interactions, no changes in the sensogram should occur, reassuring the specificity of the sensor.
If not mentioned otherwise, the volume for sample and blocking solution in RIfS is 100 µL, for 1-λ reflectometry 400 µL, the regeneration volume is 500 µL for both. Due to the larger flow cell in 1-λ reflectometry, the sample volume is higher. For blocking and regeneration, an excess of solutions is used in RIfS and these volumes are adopted to the 1-λ reflectometry to save material and money. The pump velocity for sample solutions is 0.5 µL/s and 2 µL/s for RIfS and 1-λ reflectometry, respectively, the regeneration velocity is 5 µL/s for both methods.
Sensor measurements are performed with TRIS buffer containing 1% DMSO. To prevent gas generation in the fluidic system, the buffer was degassed beforehand.

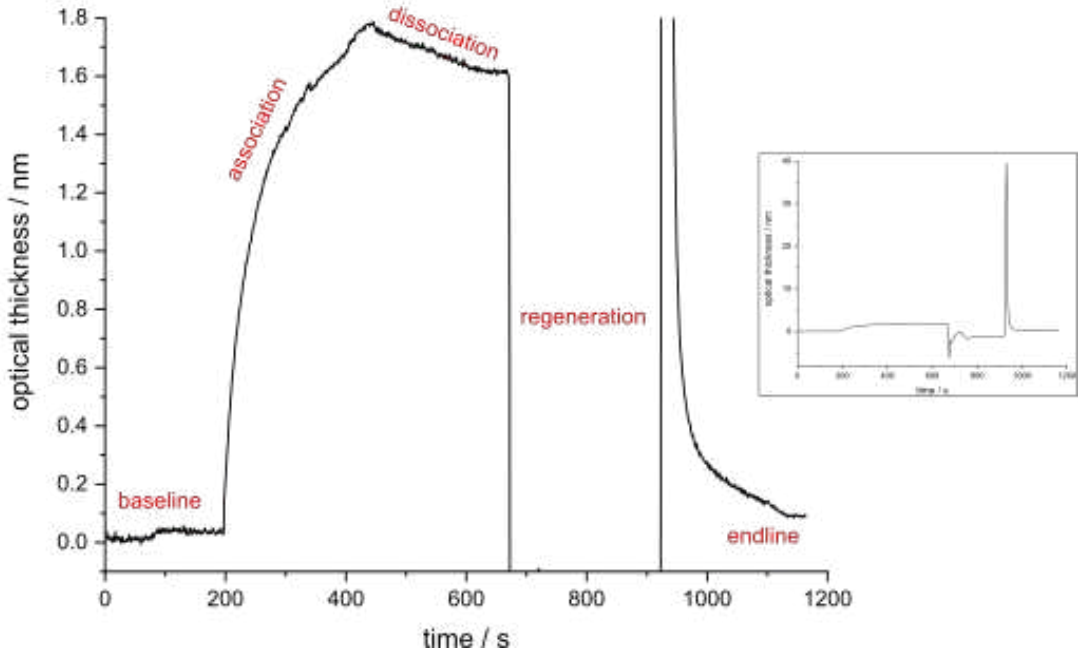


**Figure 3.9:** Exemplary sensogram of a RIfS measurement with specified baseline (flushing buffer), association phase while flushing with sample, dissociation phase while flushing with buffer, regeneration recorded while flushing with a regeneration medium and endline when flushing buffer.

### Direct Assay

Kinase solution as sample is flushed over the sensor. Due to interactions between the inhibitor on the transducer and the kinases an increase in optical thickness is recorded, observable in the association phase of the binding curve, see Figure 3.9. If not mentioned otherwise, kinase solutions have a concentration of 2 µg/mL.

### Binding Inhibition Assay

Binding inhibition assays require a pre-incubation of the kinases with the inhibitor in the homogeneous phase, here in TRIS buffer. The inhibitor is added at a molar excess of 1-100 to the kinase concentration and the solution is incubated for 15 minutes while shaken at 400 rpm at 30°C. Afterwards, the solution is flushed over the sensor, to initiate the association phase.

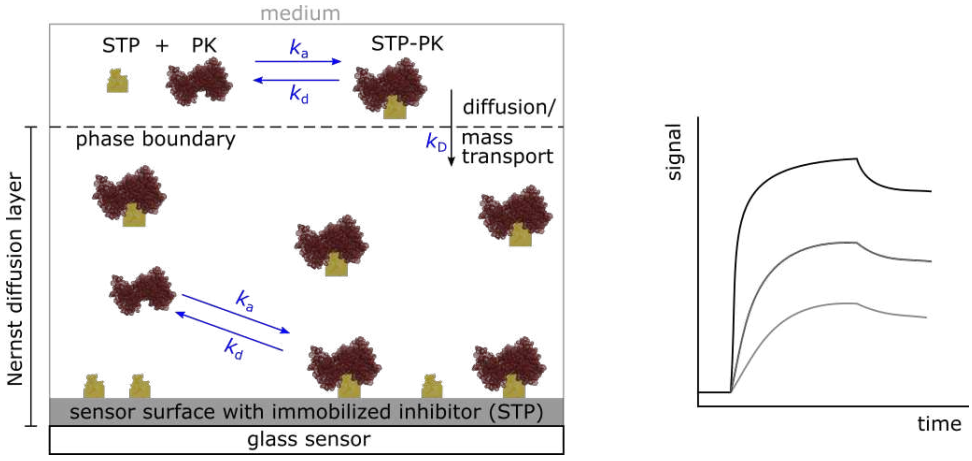


**Figure 3.10:** Schematic description of a binding inhibition assay on a sensor with the inhibitor immobilized to the transducer surface. Protein kinase interacts with the inhibitor in solution in a pre-incubation. Flushing this solution over the sensor surface, only native kinases without inhibitor bound can interact with the inhibitor immobilized to the transducer. Depending on the concentration of the free inhibitor in the pre-incubation, the sensor signal decreases.

### Regeneration

Two strategies are followed to regenerate the transducer surface in RIfS after measurements. First, classical regeneration media, such as diverse chaotropes, acids and bases, detergents and electrolytes, are tested. All these classical regeneration media were successfully applied for regeneration of sensors in RIfS or SPR [4, 17, 58, 125, 138]. An overview over the tested media and their combinations is given in Figure 3.11.

To quantitatively compare the regeneration, the effectivity $R_e$, according to Andersson et al. was calculated with a slight modification (Eq. 3) [139]. In this thesis, the effectivity of the regeneration is referred to the optical thickness of the last endline in the set of experiments. If there are several regeneration cycles on one sensor, each cycle is thus evaluated separately, referring the change in optical thickness to the endline of the cycle before. This modification of evaluation should prevent an overrating of regeneration media, which are not used in the first

regeneration cycle while it avoids to prepare new transducers each time.

$$R_e = 100 - \frac{\text{optical thickness regeneration}}{\text{optical thickness last endline}} \cdot 100\% \tag{3}$$

A graphical description of the calculation of $R_e$ is shown in Section 4.3.2 in Figure 4.11.
In this study, FAK or TGFβ as kinases are flushed over an AMD-STP-sensor. After the association and dissociation phase, the regeneration is evaluated. The regenerating components in the media are either tested alone or in repeated regeneration steps on the same sensor. Several regeneration cycles are performed on the same sensor, until sufficient regeneration. Regeneration is defined as sufficient, when the optical thickness of the baseline, prior to any association or dissociation, is reached. For RIfS evaluation in this work, the change in optical thickness is expected to be regenerated to reach zero. Then, another step of kinase association is performed, to judge any improvement or possible impairment of the sensor surface for reuse. If the second kinase association is similar to the first one, further regeneration is tested. If kinase association is not successful, a new transducer is installed in the setup, and the whole process starts again with the association phase, dissociation phase and regeneration with a new medium.

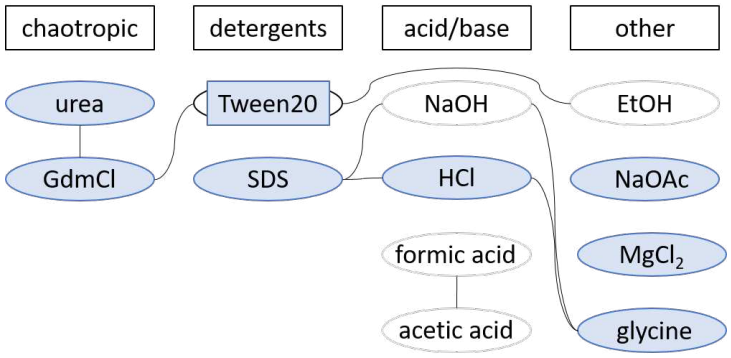


**Figure 3.11:** Overview on the tested combinations of classical regeneration compounds. Blue highlighted compounds were tested in single and repeated regeneration steps.

With classical regeneration media, no full regeneration is reached. Thus, a cocktail strategy, developed by Andersson et al., is tested as second strategy [139]. The cocktails are grouped into acidic (A), basic (B), chaotropic (C), detergent (D), ionic (I) and non-polar water soluble (U) compounds. The specific ingredients of all cocktails is given in Table 4.6. For measurements with only one cocktail, the cocktail is diluted 1:2 using milliQ water. Further binary mixtures of cocktails are all prepared with equal parts of the two cocktials and milliQ water, e.g. the mixture of BDw consists of one part cocktail B, one part cocktail D and one part milliQ water.

**Kinetic Evaluation**

The binding affinity and kinetic of drugs/inhibitors (I) interacting with enzymes/proteins (P) are described by the mass law of action (Equation 4). A logistic curve of the signal recording the interaction plotted logarithmically against the related protein concentration is evaluated as dose-response curve, see Figure 4.7 B [140, 141]. By the mass law of action, the binding affinity

is defined by the association or dissociation constant ($K_a\,[\mathrm{M}^{-1}]$, $K_d\,[\mathrm{M}]$), see Equation 4.

$$P + I \underset{k_d}{\overset{k_a}{\rightleftarrows}} PI \qquad \Rightarrow \qquad K_a = \frac{[PI]}{[P]\cdot[I]} = \frac{k_a}{k_d} = \frac{1}{K_d} \tag{4}$$

In RIfS, the protein as sample is flushed over the sensor. These flow conditions lead to a pseudo-first order kinetics, with the observable rate constant $k_{obs}$.

$$\Gamma(t) = \Gamma(eq)\cdot(1 - e^{-k_{obs}\cdot t}) \tag{5}$$

In Equation 5, the amount of bound protein, interacting with inhibiors on the sensor surface (surface loading at a specific time, $\Gamma(t)$) is defined as the surface loading at the equilibrium ($\Gamma(eq)$) of the association and dissociation rate constants $k_a$ and $k_d$ and an exponential term of $k_{obs}$ [119, 123, 124]. For the evaluation of the kinetic data, without consideration of the mass transport limitations, the curved part of the association phase of a sensorgram is fittet according Equation 5, see Figure 4.8 A. While $k_{obs}$ is defined by $k_a$ and $k_d$, see Equation 6, the kinetic rate constants are calculated via a linear fit of $k_{obs}$ versus the related protein concentration $[P]$, see Figure 4.8 B.

$$k_{obs} = k_a \cdot [P] + k_d \tag{6}$$

### 3.2.6 Surface Analysis

**Table 3.12:** Hard- and software used for MALDI-TOF-MS, ATR-IR and Raman microscopy.

| | |
|---|---|
| ultrafleXtreme | Bruker, Billerica, Massachusetts-USA |
| target plate MTP 384 ground steel | Bruker, Billerica, Massachusetts-USA |
| VIP WSO Adapter ground steel | Bruker, Billerica, Massachusetts-USA |
| ITO slide glass sample plates | Bruker, Billerica, Massachusetts-USA |
| flexControl 3.4 | Bruker, Billerica, Massachusetts-USA |
| flexAnalysis 3.4 | Bruker, Billerica, Massachusetts-USA |
| mMass 3.0 | Open Source Mass Spectrometry Tool, Martin Strohalm |
| Cary 630 FTIR Spectrometer | Agilent Technologies, Santa Clara, California-USA |
| MicroLab FTIR Software | Agilent Technologies, Santa Clara, California-USA |
| LabRam HR | Horiba Scientific, Palaiseau-France |
| SabSpec 6 | Horiba Scientific, Palaiseau-France |

**RIfS Transducer Preparation for Surface Analysis**

Surface analysis of the transducers, is performed after RIfS analysis of kinases, but the measurement protocol is stopped at different steps: after the dissociation or after the regeneration phase, compare Figure 3.9. The region of the transducer, where the kinase, (FAK or the protein mix 20 µg/mL, each) and the regeneration media (trypsin-EDTA and/or GdmCl) had contact to the transducer surface is marked manually by scratching on the backside of the transducer),

and the transducer is stored at 4°C until further analysis.

**MALDI-TOF-MS Measurements**

MALDI-TOF-MS measurements are performed at the working group of Prof. Martina Marchetti-Deschmann at the Institute of Chemical Technologies and Analytics, TU Wien.

### Sample Preparation on Standard MALDI Target Plate

1 µL of a 0.1 mg/mL or 1 mg/mL-solution of FAK in TRIS or a 1 µg/mL-solution of STP in TRIS is dropped in a spot on the standard target plate and dried at ambient temperature. Afterwards, 1 µL of the matrix, sinapinic acid (SA), 7 mg/mL in 30% acetonitrile and 70% trifluoroacetic acid (0.1%) (SA7), is dropped on the spot and dried. Finally, the plate is inserted into the MALDI-TOF instrument for analysis.

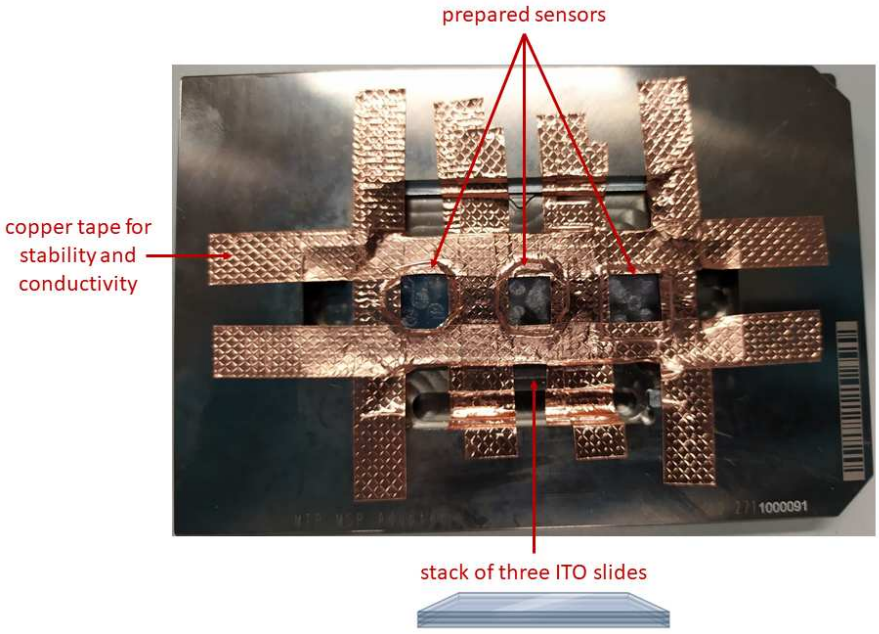


**Figure 3.12:** Photograph of the target plate constructed in-house for the MALDI-TOF-MS investigation of the transducer surface. The basis target plate is an adapter onto which a stack of three ITO slides is mounted. On top of these slides, three transducers are layed side by side and fixed with conductive copper tape.

### Sample and Target Preparation for MALDI-TOF-MS Investigation of the Transducer Surface

RIfS transducers, that are only modified with AMD or AMD and STP, as well as the transducers previously used in RIfS with kinases being flushed over the surface, are handled similar to the standard target plate. A droplet of 5 µL of a 0.1 mg/mL-FAK solution is placed on an AMD- or AMD-STP-transducer and dried. Approximately 3 µL of the SA7 solution is then dropped directly onto the dried sample on the transducer and the sample is dried. This dried-droplet method was repeated three times: This method is named d-d3 in the following. In order to measure STP as a sample, AMD-transducers void of STP are used. 5 µL of a 1 µg/mL-solution

of STP are dropped onto the transducer surface, followed by the method d-d3 after the sample droplet has dried.
To ensure enough conductivity on the transducers during the measurements for MALDI-TOF-MS analysis, RIfS transducers are placed on the target on a stack of three ITO glass slides and then mounted on an adapter constructed in-house, see Figure 3.12. Three transducers are layed side by side on top of this construction. The construct is then fixed with conducting copper adhesive tape, to assure enough stability and conductivity.

**Tryptic Digestion**
0.6 µL of a 30 µM FAK solution on an AMD-STP-transducer is dried and then tryptically digested at 37°C over night. The droplet with the digest solution is then dried and matrix is added using the method d-d3. The transducer is attached to the target construct and introduced into the MALDI-TOF-MS. For reference, a self-digestion of trypsin and a digestion of the same amount of FAK as on the transducer, are prepared in solution and also incubated at 37°C on a vibrating table at 300 rpm over night. Both blanks are dropped on the standard target plate (1 µL), dried and overlaid with 1 µL of SA7 as matrix.

**MALDI-MS Measurements**
MALDI-TOF-MS-measurements are performed in a reflectron mode. The characteristics depend on the sample: For FAK, the mass range is 30000-36000 m/z and a laser power of 90-100%. The reference masses cover a range of 24-66 kDa. For STP, the mass range is 300-600 m/z with a laser power of 50%. The reference masses cover a range of 300-590 Da. Every measurement includes 2000 laser shots with a frequence of 2 kHz, and the spectra are summarized over 16000 shots.

**ATR-IR Measurements**
Attenuated total reflection-Fourier transform infrared spectroscopy is conducted by Leon Biesterfeld, a member of the working group of Prof. Jannika Lauth, Eberhard Karls Universität Tübingen, at the Leibniz Universität Hannover.
The transducers are placed on the ATR crystal and data recorded in the wavenumber range of 650-400 $cm^{-1}$. Between each measurement, the measuring tip is cleaned with isopropanol and dried with compressed air.

**Raman Microscopy**
Raman microscopy on RIfS transducers is performed by Prof. Natalia Ivleva at the Technische Universität München. Laser light is irradiated on the transducers at 785 nm with a laser filter of 100%. The spectra are recorded with an acquisition time of 10 s and 50 accumulations via an objective with 100x augmentation.

### 3.2.7 Magnetic Nanoparticles

**Table 3.13:** Hard- and software used for the analysis of the kinase after extraction with magnetic nanoparticles.

| | |
|---|---|
| Cary Eclipse Fluorescence Spectrometer | Agilent Technologies, Santa Clara, California-USA |
| Cary Eclipse WinFLR 1.1 (132) | Agilent Technologies, Santa Clara, California-USA |
| SuperMag Multitube Separator | Ocean NanoTech, San Diego, California-USA |

#### Coating of Magnetic Nanoparticles

The dextran-coating of commercial magnetic nanoparticles (see Table 3.1) is modified to create a surface comparable to the senors, see Section 3.2.3. The activation of the particles follows the protocol by the vendor: 500 µL of the particle stock solution are mixed with 0.8 mg EDC and 1.6 mg NHS in 125 µL MES buffer for 45 minutes on a vibrating table with 400 rpm at ambient temperature. The particles are magnetically separated from the solution and washed three times with PBS buffer. After activation, the particles are resuspended in 115 µL PBS and 35 µL of STP solution in DMSO (1 mg/mL) and the mixture is incubated for three hours at 400 rpm on a vibrating table at ambient temperature, see Figure 3.13. Again, the particles are separated magnetically and washed with PBS buffer three times. Finally, the magnetic nanoparticles coated with STP (NP-STP) are resuspended in 200 µL PBS and stored at 4°C.

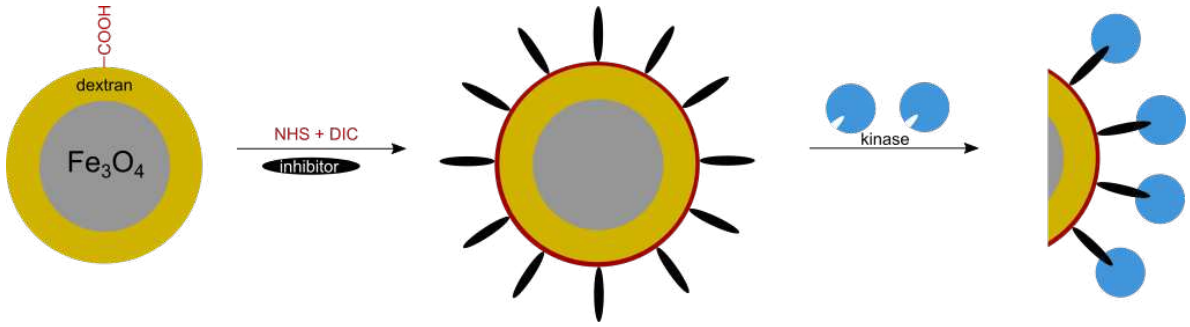


**Figure 3.13:** Surface modification of the magnetic nanoparticles, functionalized with carboxylic acids on a coating layer made of dextran. The refunctionalization with NHS and EDC and subsequent covalent binding of the inhibitor via its amino group is similar to the transducer modification presented in Figure 3.3. As last step, the binding of kinases to the immobilized inhibitor is displayed.

#### Selective Extraction of Kinases from Aqueous Solutions using Magnetic Nanoparticles with Immobilized Inhibitors

For measurements of the protein fluorescence, which arises from its tryptophan moieties, the total volume used for each measurement is 600 µL in TRIS buffer. FAK with a stock solution of 1 mg/mL is incubated with NP-STP particles at a volume ratio of 1:10 (FAK:NP-STP), interacting with the inhibitor on the surface, see Figure 3.13. After 15 minutes of incubation at 400 rpm at ambient temperature, the particles are separated magnetically, as shown in Figure 3.14, and the supernatant is analyzed for fluorescence at 345 nm. The residue is resuspended in a solution of GdmCl (6 M) as regeneration medium and incubated for 15 minutes, 400 rpm

at ambient temperature. The particles are removed with a magnet and the fluorescence of the supernatant is measured.

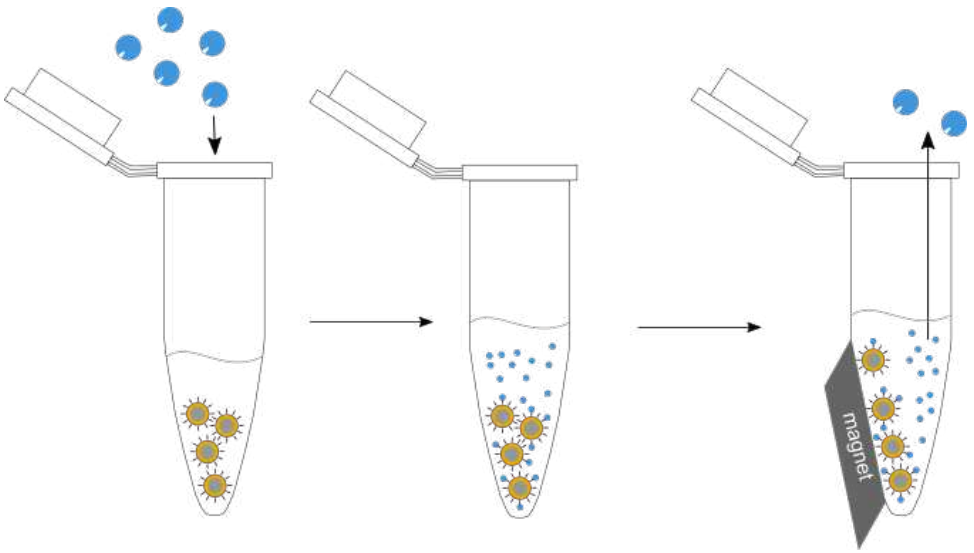


**Figure 3.14:** Sktech of the kinase extraction protocol in solution with modified magnetic nanoparticles.

"Insanity is doing the same thing over and over again and expecting different results."

Albert Einstein

# 4 Results and Discussion

## 4.1 Docking Simulations: Theoretical Investigation of the Interactionss between the Chosen Model Inhibitors and Protein Kinases

Docking simulations are conducted with various protein kinases and inhibitors. Due to several hits in the pdb-data base for one protein kinase, depending on the underlying crystal structure of the protein, simulations are made with different protein structures and the average of the simulated free binding energies are compared. The amino acid sequence of the protein kinases available for experiments are also considered in the simulations.
In Figure 4.1, an overview over the simulated free binding energies of several inhibitors with the binding pocket of several protein kinase structures is given. The more negative the simulated free binding energy, the stronger are the interactions between receptor and ligand. It is already published, that protein-ligand interactions, simulated with AutoDock Vina, mostly show binding energies between -15 and -3 kcal/mol. This well corroborates the data of this work, see Figure 4.1 and Table 4.1, where most interactions are simulated to -12 to -6 kcal/mol [42, 43]. For data comparison in this work, only the highest binding energy for interactions in the binding pocket is depicted. Not only is there a difference in the energy depending on the inhibitors, but also differences depending on the protein kinase. Clearly, every protein kinase possesses a specific arrangement of the amino acids in the binding pocket, providing perfect interaction possibilities for only a small number or even only one specific inhibitor. Based on the simulations, specific kinase-inhibitor pairings are shown to have stronger interactions than others. Figure 4.1 shows, that fragment1 and fragment2 both show weaker interactions towards the ATP-binding pocket of the protein kinases than STP, imatinib > dasatinib > fasudil.
Analysing the quantitative results of the docking simulations, considering the strongest simulated binding in the ATP-binding pocket, it can be seen, that STP and imatinib have similar binding energies to all kinases investigated. Both inhibitors build the strongest interactions to the proteins' ATP-binding pockets. This finding corroborates literature studies, where STP was found to be a good inhibitor for ATP-binding kinases [19–21, 23, 44, 46]. Cavasotto et al. also showed high binding energies of -8.2 kcal/mol for the interaction of the catalytic subunit of PKA with STP, as in this thesis the binding energies of -8.6 kcal/mol are calculated.
Imatinib, which is approved as a drug to inhibit the enzyme BCR-ABL, was not expected to show only this little selectivity towards other tyrosine- or serin/threonine-kinases, as it can be seen in Figure 4.1. Nevertheless, other studies also showed inhibition of several other kinases by imatinib [2, 26]. Several kinases (ABL1, ABL1 (T351I), CLK1, MAPR8, MAPK10, KIT, LCK), which interact with both STP and imatinib, had $K_d$-values for STP similar to those of imatinib [142]. As seen in Figure 4.1 and also depicted in Table 4.1, interactions of imatinib with all investigated kinases are simulated to have free binding energies between -9.6 and -8.4 kcal/mol. Some of the simulated binding energies are even higher with imatinib than with STP, see Table 4.1, however, the differences in binding energies between the inhibitors STP and imatinib to all investigated kinases were not significant.

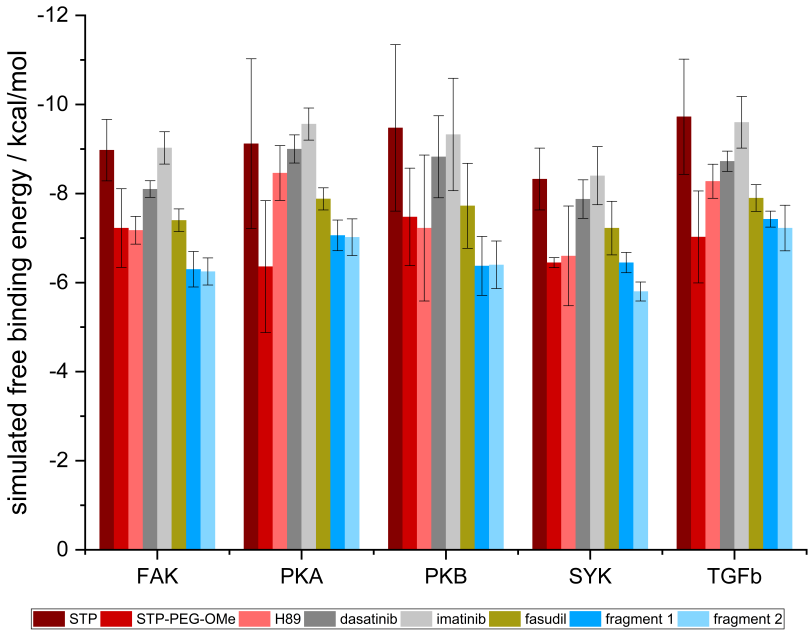


**Figure 4.1:** The simulated free binding energies of various kinase-inhibitor pairs show the specificity of the interaction. All docking simulations are calculated with several protein kinase structures with the inhibitors present in the protein binding pocket. Binding energies between -15 and -3 kcal/mol are common for protein-small molecule simulations with AutoDock Vina [42, 43].

Dasatinib, also an established drug in similar pharmaceutical application as imatinib [26], shows slightly lower binding energies than imatinib of -8.8 to -8.1 kcal/mol. The two fragments are simulated to lower binding energies than the other inhibitors (-7.4 to -6.3 kcal/mol). This finding is common in literature, where fragments are often found to have lower binding affinities. During the drug development process, suitable fragments are linked together, building an inhibitor with higher binding energies. [143–147]. This could be a reason, why fragment1 and fragment2 are not intensively discussed in literature as molecules of pharmaceutical interest. The two fragments were tested based on promising results in a dissertation [148].

To investigate changes in binding energies, when STP is covalently bound to the transducer surface via a biopolymer linker (see Section 4.3.1), simulations with STP-PEG-OMe are conducted, in addition to the unaltered inhibitors. The simulated binding energies for STP-PEG-OMe are lowered to 64-84% of those of free STP, depending on the kinase investigated, compare also Table 4.1. This provides evidence that the linker impairs the interaction with the protein as the orientation of the molecule in the binding pocket might be hindered. These results are the first indication that modifications of the small molecule, e.g. labeling, influences the interactions with the protein. Thus, a decreased interaction between STP, that is covalently bound to the transducer surface, and the kinases investigated can be presumed.

Since all previous discussed results are from simulations in the ATP-binding pocket of the kinases, by widening the simulation range, interactions of inhibitors with the whole protein are conducted as well, showing strong interactions outside the binding pocket. In nearly all combinations of proteins and inhibitors, the two conformations with highest binding energies are located in the binding pocket. Further conformations are often found for non-specific interaction

sites with free binding energies of 84 up to 95% of the simulated affinities in the ATP-binding pocket. In Figure 4.2, the simulation of the nine strongest binding modes are shown exemplarily for STP as ligand simulated with the FAK fragment which is used in the experimental part of this work. These docking simulations show, that non-specific interactions are likely, even though the two highest affinities are found in the ATP-binding pocket.

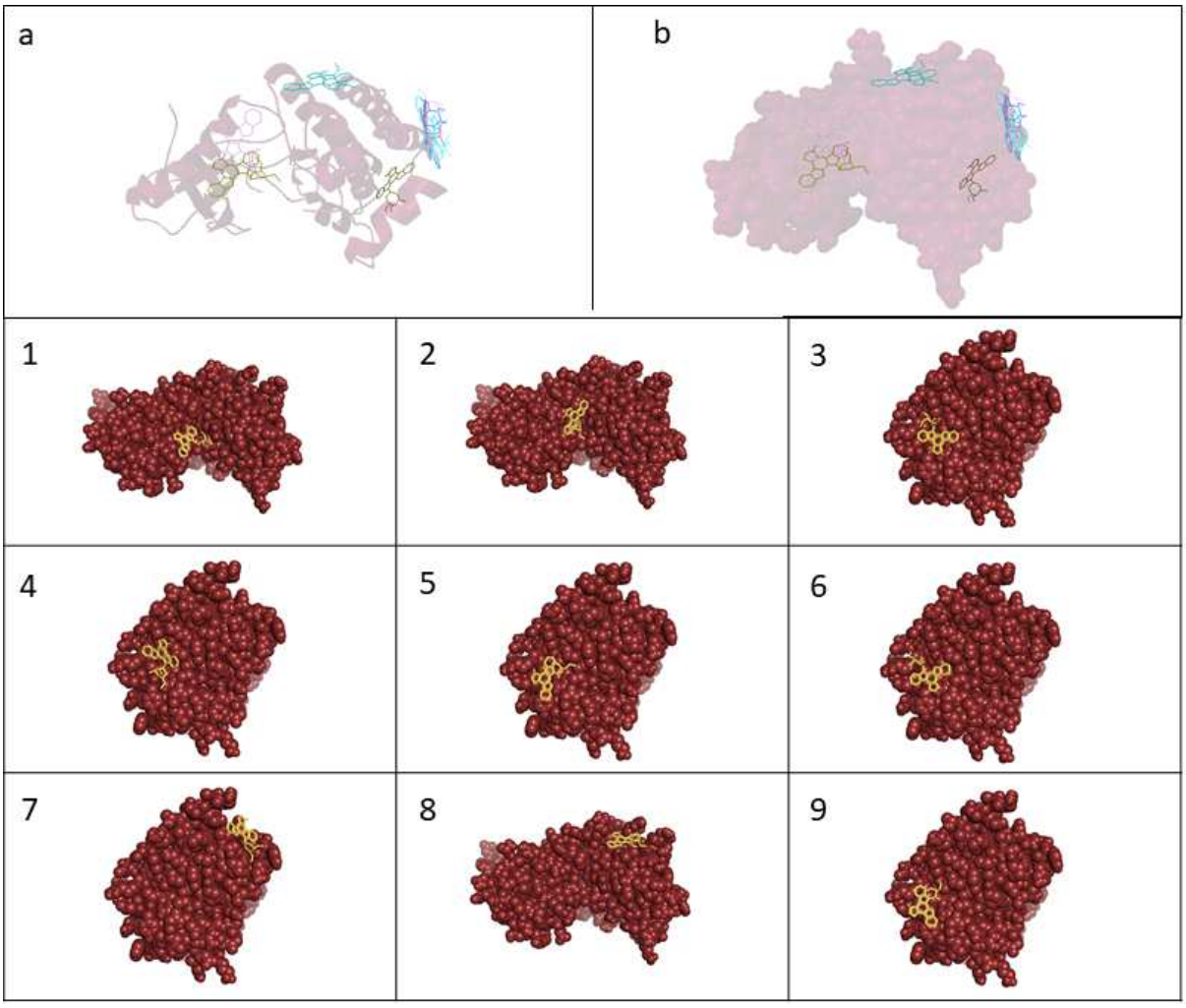


**Figure 4.2:** The output of the docking simulation of STP with the FAK fragment is shown: a and b: all nine simulated STP positions on FAK, 1-9: simulated STP positions are shown separately, sorted from high to lower binding strength, 1: -8.1 kcal/mol, 2: -7.4 kcal/mol, 3: -7.2 kcal/mol, 4: -7.1 kcal/mol, 5: -7.1 kcal/mol, 6: -7.1 kcal/mol, 7: -6.9 kcal/mol, 8: -6.9 kcal/mol, 9: -6.8 kcal/mol. The structures in 3-7 and 9 are rotated clockwise by 90° along a vertical axis for better visualization.

**Table 4.1:** All simulated free binding energies for the strongest interaction between different inhibitors and protein kinases simulated over the full protein and in the binding pocket, see adjustments for the GridBox in Section 3.2.1. For most protein kinase inhibitor pairs, the strongest binding of the whole protein lays in the binding pocket. Simulations of the inhibitors interacting only in the SYK binding pocket were not conducted.

| **Inhibitor** | **Protein Kinase** | **Simulated Free Binding Energy [kcal/mol]** | |
|---|---|---|---|
| | | full protein | in binding pocket |
| dasatinib | FAK | -7.9 | -8.1 |
| | PKA | -8.7 | -8.2 |
| | PKB | -8.8 | -8.8 |
| | TGF$\beta$ | -8.6 | -8.7 |
| | SYK | -7.9 | |
| fasudil | FAK | -7.4 | -7.4 |
| | PKA | -7.3 | -7.2 |
| | PKB | -7.4 | -7.4 |
| | TGF$\beta$ | -7.9 | -7.9 |
| | SYK | -7.2 | |
| fragment1 | FAK | -6.4 | -6.3 |
| | PKA | -6.8 | -6.6 |
| | PKB | -6.4 | -6.4 |
| | TGF$\beta$ | -7.4 | -7.4 |
| | SYK | -6.5 | |
| fragment2 | FAK | -6.4 | -6.3 |
| | PKA | -6.7 | -6.6 |
| | PKB | -6.2 | -6.4 |
| | TGF$\beta$ | -6.4 | -7.2 |
| | SYK | -5.8 | |
| H89 | FAK | -6.9 | -7.2 |
| | PKA | -7.5 | -7.6 |
| | PKB | -7.1 | -7.2 |
| | TGF$\beta$ | -8.1 | -8.3 |
| | SYK | -6.6 | |
| imatinib | FAK | -8.0 | -9.0 |
| | PKA | -8.6 | -8.4 |
| | PKB | -8.3 | -9.3 |
| | TGF$\beta$ | -9.4 | -9.6 |
| | SYK | -8.4 | |
| STP | FAK | -8.9 | -8.6 |
| | PKA | -9.1 | -8.6 |
| | PKB | -9.1 | -9.5 |
| | TGF$\beta$ | -11.0 | -9.7 |
| | SYK | -8.4 | |
| STP-4PEG-OH | FAK | -7.2 | -7.2 |
| | PKA | -7.3 | -5.5 |
| | PKB | -7.5 | -7.5 |
| | TGF$\beta$ | -8.3 | -7.0 |
| | SYK | -6.5 | |

## 4.2 Microscale Thermophoresis: Experimental Confirmation of Simulations

Results of the docking simulation in Section 4.1 are compared to MST measurements. Using labelled STP (STP-Red) fluorescence detection, direct and competitive assays are performed. In the direct assay, the concentration of STP-Red is held constant while protein kinases are titrated.
Because the MO.Control Software automatically chooses the set point for evaluation depending on a quality check based on the S/N ratio, the evaluation of every experiment slightly differs. The set point influences the output of the evaluation, in extreme cases by changing the direction of the dose-response curve. Therefore, the set point is defined manually for all experiments, regardless of the quality check. For all evaluations, the set point is defined at 2 seconds after the laser was turned on. Measurements in specific capillaries are rated to be outliers, if there is a visible inconsistency of the initial fluorescence signal, which is given by the MO.Control Software for every capillary. The evaluation is conducted using the software origin. The sigmoidal dependency of the dose-response curve directly reveals the $IC_{50}$-value as the inflection point. Using the concentration of STP-Red in the assay and the $IC_{50}$-value, the $K_d$-value can be calculated by a modulation of the Cheng-Prusoff relationship, shown in Equation 7, where the $IC_{50}$-value is higher than or equal to the $K_d$-value [149, 150].

$$K_d = IC_{50} - \frac{c(STP - Red)}{2} \tag{7}$$

Depending on the small amount of STP-Red required for the assays, there is no sufficient difference comparing the two thermodynamic values, as can be seen in Table 4.2.

Clearly, STP-Red interacts with different protein kinases, which are all described as ATP-competitive. All kinases investigated (FAK, PKA, PKB, protein mix, TGF$\beta$) strongly interact with STP-Red, resulting in evaluable fluorescence signals. By increasing the concentration of the kinase, the fluorescence signal decreases faster. From capillary 1 to 16, which are inserted in the Monolith NT.115, the concentration of kinase is reduced by a factor of 2 in every capillary. Exemplarily, the fluorescence signal of all 16 capillaries is shown in Figure 4.3, A. STP-Red molecules that interact with the kinases in the protein mix as target, are thus involved in a complex with a larger size. Therefore, their Brownian motion changes, which influences the increase of the fluorescence signal after the laser of the MST investigation was turned on. In Figure 4.3 A, an increase of the fluorescence signal with decreasing concentration of protein mix (from capillary 1 to 16) is shown, which indicates an interaction between STP-Red an the protein mix. Similar behavior is recorded for the other kinases.
$K_d$-values of the direct MST measurements with STP-Red and different kinases, which are calculated via the $IC_{50}$-values, defined as the turning point in the dose-response curve in Figure 4.3 B, are shown in Table 4.2. All values are in the same order of magnitude (606 nM -1.27 µM $K_d$), indicating similar interactions between the different kinases and STP-Red. This well

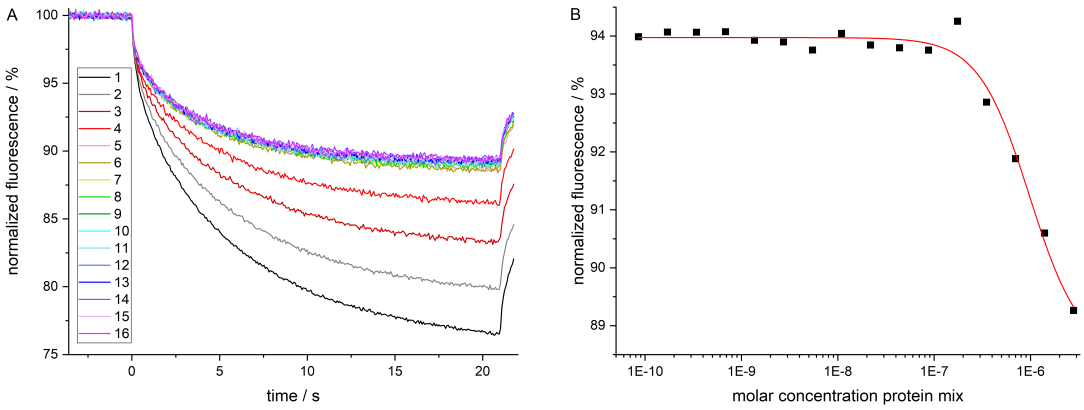


**Figure 4.3:** A: Fluorescence curves of the MST measurements of STP-Red as labelled compound in interaction with the protein mix. Capillary 1 is with the highest protein concentration, which is halfed every next capillary. B: Dose-response curve of the MST measurements of STP-Red as labelled compound in interaction with the protein mix. The coefficient of determination is 0.981. More information on these graphs is given in Section 3.2.2.

corroborates the findings from the docking simulations in Section 4.1, where similar binding energies of the kinases to STP are simulated (-8.6 to -9.7 kcal/mol): As the binding energy and the dissociation constants are connected in the Van't Hoff equation (Equation 8). A stronger binding ($\Delta_b$G more negative) is found for higher $K_a$ and smaller $K_d$-values.

$$\Delta_b G = -RT \cdot ln(K_A) = RT \cdot ln(K_d) \tag{8}$$

**Table 4.2:** Dissociation constants calculated by MST measurements with STP-Red as fluorophore at constant concentration and different protein kinases titrated using 16 different capillaries. The $K_d$-values are evaluated by the $IC_{50}$-values of the dose-response curves (Equation 7) and the concentration of the STP-Red in each assay of 40 nM.

| **Protein Kinase** | $IC_{50}$ | $K_d$ |
|---|---|---|
| FAK | 802 nM | 796 nM |
| PKA | 626 nM | 606 nM |
| PKB (AKT1) | 1.28 µM | 1.27 µM |
| protein mix | 793 nM | 788 nM |
| TGF$\beta$ | 820 nM | 800 nM |

To not only illustrate the direct interactions with protein kinases and STP, additional competitive displacement assays are conducted. For this, STP-Red and the kinase concentration are held constant, forming an STP-Red/kinase-complex. Then, the complex is titrated with free inhibitors BisX, fasudil and imatinib to replace STP-Red from the kinase releasing the complex. Different concentration ratios to STP-Red are tested, with the concentration of free inhibitor at 4 orders of magnitude higher than STP-Red at maximum and one order of magnitude lower than STP-Red at minimum. In theory, the dose-response curves should be reversed in their direction compared to one of the direct assay, if the unlabeled free inhibitors interact

with the kinase competitive to STP-Red, displacing the fluorescent STP-Red molecules from the protein, see Figures 4.4 A and B. This was observed for BisX, where the increase of the BisX concentration decreases the fluorescence signal. However, titrating fasudil or imatinib to the STP-Red/kinase-complex, Figure 4.4 C and D, the contrary is observed: With increasing concentration of the free inhibitor, the fluorescence signal increases, reversing the slope of the dose-response.

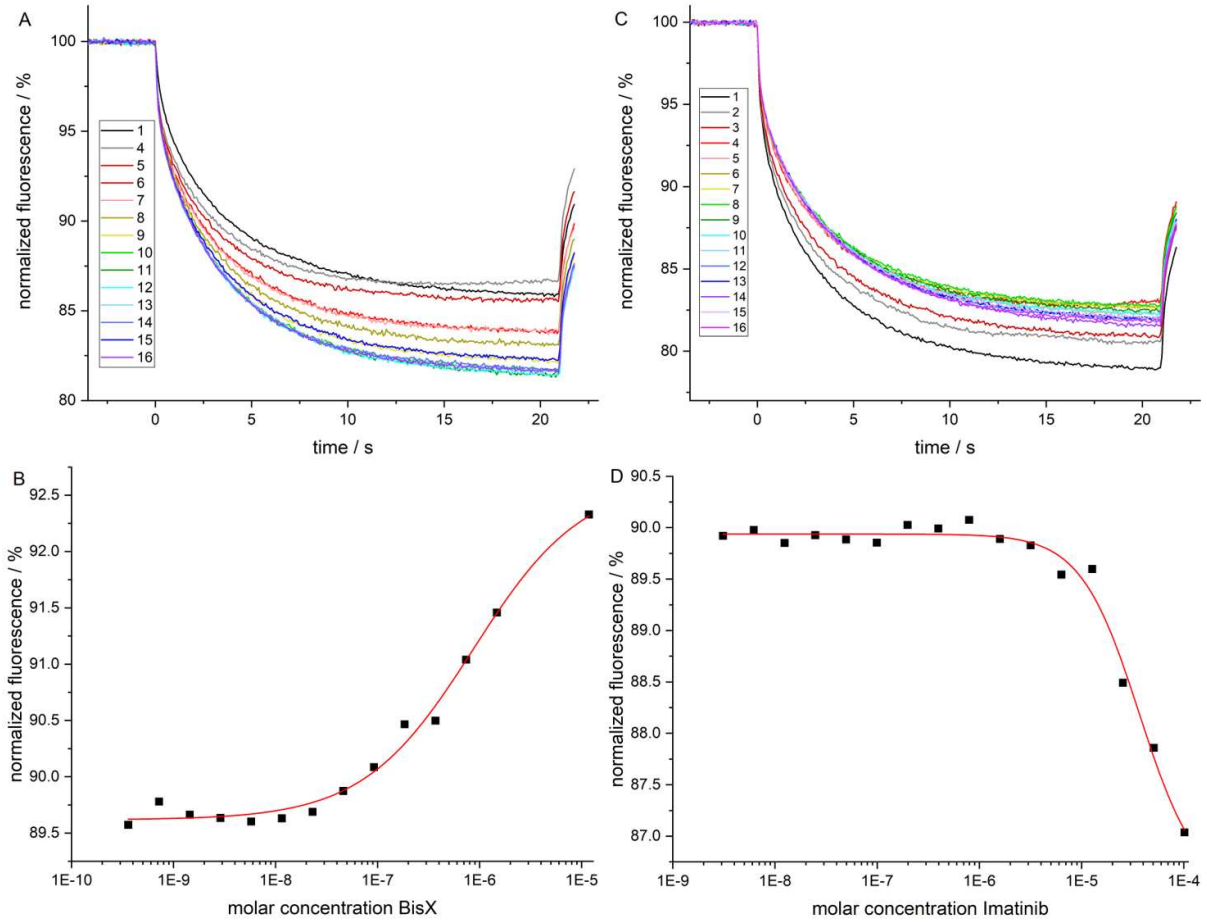


**Figure 4.4:** Results of the competitive MST measurements with fluorescent STP-Red and FAK in a complex at a constant concentration (STP 40 nM, FAK 40 µM). Competitive inhibitors are titrated. The fluorescence is normalized to the origin fluorescence of each capillary prior to the measurements. A: fluorescence signal with BisX as free inhibitor, B: corresponding dose-response curve with a coefficient of determination of 0.990, C: fluorescence signal with imatinib as free inhibitor, D: corresponding dose-response curve with a coefficient of determination of 0.985.

Due to the measurement setup and evaluation mode of MST, the direction of the dose-response curve cannot provide information about the affinity between the inhibitors and kinases. Specific assay conditions such as pH-value, type of formed complex or additives also influence the fluorescence. For instance, measurements in buffer and cell lysate may show different slopes of the dose-response curves. Measurements with different fluorescence labels and the detection of initial tryptophan fluorescence of the protein, or autocompetition with unlabeled compounds can also influence the slope of the dose-response curves [109] [151, 152]. No dependence of the curve by single or multiple binding towards the protein was found in other studies, which could

be another explanation for the shapes in the fluorescence signal is given [151]:
The structure of BisX is highly similar to STP, see Figure 3.4, so it is expected to be more competitive to the STP-binding sites of the kinases than fasudil or imatinib. In the MST measurements BisX replaces STP-Red upon increasing its concentration, resulting in a disruption of the STP-Red/kinase-complex. This release of STP-Red initiates the opposite effect of the fluorescence signal, compared to the direct assay. Fasudil and imatinib have different molecular structures compared to STP and can therefore be expected to interact with the kinase in different regions and likely in addition to STP-Red. With increasing concentration of fasudil or imatinib, the STP-Red/kinase-complex will thus further increase in mass. This effect is comparable to the formation of the STP-Red/kinase-complex in the direct assay and similar dose-response curves as in the direct assays are observed. This holds true for all three proteins tested: FAK, PKA and TGF$\beta$.

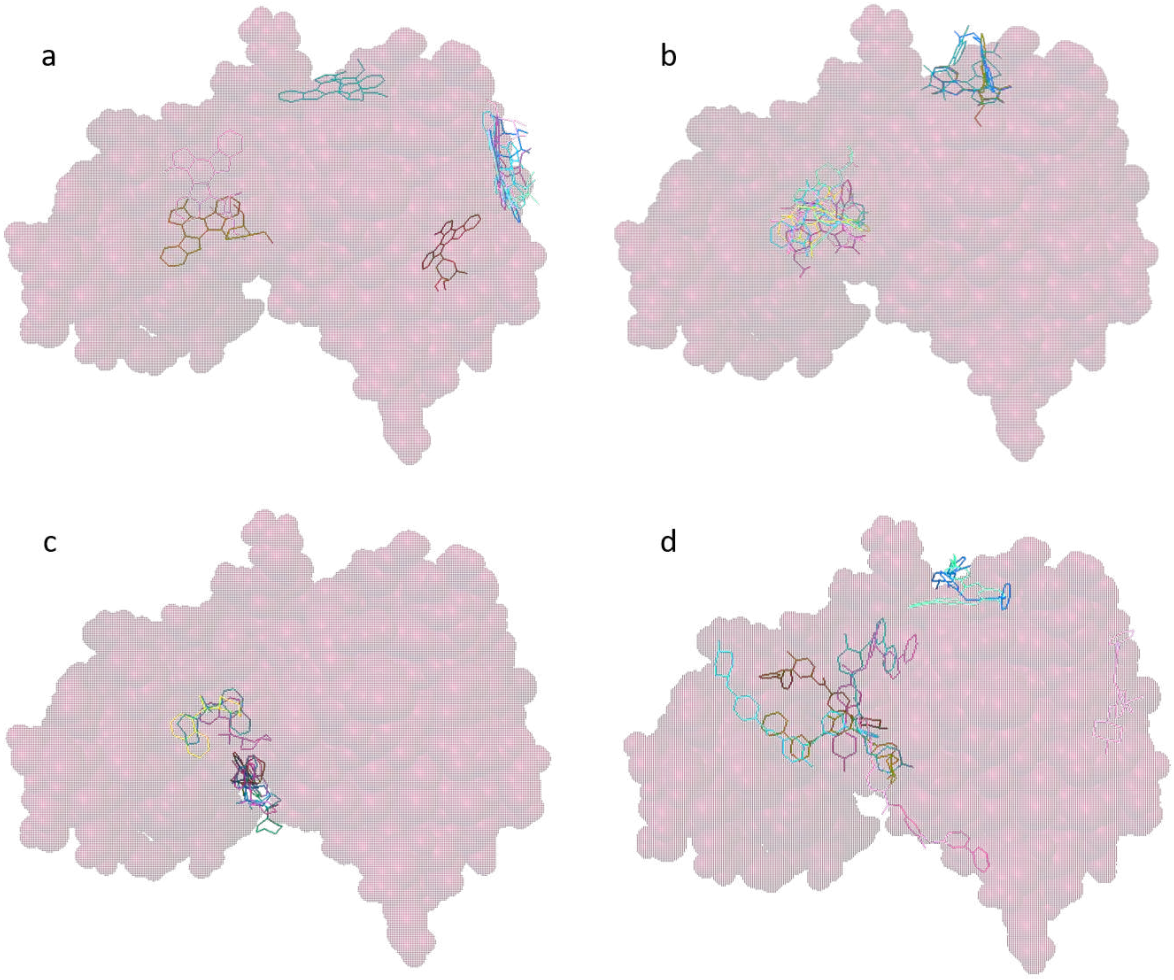


**Figure 4.5:** Structure of the FAK fragment in spheres, after docking simulations with different inhibitors, as already shown for STP-Red interacting with FAK in Figure 4.2 b. The nine interactions sites of the inhibitors with the highest binding energy of each complex are depicted in each panel. a: STP - b: BisX - c: fasudil - d: imatinib.

This hypothesis is confirmed by comparison with the results of the docking simulations for

these four inhibitors with FAK. Considering the nine binding sites, shown in Figure 4.5, with the highest simulated binding energies of BisX to FAK (Figure 4.5 b) only two regions of the kinase are occupied. These are two regions, that are also involved in the interaction with STP, see Figure 4.5 a. During the MST analysis, STP-Red first becomes complexed by the kinase and may become replaced by BisX, fasudil or imatinib when added at different concentrations. If the free inhibitor had the same binding sites as STP-Red on FAK, a competitive displacement assay would be present. This is true for BisX being in contact with FAK replacing STP-Red in the complex. STP-Red is then present in the solution in its uncomplexed free form. However, the other inhibitors are likely to occupy different binding sites on the kinase, compared to those specific for STP, which can be expected by the Figures 4.5 c and d. This holds true for the docking simulations of fasudil and imatinib interacting with FAK.
This hypothesis however, is not in accordance with literature or supporting information provided by nanotemper [109, 151, 152], but well supported by the data and well explaining the differences in the slopes of the dose-response curves obtained by MST in this study, where in constant assay conditions (pH value, additives), only the inhibitor did change.
An advantage of the competitive assays over the direct assays is the detection of the kinases interacting with unlabeled inhibitors, which reduces influences on the binding characteristics as already discussed in Section 2.

As in the competitive assays, the concentration of the kinase is held constant, the $K_d$-values are equal to the $IC_{50}$-values. The results of the competitive assay are iven in Table 4.3. It can be seen, that the constants describing the affinity, $K_d$ and $IC_{50}$, differ dependent on the ratio STP-Red:kinase as well as on the inhibitor added. For fasudil and imatinib, the thermodynamic values are higher than the ones for BisX, while imatinib more stongly binds to the kinases than fasudil.

**Table 4.3:** Dissociation constants calculated from MST measurements with STP-Red and different protein kinases in competitive assays titrating the inhibitors BisX, fasudil or imatinib. The $K_d$-values are equal to the $IC_{50}$-values of the dose-responce curves due to the low concentration of the kinase in each assay, see Equation 7. Fasudil and imatinib were not tested against all ratios of STP-Red to the protein kinases.

| **Protein Kinase** | **Ratio STP-Red:Kinase** | $K_d = IC_{50}$ | | |
|---|---|---|---|---|
| | | BisX | fasudil | imatinib |
| FAK | 1:1 | 860 nM | 125 µM | 32 µM |
| FAK | 1:2 | 43 µM | | |
| PKA | 1:2 | 46 µM | 202 µM | 42 µM |
| TGF$\beta$ | 1:2 | 3 µM | 48 µM | 27 µM |
| TGF$\beta$ | 1:22 | 544 nM | | |

Different $K_d$-values for the same kinase-inhibitor pairs at different ratios of STP-Red to kinases show, that the thermodynamic of the interaction not only depends on the inhibitor chosen, but also on the concentration of the kinase used in each assay. This shows, that a fair comparison

of affinity constants to published data is difficult.

There is a lack of published affinity data for the protein kinase-inhibitor pairs investigated here. Available data from literature are given in Table 4.4. The comparison reveals, that MST investigations in this work result in higher thermodynamic values than those published, differing by up to two orders of magnitude. Differences can, however, be expected with regard to different assay types, analytical methods and data evaluation. Furthermore, the MST data are created with labeled STP, which might further change affinities.

The comparison of the data in Table 4.4 with the results of the theoretical docking simulations as well as the experimental investigations with MST show, that interactions of the protein kinase-inhibitor pairs, can be expected to be sufficient for a further development of RIfS assay.

**Table 4.4:** Affinity data of different protein kinases and inhibitors evaluated by MST and compared to literature data.

| **Protein Kinase** | **MST** | **Literature** | | | |
|---|---|---|---|---|---|
| | $K_d/IC_{50}$ | $K_d$ | $IC_{50}$ | **Assay Type** | **Source** |
| | | **fasudil** | | | |
| PKA | 202 µM | 5.7 µM | | SPR | [153] |
| | | **STP** | | | |
| FAK | 796 nM/802 nM | 10-100 nM | | fluorescence microscopy in cells | [154] |
| PKA | 606 nM/626 nM | 8.2 nM<br>2 nM<br>5 nM | <br>1.2 nM<br>15 nM | enzyme assay<br>enzyme assay<br>phosphorylation assay | [46]<br>[44]<br>[45] |
| TGF$\beta$ | 800 nM/820 nM | 50 nM (TGF$\alpha$) | | labeled to RNA, hybridization in cells | [155] |
| | | **various inhibitors** | | | |
| FAK | | 0.07 nM-20 µM | 0.6-50 nM | Review | [156–158] |
| PKA | | 2 nM-500 µM | | phosphotransferase assay | [159, 160] |

## 4.3 Sensor Measurements: Transfer from Simulated and Experimentally Proven Systems to New Methods for Kinase and Inhibitor Screening

### 4.3.1 Direct Assays

Direct assays on a RIfS transducer are the first step in the development of a sensor method to perform binding inhibition assays as well as kinase and inhibitor screening. In pre-tests a transducer with AMD immobilized as biopolymer performed better than PEG surfaces. The biopolymer layer not only increased the distance between the glass substrate and the inhibitor covalently bound to the biopolymer, creating a higher flexibility for sterically hindered interactions with larger binding partners, but also best prevented any non-specific binding of the protein to the sensor surface. Tests with ovalbumin, human and bovine serum albumin on an AMD-transducer as well as on an AMD-STP-transducer did not reveal any changes in optical thickness, see Figure 4.6. This proves, that the AMD-layer is effective in preventing non-specific binding of proteins and also non-specific binding to STP bound to the transducer.

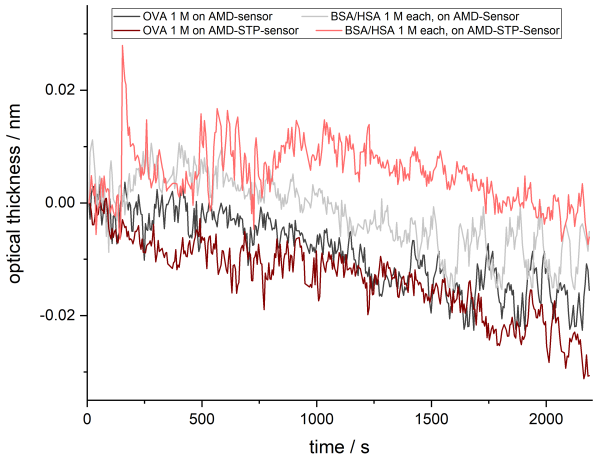


**Figure 4.6:** Diverse proteins (ovalbumin (OVA), human serum albumin (HSA), bovine serum albumin (BSA)), are each measured in a concentration of 1 M in RIfS using an AMD-transducer and an AMD-STP-transducer. The lack of changes in optical thickness proofs the prevention of non-specific interactions of possible matrix proteins with the sensor surfaces, see Section 3.2.5.

To calculate kinetic data of the interaction between the protein kinase and the inhibitor which is bound to the sensor surface, a concentration series of a kinase is measured in RIfS. First, interactions between FAK as kinase and STP as inhibitor on the transducer are analyzed, see Section 3.2.5. Except of the highest concentration, the measurements are conducted in triplicates. A clear increase in optical thickness indicates the binding of FAK to the inhibitor, see 4.7 A, however, a high endline reveals insufficient regeneration of the sensor surface. Thus, each measurement is performed on a newly produced transducer. Strategies to overcome the regeneration challenges are discussed in Section 4.3.2. Owing to a certain variability of the surface of the individual transducers, prepared manually, the measured changes in optical thickness slightly differ with a standard deviation between 0.001-0.147 nm. During the dissociation

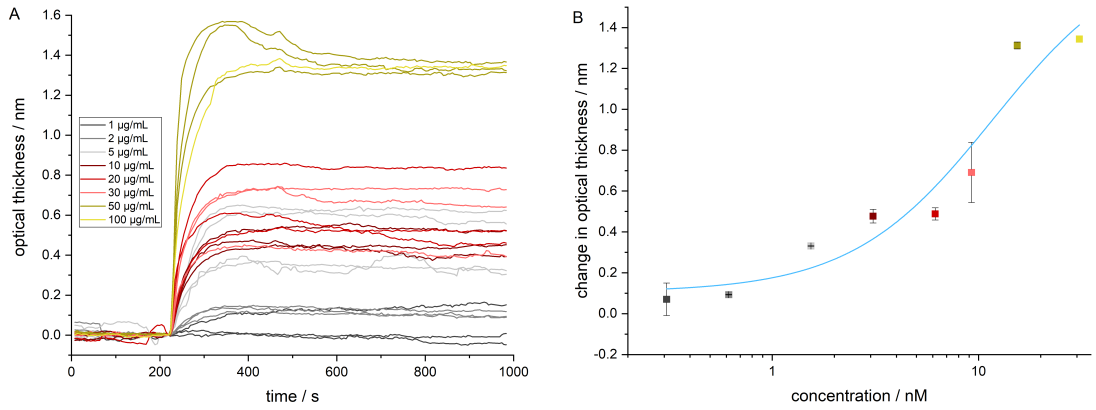


**Figure 4.7:** A: Binding curves of direct assays in RIfS using different FAK concentrations (from 1 µg/mL up to 100 µg/mL) on AMD-STP-transducers. Each measurement is performed on a new transducer. B: Dose-response curve of the RIfS measurements displayed in A. The coefficient of determination is 0.932.

phase, no dissociation of the FAK from the sensor is seen, which would be common for RIfS [119, 123, 124, 161]. Reasons are discussed in Section 4.3.2.

For further kinetic evaluations, the results of triplicate measurements per concentration are averaged and the change in optical thickness is plotted against the concentration in a logarithmic scale to obtain dose-response curves. With a high coefficient of determination of 0.932, the expected sigmoidal dependence is apparent.

A kinetic evaluation of the sensograms is reached following common protocols as described in Section 3.2.5: The curvature of the association phase in the binding curve is fitted exponentially, as described in Section 3.2.5. An example of such a fit is displayed in Figure 4.8 A. By plotting the observable rate constant $k_{obs}$ against the protein concentration, a linear dependency with a coefficient of determination of 0.726 is obtained, see Figure 4.8 B for the association of FAK on an AMD-STP-transducer. The low correlation coefficient can be explained by the fact, that each measurement was performed on a new transducer, reducing the reproducibility. As explained earlier in Section 2, $k_a$ and $k_d$ can be calculated by the observable rate constant $k_{obs}$ and its linear dependency on the protein concentration. In Figure 4.8 B, $k_{obs}$ is displayed for each concentration of FAK. The slope of the linear regression defining $k_a$ is 1.24 $L\ \mu mol^{-1}\ s^{-1}$, the intercept $k_d$ is $2.6{\cdot}10^{-3}\,s^{-1}$. The calculation of the dissociation rate constant would be possible via the intercept here, but error-prone. More precise data could be generated by evaluating the curvature of the dissociation phase in the sensogram [123]. However, for the kinases, no dissociation is observed in RIfS, see Figure 4.7 A. Thus, the dissociation constant $K_d$ is estimated form Figure 4.8 B to 18.19 nM.

$$K_d = \frac{k_d}{k_a} = \frac{0.02256\ s^{-1}}{0.00124\ L\ nmol^{-1}\ s^{-1}} = 18.19\ nM \tag{9}$$

Comparing the values obtained by MST vs. RIfS, a difference of over 1.4 orders of magnitude is present for the dissociation constant $K_d$ for the interaction between STP and FAK: 796 nM (MST) vs 18.2 nM (RIfS), see also Table 4.5. It seems, that the heterogeneous assay on the

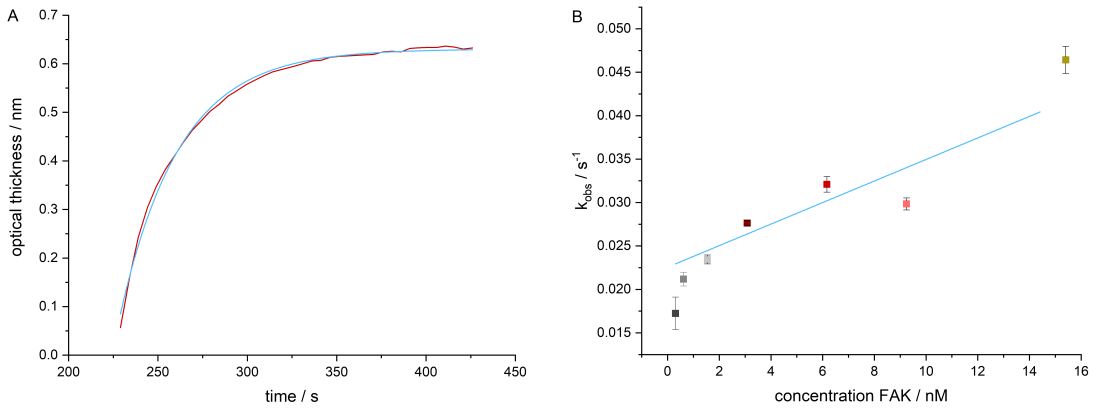


**Figure 4.8:** A: Example of an exponential fit of the curvation of the binding curves in Figure 4.7. The fit is calculated using the average of the triplicate measurements for each protein concentration. B: Linear fit of the observable rate constant $k_{obs}$ from the association and dissociation rate constants. $k_{obs}$ is determined by the exponential data of the curvature in A. The coefficient of determination is 0.726. Kinetic data: $k_a = 1.24\ L\ \mu mol^{-1}\ s^{-1}$, $k_d = 2.5 \cdot 10^{-3}\ s^{-1}$, $K_d = 18.19\ nM$.

sensor results in a stronger interaction of the protein with the inhibitor-loaded surface, than the direct interaction in the homogeneous assay of MST. Regardless of the data compared here from two different measurement methods, more precise data are often evaluated for heterogeneous assays, as homogeneous methods are more susceptible to, for example, matrix effects [162]. The strong interactions are already expected form the lack of a dissociation and the challenges in regeneration. Similar data can be found in already published data, e.g. by Kabir et al. who described $K_d$-values from 10-100 nM evaluated via fluorescence microscopy, even in cells [154].

Similar experiments with direct assays using concentration series were performed with 1-λ reflectometry. Besides the excited light, another difference to RIfS measurements is the output of the data. While RIfS measures the changes in the optical thickness, 1-λ reflectometry records the changes in the intensity of the recorded images. As in RIfS sensograms, in 1-λ reflectometry no dissociation is observed. The kinetic evaluation of the data is the same. Experiments are conducted with the protein mix, consisting of various proteins, including PKA, see Section 3.1. To enable a rough estimation of the binding kinetics, the assumption is made, that all protein in the protein mix is PKA. The transducer of the concentration series of the protein mix is modified with AMD and STP and the analysis of the sensograms reveals thermodynamic $K_d$ values of 20 nM by exponential evaluation. This is well corroborated by diverse studies with autoradiography, enzyme or phosphorylation assays and fluorescence polarization with $K_d$-values between 5 and 44 nM and $IC_{50}$-values between 1.2 and 15 nM [20, 21, 44, 45]. On other transducers, another inhibitor fragment1 is immobilized and a $K_d$-value of 319 nM is determined for the protein mix as titrated analyte. Clearly, the assay developed here is able to determine differences in the kinetic behavior depending on different protein-inhibitor pairings. These results serve as a proof of principle: Kinase screening in the heterogeneous phase is possible, using either RIfS or 1-λ reflectometry.

With the assumption made before, that all proteins in the protein mix are PKA, a comparison to docking simulations and the results is possible. As seen in Table 4.5, the simulated

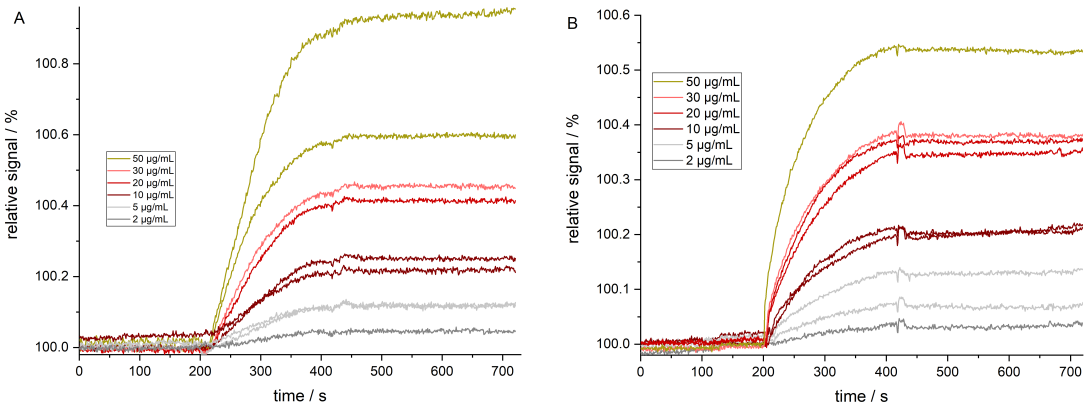


**Figure 4.9:** Binding curves of a direct assay of the protein mix from analyses by 1-λ reflectometry using a new transducer for each measurement, with two different inhibitors immobilized on the transducer surface A: on an AMD-STP-transducer, B: on an AMD-fragment1-transducer, for structures of inhibitors see Figure 3.4. For a better visualization and comparability to RIfS sensograms, the signals of the 1-λ reflectometry are inverted.

binding energies for the system STP-FAK and STP-PKA are similar with -8.9 kcal/mol and -9.1 kcal/mol. Likewise, the $K_d$-values determined by the sensor assays are similar with 18 nM for the system STP-FAK and 20 nM for STP-protein mix. Furthermore, also from examining the corresponding MST measurements, $K_d$-values similar for STP-FAK, STP-PKA and STP-protein mix obtained (796 nM, 606 nM and 788 nM). In contrast, for the systems fragment1-PKA and fragment1-protein mix a weaker binding energy of -6.8 kcal/mol was simulated, well reflected by the higher $K_d$-value of 319 nM, determined with 1-λ reflectometry. Differences between kinase-inhibitor-pairs can be determined by docking simulations, MST and the sensor assays in RIfS and 1-λ reflectometry. Absolute values differ as expected from experimental differences for MST and the biosensor assays.

**Table 4.5:** Dissociation constants determined experimentally by MST and RIfS (in blue) or 1-λ reflectometry (in purple) in direct assays compared to the simulated free binding energies of various inhibitors on the full protein structure, see Table 4.1. Since the protein mix is evaluated, assuming all proteins being PKA, the values are compared directly, data from purified PKA are highlighted in bold.

| **Inhibitor** | **Protein Kinase** | $K_d$ [nM] | | **Simulated Free Binding Energy [kcal/mol]** |
|---|---|---|---|---|
| | | MST | sensors | docking simulation |
| fragment1 | **PKA**, protein mix | | 319 | **-6.8** |
| STP | FAK | 796 | 18 | -8.9 |
| STP | **PKA**, protein mix | **606**, 788 | 20 | **-9.1** |

### 4.3.2 Regeneration

All investigations on the sensors show insufficient regeneration, regardless of the conducted assay and the kinase-inhibitor pair used. Therefore, each measurement requires a new transducer,

which turns RIfS and 1-λ reflectometry into less sustainable methods. A further challenge is the lower reproducibility of measurements, owing to variations of the transducer surfaces introduced by the manual preparation of the transducers. In order to improve the regeneration of the sensors, a large study on regeneration media is conducted.
As described in Section 3.2.5, two different strategies are investigated: first, classical regeneration media known for sensor investigations are tested primarily while second, different cocktails of regeneration media are screened.
The classical regeneration media are composed of chaotropes, detergents, acids or bases, as summarized in in Figure 3.11. Various combinations are investigated. According to Equation 3, the regeneration efficiency is determined, see Figure 4.11.

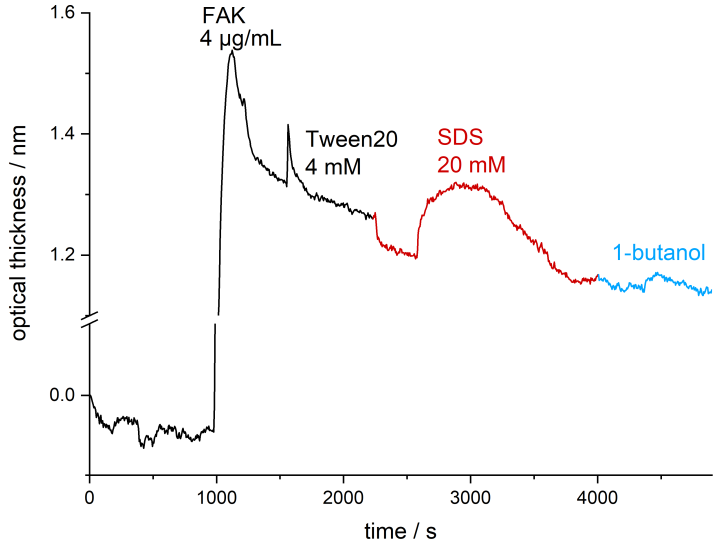


**Figure 4.10:** RIfS sensograms of the regeneration study with micelles. After an association of FAK on the AMD-STP-transducer and a regeneration experiment with Tween20, SDS is flushed over the sensor with the expectation to form mixed micelles with Tween20 [163–167]. By flushing 1-butanol, the micelles are expected to be removed from the sensor surface. The $R_e$ of 14% shows unsuccessful regeneration.

The best regeneration is achieved with a combination of HCl followed by an aqueous solution of SDS, a single regeneration cycle reaches an efficiency of $R_e$=95% in some experiments. In others, however, only 45% regeneration efficiency was reached. Using 5% Tween20, $R_e$-values of 76% are reached consistently. However, the association in a second analysis of kinases on the same sensor shows, that the sensor surface is affected, visible in a lower increase in optical thickness of only 24% of the original association signal. Detergents as regeneration media are expected to disrupt intra- and intermolecular interactions of the protein, while neutral detergents, such as Tween or Triton, are described to be less destructive than ionic detergents, such as SDS [168]. Additional to the expected regeneration characteristics, Tween20 is known to prevent adsorption of proteins such as those present on the sensor [169]. Tween20 or Tween80 are often included in MST measurements to prevent the sorption of the the protein to the capillaries' inner surfaces. Additional washing cycles did not improve the association in further uses of the sensor. So despite acceptable regenerations, Tween20 alone is not further considered

as regeneration medium.
However, Tween 20 is further tried to be removed from the transducer surface. After regeneration with Tween20 (4 mM), an aqueous solution of SDS (20 mM) is flushed over the sensor, since SDS is known to form micelles. The critical micellar concentration for SDS is 4-8 mM, decreasing with addition of additives or in buffer to 2-3 mM. Thus, mixed micelles with SDS and Tween are expected to be formed [163–167]. By flushing the sensor with 1-butanol, the micelles and all free detergent molecules are expected to become removed from the sensor surface. However, this process fails to restore the original optical thickness, as seen in Figure 4.10 and by the low $R_e$-value of 14%.
Unfortunately, neither of the other regeneration media tested nor combinations thereof reach a regeneration efficiency of more than 25%.
The experiments with classically known regeneration compounds and the combination of them are performed dependent on practical experience. In the second approach, a well known strategy to search suitable regeneration media is followed: using cocktails as described by Andersson et al [139]. Each cocktail consists of several compounds with similar chemical properties, summarized in Table 4.6 in Section 3.2.5. By combining the compounds in cocktails, such as formic acid, phosphoric acid, malonic acid and oxalic acid for the acidic cocktail, see also Table 4.6, the influence of the regeneration media on the protein-surface interactions can be intensified and the best characteristics for regeneration may be determined. Originally, the method was applied in SPR to break antibody-antigen interactions, but is used here to establish a suitable regeneration protocol [139].
First, each cocktail in Table 4.6 is tested separately. The acidic cocktail A and the basic cocktail B work based on changes in the pH value and thus ionize the side groups of the protein, which changes its charge and breaks electrostatic forces leading to a denaturation of the protein [170–172]. Working with glass transducers as in RIfS and 1-λ reflectometry, bases can damage the glass substrate irreversibly, so the concentration has to be kept low [139, 173]. Chaotropes in cocktail C are expected to denature proteins by interfering with their hydrophobic environment and therefore impacting hydrogen bond formation and ionic strength. The same should apply for non-polar, water soluble compounds as combined in cocktail U [139]. Less harmful to the transducer substrate than the pH changes is the influence of salts (cocktail I, ionic) on the coulomb interactions of the protein and the sensor surface [139, 173]. All these alterations in the protein structure, charge or environment also influence the interactions between the proteins and the inhibitors, resulting in weaker binding and regeneration. Unfortunately, non of these cocktails, each used as a regeneration medium alone, result in $R_e$>37%. Therefore, the cocktails are mixed to combine their effects. As defined in Section 3.2.5, each mixture consists of three fractions of equal volume, which are either a cocktail or milliQ water. The mixture is named with a three-letter code, such as UDw (one part cocktail U + one part cocktail D + one part milliQ water). Each mixture is treated as one individual regeneration medium.
The mixture of DUw, detergents mixed with non-polar water soluble solutions, shows promising results with an effective regeneration of 97%. However, also in the cocktail mixture, the use of detergents for regeneration reduces the sensor capacity, visible in diminished kinase association

in subsequent assays. The mixture BDw is second best with 75% regeneration. Again, detergents are part of the mixture. The association of kinase in a second assay on the sensor after the regeneration was, however, not impaired. The elevated pH value of the cocktail seems to prevent the impact of detergents on the sensor surface and thus on further FAK association. However, a regeneration efficiency of 75% is insufficient.

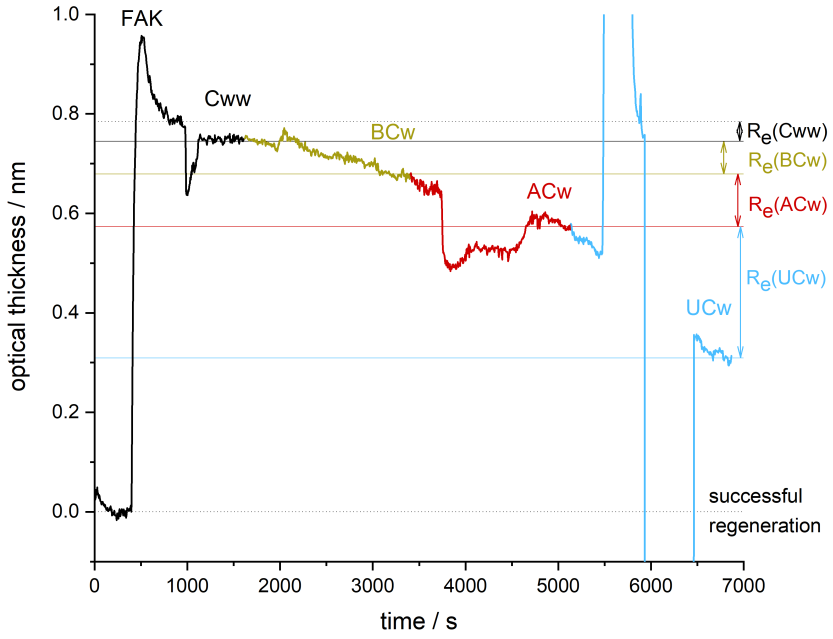


**Figure 4.11:** RIfS binding curves of various regeneration cycles on an AMD-STP-transducer after the association of FAK 40 µg/mL (black signal at the beginning). Regeneration tests with the cocktail mixtures of Cww (black, $R_e$=7%), BCw (gold, $R_e$=13%), ACw (red, $R_e$=27%) and UCw (blue, $R_e$=61%) are displayed, all showing insufficient regeneration. Table 4.6 summarizes the composition of the cocktails.

The cocktail C of chelating compounds and also mixtures with this cocktail C, show regeneration efficiencies lower than 40%. The goal of EDTA in cocktail C is to competitively bind metals from proteins and therefore change the protein folding [169]. No significant influence of the regeneration with mixtures including cocktail C is observed and thus, cocktail C is not further investigated.

The most promising cocktails U, D and B are further investigated, e.g. as the mixtures DUU, BDU, UUw, UUU. With an $R_e$-value of 71%, the mixture of UUw shows good regeneration in combination with a good reproducibility. FAK association in subsequent assays is successful, reaching an optical thickness of 85-90% of the original value. $R_e$-values of 75% and 71% by the cocktail mixtures BDw and UUw for the system FAK interacting with the AMD-STP-transducer are not sufficient to increase the precision compared to single measurements, each on a new transducer, as described in Sections 4.3.1 and 4.3.4. Other mixtures and new combinations do not improve the regeneration.

In Table 4.7, the best mixtures for FAK regeneration are highlighted in bold. A possible explanation for the failure of complete regeneration is, that FAK can interact with STP also outside the ATP-binding pocket in an allosteric binding mode as already discussed in Section

4.2 and verified with the docking simulations (Section 4.1). It is thus likely, that one molecule of FAK is involved in several interaction with the STP molecules on the transducer, forming a tightly bound protein layer on the transducer surface. This layer might be hard to disrupt by the regeneration media, due to a limited access to the binding regions of the proteins to the surface.

In order to avoid additional allosteric binding of the kinase to the transducer surface, self-assembled monolayers are investigated. Instead of AMD as biopolymer layer on the transducer, two polyethylene glycoles (PEGs) are used in a mixture, see Section 3.2.3: a short PEG with a non-reactive end towards the aqueous phase and a long PEG providing an amino-surface also towards the aqueous solution. The amine is used to covalently couple the inhibitor. With different ratios of these two PEGs during the surface modification, an amount of the inhibitor, diluted specifically to 1/10000 per possible binding site, is reached. This transducer modification is hoped to prevent several binding sites of the protein to be involved in the interactions with the inhibitors on the surface as well as provide a binding partner to the protein, further away from the transducer surface to interact in the ATP-binding site without steric hindrance.

All investigations with PEG instead of AMD show smaller changes in the optical thickness for the association of protein kinases. Furthermore, the regeneration of the kinase associated on self-assebled monolayers could not be improved. Therefore, the method with self-assembled monolayers, is not further investigated.

For TGFβ, the cocktail mixture UUw only reaches a regeneration of $R_e$=33%, compared to $R_e$=71% for FAK. Regeneration tests with the mixed cocktail approach with TGFβ on an AMD-STP-transducer show best results with the cocktail mixture UDw and a regeneration efficiency of $R_e$=50%. In Table 4.7, the best mixtures for TGFβ regeneration are highlighted in italic.

**Table 4.6:** Overview on regeneration cocktails, according to [139].

| **Label** | **Ingredients in Water** |
|---|---|
| A - acids | FA, $H_3PO_4$, malonic acid, oxalic acid - each 0.15 M - pH 5 (with NaOH 1 M) |
| B - bases | ethanolamine, glycine, $Na_3PO_4$, piperazine - each 0.2 M - pH 9.2 (with HCl 1 M) |
| C - chelating | $Na_2$−EDTA - 20 mM |
| D - detergents | CHAPS, Triton X-100 - each 0.3% (w/w), Tween20, Tween80, Zwittergent 3-12 - each 0.3% (v/v) |
| I - ionic | GdmCl (1.83 M), KSCN (0.46 M), $MgCl_2$ (1.83 M), urea (0.92 M) |
| U - non-polar water soluble | 1-butanol, acetonitrile, DMSO, EtOH, formamide - in equal amounts |

Reasons for the regeneration differences regarding different kinases are differences in the protein structures (primary to quarterny) with different interaction sites and binding energies. As seen in the docking simulations in Section 4.1 and also in the results of the competitive assays investigated with MST in Section 4.2, the inhibitors bind in the ATP-binding pocket, but also nonspecific interactions outside of this region are likely. Both interaction types are different

for every protein kinase resulting in a different number of binding sites and strengths of the association, changing the requirements on the regeneration.

**Table 4.7:** Overview on tested combinations of regeneration cocktails, see Table 4.6. All cocktails are mixed with three equal volumes of the cocktails, indicated by a three-letter code. In most experiments the third part is milliQ water, represented with a w. Mixture abbreviations given in bold show best regeneration for FAK, italic written mixture abbreviations show best regeneration for TGFβ both on an AMD-STP-transducer. $R_e$-values of the best FAK regeneration are added, even though not all are reproducible, according to [139].

| | A | B | C | D | I | U |
|---|---|---|---|---|---|---|
| A | Aww, - | BAw, 18% | ACw, 30% | ADw, 67% | AIw, 21% | AUw, - |
| B | BAw, 18% | Bww, 17% | BCw, 19% | **BDw, 75%**<br>BDU, 30% | | BDU, 30% |
| C | ACw, 30% | BCw, 19% | Cww, 4% | DCw, 41% | ICw, 9% | UCw, 68% |
| D | ADw, 67% | **BDw, 75%**<br>BDU, 30% | DCw, 41% | Dww, 6% | IDw, 23% | **DUw, 97%**<br>BDU, 30%<br>*UDw, 19%*<br>DUU, - |
| I | AIw, 21% | | ICw, 9% | IDw, 23% | Iww, 20% | |
| U | AUw, - | BDU, 30% | UCw, 68% | **DUw, 97%**<br>*UDw, 19%*<br>BDU, 30%<br>DUU, - | | Uww, 58%<br>**UUw, 71%**<br>UUU, 49% |

To study the effect of the regeneration medium on the sensor surface, a pre-incubation with the mixture UUw is tested on an AMD-STP-transducer in RIfS, prior to kinase association on the sensor. Astonishingly, neither the kinase association is altered compared to the association of a kinase to a fresh transducer, nor the regeneration efficiency after the dissociation phase.
While the regeneration medium provides information on the chemical interaction between sensor and associated molecules, different media address different types of interactions. Every system would require a separate optimization of the regeneration process. Andersson et al., for instance, found that only one of their 13 systems tested was influenced by the cocktail UUw, which is found as one of the best regeneration medium for FAK on the AMD-STP-transducer in their study. In other studies, aqueous $NaHCO_3$ (100 mM, pH 8.7) was a good regeneration medium for SPR with STP as inhibitor on a PKA wild type-sensor, but this medium failed in our study [139, 174]. Clearly, the sensor surface is relevant for the strength of the interaction, since the interaction between protein and STP is altered, owing to the molecule immobilized on the transducer.
In an expanded study, trypsin-EDTA is used to achieve a tryptic digestion of the associated protein kinase directly on the transducer surface, followed by a rinsing with common regeneration medium, e.g. GdmCl. However, regeneration studies of associated FAK with Trypsin-EDTA followed by GdmCl only reach efficiencies between 45 and 60%. It is likely, that trypsin have only limited excess to the amino acid sequence given the tight protein layer on the sensor.
Since the best regeneration methods vary for different kinases and did not improve the precision of the results, sensor investigations were performed as non-regenerated measurements, each as-

say on a new transducer. The variance between these measurements, owing to the differences in the manually prepared transducer surfaces, had to be accepted.

Only very few studies report such severe problems with the regeneration. If this is due to the lack on literature to publish negative data or the fact, that mostly regeneration performances are successful, cannot be defined here. The dense coverage of a transducer surface due to the high concentration of protein hinders the regeneration process, due to irreversible interactions on RIfS sensors [3]. Challenges were often found, when the sensing element is a protein, e.g. for an antibody-antigen interaction. Suitable methods provide both, a good regeneration of the proteins from the sensor surface and a formation of a new sensing layer afterwards [175]. In some cases regeneration was successful but the activity of the surface suffered in subsequent measurements [138]. In general, it is unlikely to find a regeneration media that is suitable for every protein and application [139, 168].

The missing regeneration raises the question of the origin of the strong interactions between STP on the transducer and the associated protein. Assumptions are:

1. Owing to the molecular structure of the inhbitors, all containing aromatic moieties, a stimulation by the light, irradiated on the transducer during the RIfS measurements, is possible. This might lead to photoactivation and results in the formation of covalent bonds between the inhibitor on the transducer and the protein. All inhibitors absorb at wavelengths between 250 and 400 nm, well in the range of the white light irradiated by the halogen RIfS lamp, see Figure 4.12. This absorbed energy might support the formation of a covalent bond towards the kinase. Using 1-λ reflectometry, green light with a wavelength of 535 nm is used, not within the absorption bands of the inhibitors. Since the regeneration of assays investigated with 1-λ reflectometry is incomplete as well, covalent bond formation is unlikely.

2. As seen in the docking simulations, interactions between the inhibitors with the kinases also occur allosterically outside the ATP-binding pocket. If proteins are in contact with the inhibitors on the sensor surface, it is likely, that several intermolecular interactions between the inhibitors on the sensor and one kinase are formed. The overall strength of these multiple interactions might be too strong to be completely broken during the regeneration process. However, kinase association of sensors with self-assembled PEG-monolayers, where the binding capacity is decreased significantly (1:10000 of possible binding sites), could also not be completely regenerated. With these experiments, multiple binding sites between one kinase to several inhibitors on the transducer surface are unlikely.

3. Regarding the second assumption, that one protein interacts with several inhibitor molecules on the transducer, it seems possible, that the protein folding changes upon binding, resulting in a dense monolayer of proteins on the transducer surface. In experiments of protein folding during BSA adsorption as protein on a silica-surface with SPR, a conformational change towards a flat protein structure, building a dense layer on the sensor

chip was shown in other studies [176]. This might be too dense for the regenerating compounds to act on interaction sites. Even a trypsine solution would not have access to lysine and arginine for a digestion, not able to improve following regeneration steps. It also seems possible, that the regeneration medium only changes the folding or charge of the sensor-averted part of the protein, not influencing the interactions towards the transducer. This would change the optical thickness, as observed in the unsuccessful regeneration investigations, even without removing any kinase molecules from the sensor. With the explanation of the second assumption, that regeneration of kinase associated on self-assembled PEG-monolayers is found unsuccessful, this third hypothesis has to be considered critically.

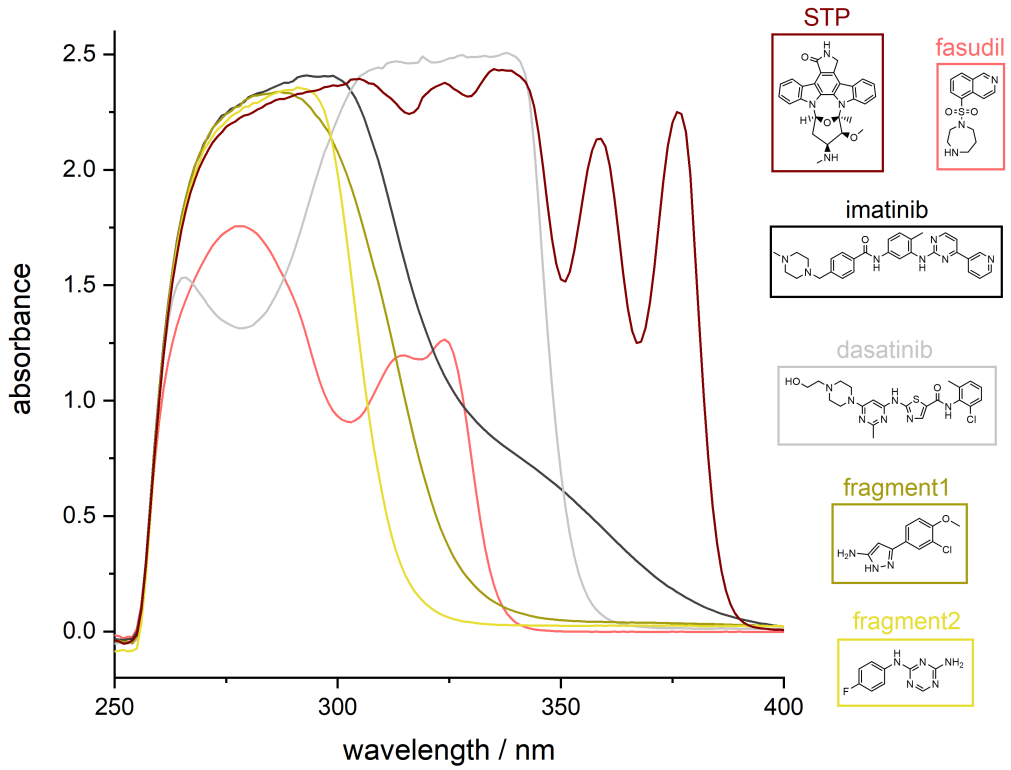


**Figure 4.12:** UV-VIS spectra of the inhibitors investigated in this study. All inhibitors show absorption between 250 and 400 nm, due to the aromatic ring systems in their molecular structure.

All assumptions are inline with binding curves in RIfS and 1-λ reflectometry not showing any signal decrease during the dissociation phase, which indicates a strong affinity of the protein to the transducer surface, see Figure 4.7 A and Figures 4.9 A and B. Intermolecular interactions lead to an equilibrium of association and dissociation, but seemingly the equilibrium is on the associated state. If the interaction results in a covalent bond (see Assumption 1), dissociation is no longer possible, explaining the missing dissociation signal and the failure of all regeneration media. If one protein molecule interacts with several inhibitor molecules on the transducer (see Assumptions 2 and 3), the association dominates over the dissociation, due to several binding sites, and the optical thickness does not decrease significantly during the dissociation phase.

Summarizing, the interaction between the protein kinase and the inhibitor on the transducer surface either involves covalent bonds or multiple binding sites, where several regions of one protein molecule interact with several inhibitors on the transducer surface.
Even if these assumptions are not thus likely and more complex processes might explain the poor regeneration, speculative interpretations are not given in this work. The surfaces of the transducers after kinase association are further investigated by surface analytical methods, see Section 4.4, to shed light on the type of interaction.

### 4.3.3 Optimization of the Sensor Surface for Referencing the Sensor Capacity

The results of the direct assays demonstrate the principal applicability of RIfS for the detection of protein kinase interactions with inhibitors including the kinetic evaluation of the binding process. In order to improve the comparison of the sensor signals, an intermediate step in the RIfS protocol is added, with the aim to quantify the coverage with inhibitor on the sensor surface. This knowledge could increase the reproducibility of the sensor surfaces by using the quantitative stable system of the biotin-streptavidin-binding as reference.
The transducers are modified with AMD and biotin, instead of AMD and STP, cf. Section 3.2.3 and Figure 4.13. The inhibitor in solution is covalently linked to biotin. Then a complex with streptavidin is formed in solution by the strong biotin-streptavidin interaction. For RIfS, this inhibitor-biotin-streptavidin complex is then bound to the AMD-biotin transducer via further free interaction sites of streptavidin towards biotin [177–180]. This creates the binding sites for protein kinases. Further steps of the RIfS measurements follow the previous protocol.

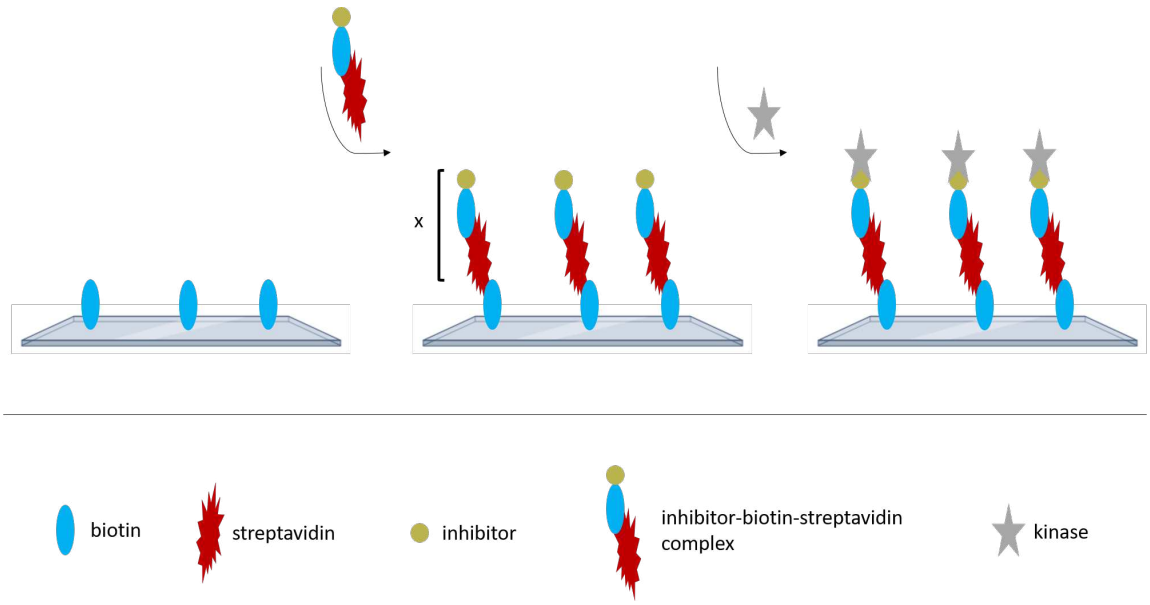


**Figure 4.13:** Sktech of the sensor system with biotin and streptavidin to be able to normalize assays on the surface capacity of different RIfS sensors. The AMD-transducer is modified with biotin, see Section 3.2.3. In RIfS, the inhibitor-biotin-streptavidin complex is bound to the AMD-biotin-transducer. Via the change of optical thickness, which is indicated by "X", mostly generated by the large streptavidin molecule, the amount of inhibitor on the sensor surface can be defined.

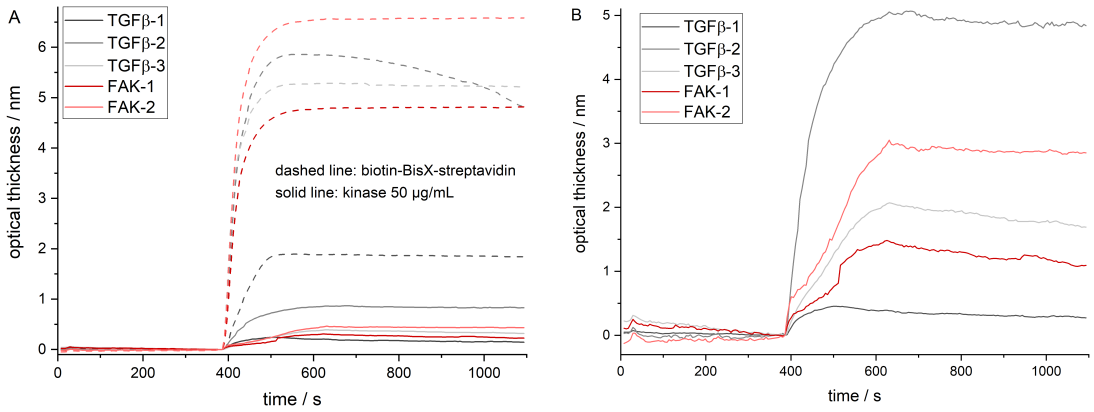


**Figure 4.14:** RIfS binding curves of a direct assay using biotin-sensors. First, a complex consisting from biotin, BisX and streptavidin is added to the transducer surface, followed by the association of FAK or TGFβ in a concentration of 50 µg/mL. A: All sensograms of the complex association and the corresponding kinase association. B: All sensograms of the kinases, adjusted to the corresponding surface capacity with BisX as inhibitor, created by association of the biotin-BisX-streptavidin complex on the biotin-sensor.

The auxiliary step of adding streptavidin is anticipated to better define the amount of inhibitor on the transducer surface: The streptavidin on the transducer surface evokes a specific increase in the RIfS sensor signal, which can then be used to account for differences in the surface capacity of different transducers. This specific change of the optical thickness is schematically depicted in Figure 4.13 with the "X" and monitored in RIfS, see Figure 4.14 A. It is expected, that the kinase association could be assessed with higher precision, by normalizing it to the amount of streptavidin, representative for the surface coverage with inhibitor. However, the precision in optical thickness for kinase association was already low with relative standard deviations between 12 and 61%, see Figure 4.14 B. Moreover, the changes in optical thickness of the tested kinases FAK and TGFβ at a concentration of 50 µg/mL are smaller than expected, from the association on AMD-STP transducers. Obviously, the auxiliary-system via biotin and streptavidin results in a lower surface capacity of the inhibitor and furthermore, the referencing of the signals does not improve the precision of the biosensor assays.

Advantages of this biotin-steptavidin system investigation, are the strong and specific interaction between these molecules and the increased distance between the glass surface of the transducer and the inhibitor. This should enhance the specificity of the kinase-inhibitor interaction due to a better access to the binding pocket by a higher flexibility for the protein kinases to locate the interaction in the sterically hindered ATP-binding pocket. In contrast, the strong interactions between biotin and streptavidin prohibit a regeneration of the surface.

Future work may focus on different auxiliar systems given the high potential for normalization in combination with better regeneration. E.g., the hybridization of DNA or RNA on the sensor as an intermediate step (such as the biotin-streptavidin system) is already known to combine these two requirements [181–184]. Further details of this auxiliary system are discussed in Section 5.

### 4.3.4 Binding Inhibition Assay: Proof of Principle

While the kinetic data calculated from the direct assay (see Section 4.3.1) demonstrate the interaction in heterogeneous phase, data in homogeneous phase can be evaluated by changing the assay type. With a binding inhibition assay, where kinase is pre-incubated with inhibitor before being injected to the sensor, the interaction in the homogeneous phase can be analyzed. The first RIfS investigations of a binding inhibition assay with kinase preincubated with STP in homogeneous phase on an AMD-STP-transducer show unexpected signals during the association phase, see Figure 4.15. Measurements with STP as sample alone result in enhanced optical thickness. As shown in Figure 4.15, the signal increases during the association phase depending on the inhibitor investigated. During the dissociation phase, where buffer is flushed over the sensor, the signal returns to the baseline. This full dissociation shows, that there are only weak and reversible interactions of STP and all other investigated inhibitors with the transducer surface.

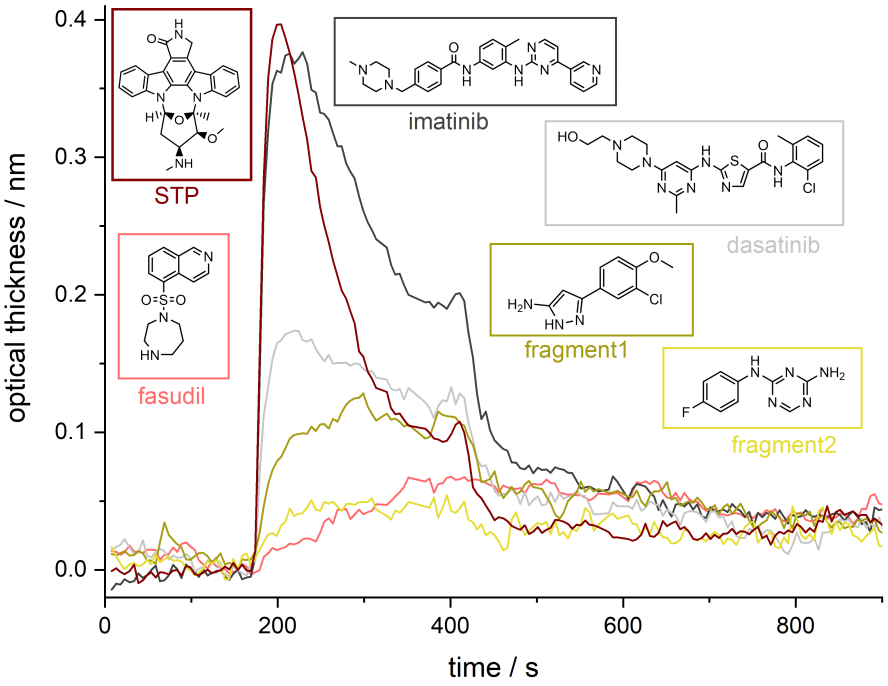


**Figure 4.15:** Sensor signal of various inhibitors (10 µg/mL) measured in RIfS with white light. High signals are observed during the association phase, returning to the baseline during the dissociation phase. The measurement protocol is similar to the investigations with kinases as sample, see Section 3.2.4.

In order to perform reliable binding inhibition assays the sensor system is changed to 1-λ reflectometry, irradiating monochromatic green light at 535 nm, instead of white light, which is used for RIfS. Beside for the irradiation with monochromatic light, 1-λ reflectometry has the benefit of using a referenced signal: the signals of the regions with inhibitor bound to the sensor surface can be referenced to the signals of the inhibitor-free sensor regions. Thus, signals generated by affinities from non-specific binding as well as differences in the initial reflectivity

can be considered and no longer influence data evaluation.
An investigation of several inhibitors as sample on an AMD-transducer with 1-λ reflectometry did not show any signal increase, see Figure 4.16, thus, the biosensor is well applicable for an binding inhibition assay.

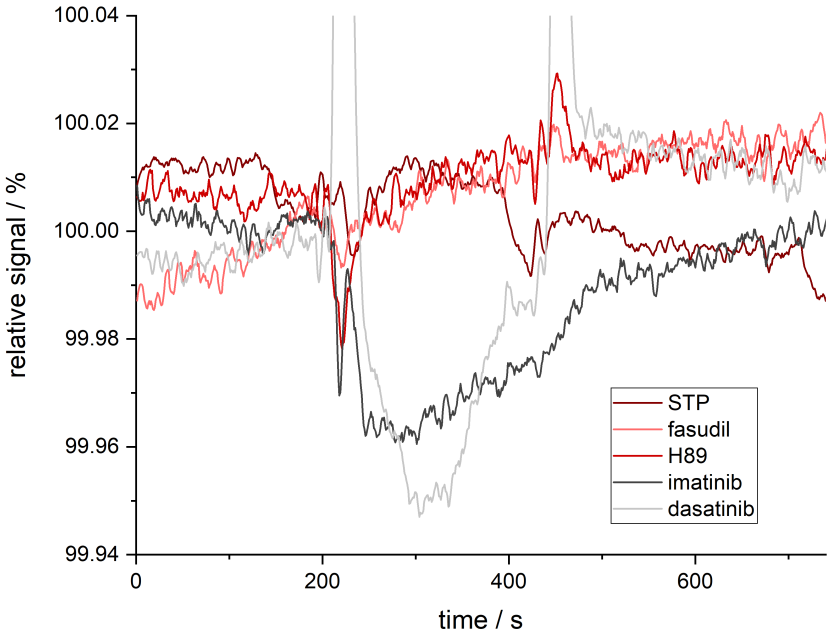


**Figure 4.16:** Signals of 1-λ reflectometry, flushing different inhibitors (10 µg/mL) over an AMD-sensor. The measurement protocol is similar to the investigations with kinases as sample, see Section 3.2.4. The green light of 535 nm is outside of the wavelengths absorbed by the inhibitors (see Figure 4.15), resulting in undisturbed signals of the binding curves. The sharp peaks at second 200 and 420 are generated by pressure pulses due to switching the autosampler and pump direction.

Binding inhibition assays are conducted with 1-λ reflectometry. Because the highest binding signals are achieved with the protein mix, the first binding inhibition assays are performed with this sample, inhibited in homogeneous phase with STP, which is added at different concentrations. The assay is performed on AMD-STP-transducers. The inhibition with equimolar concentrations of STP and the protein mix is found to be ineffective. Therefore, STP is added in excess. The pre-incubation is conducted with 5- up to 100-fold molar excess of STP to the protein mix, whose concentration is held constant at 50 µg/mL. All calculations are made, assuming all proteins in the protein mix to be PKA. In Figure 4.17, the binding curves proof a successful binding inhibition assay of the protein mix with STP on an AMD-STP-transducer. In total, three test series are conducted with different inhibitor concentrations and the data are kinetically evaluated using the average of three sensor signals of each inhibitor concentration, except of the values for the 30-fold inhibition, where air bubbles in the flow cell interrupted two of three analyses.
The kinetic evaluation is similar to the one for the direct assay. In Figure 4.18 A, the sigmoidal dependency of the inhibitor concentration is shown. The sensor signal at the end of the dissociation phases are used for evaluation and referenced to the signal of the non-inhibited protein mix sample, which was set to 100%. The kinetic evaluation in Figure 4.18 B uses the exponential

fit to each binding curve, as already shown in Figure 4.8 A. The dissociation constant is calculated as $K_d$=31.9 µM and a 41.8-fold molar excess of the inhibitor found as the half-maximum inhibition concentration. Compared with the data of the direct assay for the protein mix on an AMD-STP-transducer, the dissociation constant is more than three orders of magnitudes higher than for the direct assay: 20 nM (direct assay) and 31.9 µM (the binding inhibition assay). This comparison reveals a higher affinity for the interaction in the heterogeneous phase, compared to the interaction in homogeneous phase, which is already discussed in Section 4.3.1 when comparing data of the homogeneous assays in MST to the direct assay on the sensor in heterogeneous phase [162]. It is important to note, that the binding inhibition assay depends on and is limited by the affinity of the direct assay, as the detection is based on binding the fraction of analyte to the sensor surface, which is not inhibited in solution, see Figure 3.10.

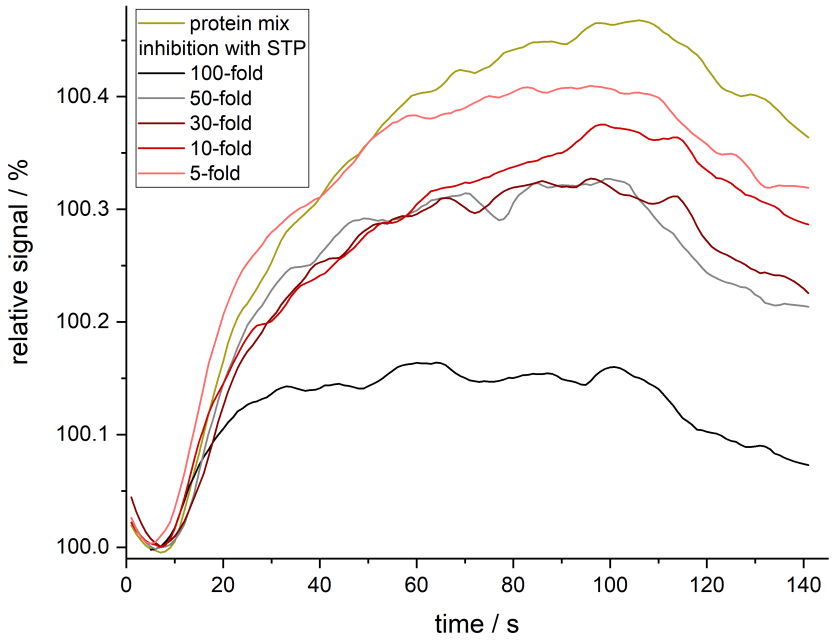


**Figure 4.17:** Binding inhibition assay with STP and the protein mix on an AMD-STP-transducer recorded with 1-λ reflectometry. The concentration of the protein mix is constant (50 µg/mL) and inhibition with STP is conducted with 5- up to 100-fold molar excess. For a better visualization and comparability to RIfS sensograms, the signals of the 1-λ reflectometry are inverted.

To explain the affinity of the binding inhibition assay, both interaction processes have to be considered. E.g. the dissociation constant of the binding inhibition assay is limited by the dissociation constant of the direct assay. Furthermore, several binding modes of the inhibitor on the protein structure, as found by the docking simulations in Section 4.1, can be expected to influence the kinetic data. Allosteric binding can lead to both added inhibitor binds to the protein kinase in solution and a binding of the kinase-inhibitor complex on the surface. Thus, the required excess of added inhibitor can be explained.

The lack of referencing the signal of each sensor to a standard, as described in Section 4.3.3, challenges further evaluation of kinetic data for protein-inhibitor-interaction. All measurement series of binding inhibition assays are performed with the same batch of transducers, in or-

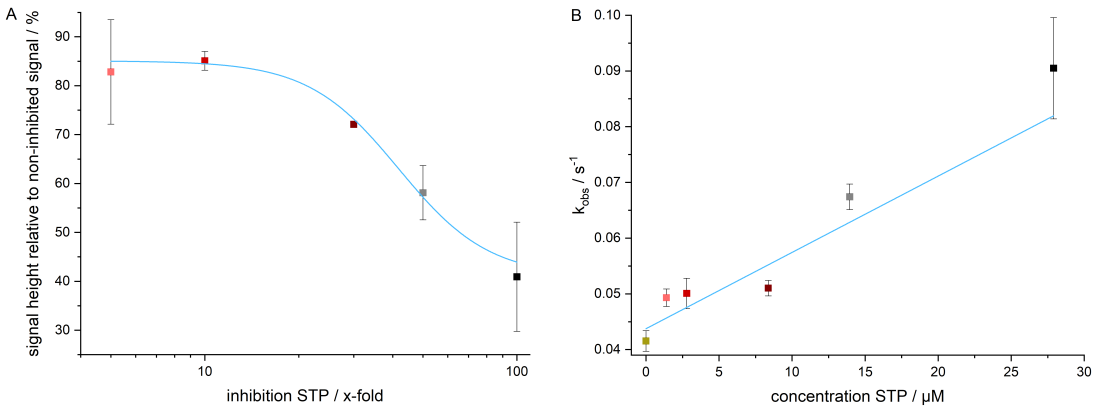


**Figure 4.18:** A: Sigmoidal dependency of the binding inhibition assay from Figure 4.17, (c(protein mix)=50 µg/mL, STP in 5-100-fold molar excess). The sensor signal at the end of the dissociation phase was referred to the sensor signal of the non-inhibited signal of the protein mix, which was set to 100%. The coefficient of determination is 0.986. B: Evaluation of the kinetic data of the binding inhibition assay via the exponential fit method, see Section 4.3.1. The coefficient of determination is 0.780. Kinetic data: $k_a = 1.37\ L\ mmol^{-1}\ s^{-1}$, $k_d = 0.04\ s^{-1}$, $K_d = 31.9\ \mu M$.

der to provide highest comparability of the sensors. Different transducer modifications were tested: AMD-transducers linked with fasudil, fragment1, fragment2, H89 and STP; different kinases: PKA and the protein mix and different small molecules for inhibition in solution: fragement2, H89 and STP. Compared to the protein mix, purified kinases show lower signals in 1-λ reflectometry. Lower signals and the need to use a new transducer for every measurement results in high standard deviations of the sensor signals, when purified kinases are used as sample. Figure 4.19 shows, that the signals of the non-inhibited samples are similar the inhibited samples.

Figure 4.20 B shows signals of the direct assay of the protein TGFβ (20 µg/mL) on an AMD-STP-transducer as well as signals of the binding inhibition assay with STP in a 100-fold molar excess recorded by 1-λ relfectometry. As expected, the averaged signals of these two experiments show clear differences: The averaged signal of the non-inhibited sample shows a signal increase of 0.10% with a relative standard deviation of 24%. For the inhibited sample, the averaged association signal shows an increase of 0.068% with a relative standard deviation of 11%. Comparing the averaged signals, the inhibition results in a 31% decrease of the non-inhibited signal. However, in the original binding curves it can be seen, that some of the non-inhibited curves overlap with the inhibition curves. In order to improve binding inhibition assays, the variance in the transducer manufacturing has to be reduced.
In Figure 4.20 A, binding curves of a direct assay of the protein mix with a concentration of 50 µg/mL on an AMD-STP-transducer and the corresponding binding inhibition assay with STP in 76-fold molar excess are displayed. While the averaged signal of the non-inhibited sample shows a signal increase of 0.305% with a relative standard deviation of 10%, the corresponding values for the averaged inhibited signals are 0.068% in signal increase and 11% relative standard deviation. The inhibition results in a 54% decrease of the non-inhibited signal, proving the principal applicability of the system.

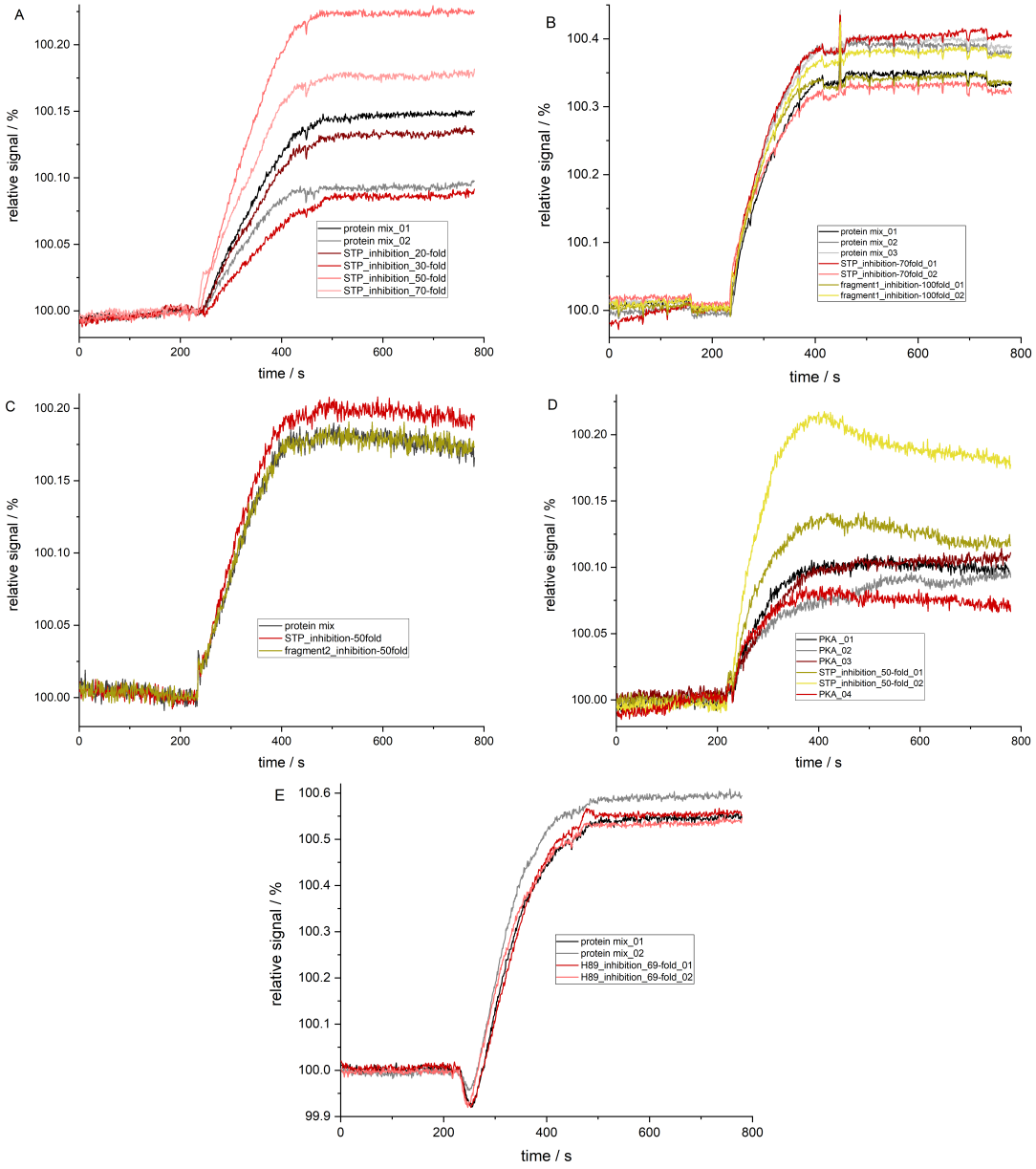


**Figure 4.19:** Examples for unsuccessful binding inhibition assays measured with 1-λ reflectometry. A: AMD-STP-transducer, protein mix 10 µg/mL, inhibition with STP in a concentration series; B: AMD-fragment1-transducer, protein mix 10 µg/mL, inhibition with STP in 70-fold molar excess or fragment1 in 100-fold molar excess; C: AMD-fragment2-transducer, protein mix 10 µg/mL, inhibition with STP or fragment2 in 50-fold molar excess; D: AMD-fasudil-transducer, PKA 20 µg/mL, inhibition with STP in 50-fold molar excess; E: AMD-H89-transducer, protein mix 50 mg/mL, inhibition with H89 in 69-fold molar excess. For a better visualization and comparability to RIfS sensograms, the signals of the 1-λ reflectometry are inverted.

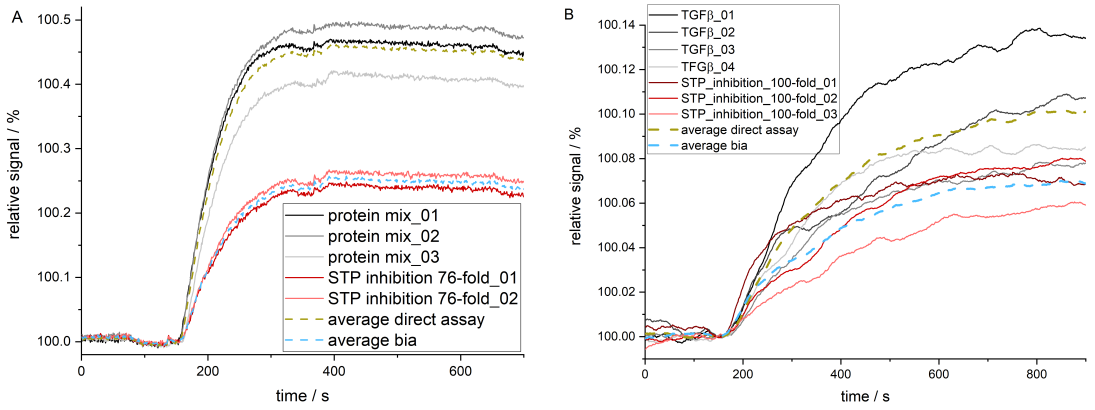


**Figure 4.20:** Proof of principle of the binding inhibition assay (bia) with different protein-inhibitor pairs and inhibitor concentrations investigated with 1-λ reflectometry. The signals of the direct assay, where only protein is the sample, are higher (black and gray curves) than the inhibited samples (red curves). Hence, the averages of the non-inhibited signals (gold dashed line) are higher than the averages of the inhibited signals (blue dashed line). A: Binding inhibition assay of the protein mix (50 µg/mL) with STP as inhibitor in 76-fold molar excess, on an AMD-STP-transducer. $\overline{X}$(kinase)=0.305%, RSD(kinase)=10%, $\overline{X}$(inhibition)=0.068%, RSD(inhibition)=11%. B: Binding inhibition assay of the protein TGFβ (20 µg/mL) with STP as inhibitor in 100-fold molar excess, on an AMD-STP-transducer. $\overline{X}$(kinase)=0.10%, RSD(kinase)=24%, $\overline{X}$(inhibition)=0.068%, RSD(inhibition)=11%. For a better visualization and comparability to RIfS sensograms, the signals of the 1-λ reflectometry are inverted.

To summarize, binding inhibition assays cannot always be evaluated for kinetic data, due to the regeneration challenges and the need to use a new transducer for every measurement. Data for the protein mix and TGFβ, however, show, that binding inhibition assays are principally possible, see Figure 4.20 A and B. Currently, however, only for kinase-inhibitor pairs revealing a high sensitivity. Interaction of protein kinases and inhibitors in the homogeneous phase are successfully recorded on the sensor, for the protein mix and TGFβ. By calculating kinetic data, differences between the interaction of kinase and inhbitor in the homogeneous phase (direct assay) and in the heterogeneous phase (binding inhibition assay) are shown. These kinetic data corroborate MST results and also the results of the docking simulations. Progress can be made by improving the regeneration (Section 4.3.2) or by a higher reproducibility in the preparation of transducers. Furthermore, auxiliary systems, e.g. by using a DNA or RNA hybridization should be investigated, see (Section 4.3.3 and Section 5).

## 4.4 Surface Analysis: Unravelling Unexpected Strong Kinase Binding

Due to the fact, that the proteins do not dissociate from the sensor surface and thus regenerations are unsuccessful, a closer look at the interaction between kinase and inhibitor bound to the sensor surface is made, attempting to prove or disprove the hypotheses from Section 4.3.2. Therefore, surface analysis of RIfS transducers before and after association with FAK is performed with MALDI-TOF-MS, ATR-IR spectroscopy and Raman microscopy.

### 4.4.1 MALDI-TOF-MS Measurements

FAK is dropped and dried on a standard target plate for proteins, sinapinic acid is used as matrix, as it is proved superior to cyano-4-hydroxycinnamic acid, see Section 3.2.6, and measured by MALDI-TOF-MS. The dried droplet method is repeated twice (d-d3, see Section 3.2.6), proved to be the best method for matrix addition. This method is also applicable for STP with its lower mass of m/z=467.5.
In Figure 4.21, the mass spectrum of 100 ng FAK on the standard protein target plate is displayed. The peak of the investigated FAK fragment with an average mass of 32.46 kDa is observed. With this as basis for MALDI-TOF-MS measurements of FAK, further investigations with AMD-STP-transducers are made. For surface analysis, FAK is dropped on to the surface of two transducers. From one, non-bound FAK is removed by washing with milliQ water after an incubation time of 10 minutes. On both transducers, matrix is added (SA7, d-d3). The transducers are then glued onto the ITO slides of the target plate constructed in-house with copper band (see Figure 3.12). This experiment simulated the measurements in RIfS, where the kinase is flushed over the surface of the AMD-STP-transducer. To investigate the applicability of MALDI-TOF-MS results, the FAK concentration of this experiment is in the range used during RIfS measurements, although a comparison of static experiments vs. experiments in flow is difficult. As seen in the spectra in Figure 4.22, only when the full amount of FAK is dried on the transducer, a small peak can be observed. When FAK is washed from the transducer surface after the incubation, no protein can be detected by MALDI-TOF-MS. This is a first indication, that the amount of FAK on the transducer of RIfS measurements is too low to be detected by MALDI-TOF-MS. And indeed, in none of the experiments with AMD-STP-FAK-transducers prepared with RIfS protein was detected.
The washing step removes all FAK molecules not interacting with the inhibitor on the transducer surface. Therefore, the concentration of FAK is reduced. The reason for this failure to detect FAK is surely the low FAK concentration of the transducer after the washing step in the static experiment simulation as well as on the RIfS transducers. Kinases interacting with the transducer surface presumably cover the transducer only with a monolayer, both in this experiments and in RIfS. In other studies, the limit of detection for lysozyme analysis on contact lenses with MALDI-TOF was found to be a monolayer with a density of approximately 15% [185]. The detection of a protein monolayer with MALDI-TOF-MS is possible, but highly influenced by the matrix chosen. The required laser power depends on the matrix. A con-

centration gradient of matrix may be formed, which is more concentrated at the edges of the droplets [186, 187]. With this knowledge, and the fact, that the matrix is dropped on the RIfS transducers in the region, where the flow cell of RIfS was located, it is likely, that the ideal concentration of matrix is not located exactly at the point of the highest concentration of FAK on the transducer. This might decrease the ionization performance of the protein.

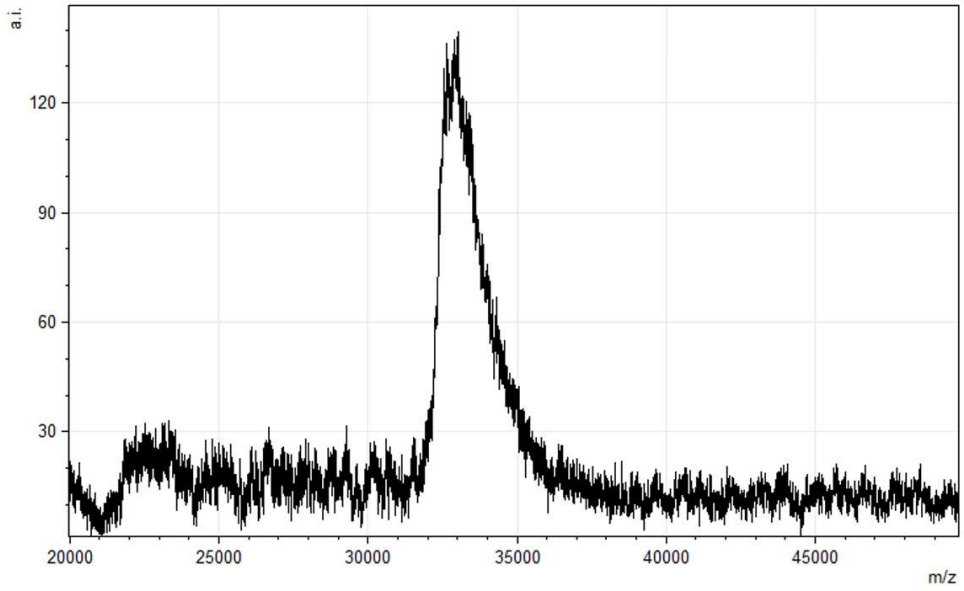


**Figure 4.21:** MALDI-TOF-MS spectrum of FAK (average mass 32.46 kDa) on the stardard protein target plate: 1 µL of a 0.1 µg/mL FAK aqueous solution is dried and matrix is added, see Section 3.2.6.

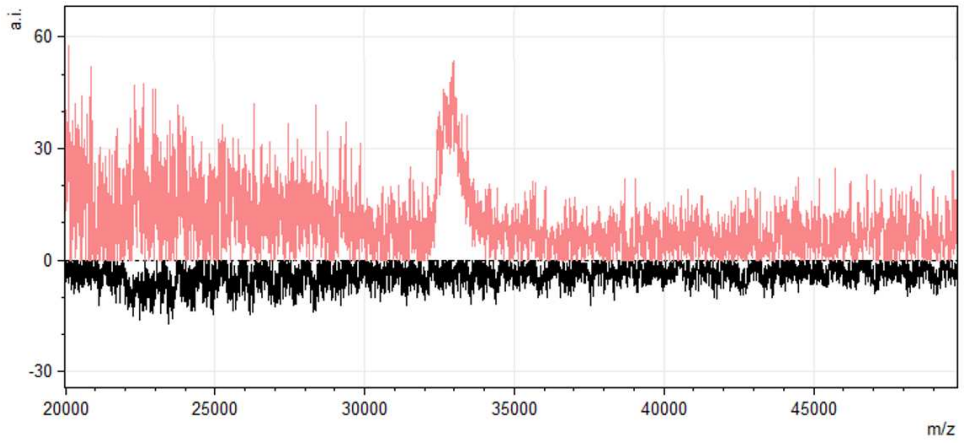


**Figure 4.22:** MALDI-TOF-MS spectra of AMD-STP-transducers incubated with 5 µL FAK solution (30 µg/mL) in a static experiment. Red: The drop of FAK solution is dried on the transducer and matrix is added. Black: The drop of FAK solution is incubated for 10 minutes, then the transducer is washed with milliQ water and dried in a stream of nitrogen. Then, sinapinic acid is added as MALDI matrix, see Section 3.2.6.

However, another reason for too high LODs is: Even if the concentration of FAK on the AMD-STP-transducers is higher than the LOD, the conductivity of the transducer as MALDI plate might be too low. With the target plate constructed in-house from ITO slides and copper tape,

suitable conductivity conditions for the sample may not be reached, resulting in diminished ionization and therefore high LODs in MALDI-TOF-MS.
A third reason for the failure of detection FAK on the transducer after RIfS investigations might be a covalent bond formation between the FAK and the STP on the transducer surface, see the first hypothesis in Section 4.3.2. If this is the case, the ionization process of MALDI is not powerful enough to break these covalent bonds. To investigate this assumption, experiments of a tryptic digestion are made. The tryptic digestion of FAK is performed in solution to provide a reference, and on an AMD-STP-transducer with dried FAK solution. The digestion in solution is measured on the standard protein target plate, while the digestions on the transducers are measured with the target plate constructed in-house. Furthermore, a self-digestion of trypsin is performed, as a control. Comparing the mass spectra for digestion in solution vs. digestion on the transducer in Figure 4.25 shows, that most of the peptide signals of the tryptic digestion in solution are not observed in the digests on the transducer (m/z-range 300-500). Some signals are related to the STP on the transducer, which can be seen by the comparison of the red (digestion on the transducer) and black (STP) curves in Figure 4.25. Here, not only the tryptic digestions are compared, but also a spectrum from an untreated AMD-STP-transducer is shown. The peak in the black trace at 466.5 m/z stems from STP, which is covalently bound to the transducer surface, cf. Figure 3.3. The signal is not seen in spectra of only an AMD-transducer. STP ionizes even without MALDI matrix added. Comparing the spectrum of an AMD-STP-transducer with matrix in Figure 4.23 with the spectrum of STP on the standard target plate without any matrix in Figure 4.24, a high intensity of peaks at 466.5 m/z, belonging to the full molecule signal of STP, are present in both spectra. Presumably, STP is activated by the absorption of light at 250-370 nm (compare its UV spectrum in Figure 4.12). Matrix molecules absorbing energy by the laser irradiation and transferring this energy towards the analyte molecules are not required for STP. The energy transfer from the laser (app. 330 nm) directly to the STP might be effective enough, to break the covalent bond, so STP on an AMD-STP-transducer is observable by MALDI-TOF-MS. This process is unlikely for kinases.
The results displayed in Figure 4.25 show, that kinase peptides from tryptic digestion on the transducer cannot be determined by MALDI-TOF-MS. While the digestion in solution shows, that the concentrations used are higher than the LOD, the reason for unsuccessful measurements on the transducer must be the insufficient conductivity on the transducer. Likewise, experiments with tryptic digestion on AMD-STP-transducers with associated FAK from an assay performed in RIfS are not successful.
While the conductivity is limiting the MALDI-TOF-MS investigations, we cannot further investigate the hypothesis of a possible covalent binding between kinase and inhbitor on the transducer with this method.

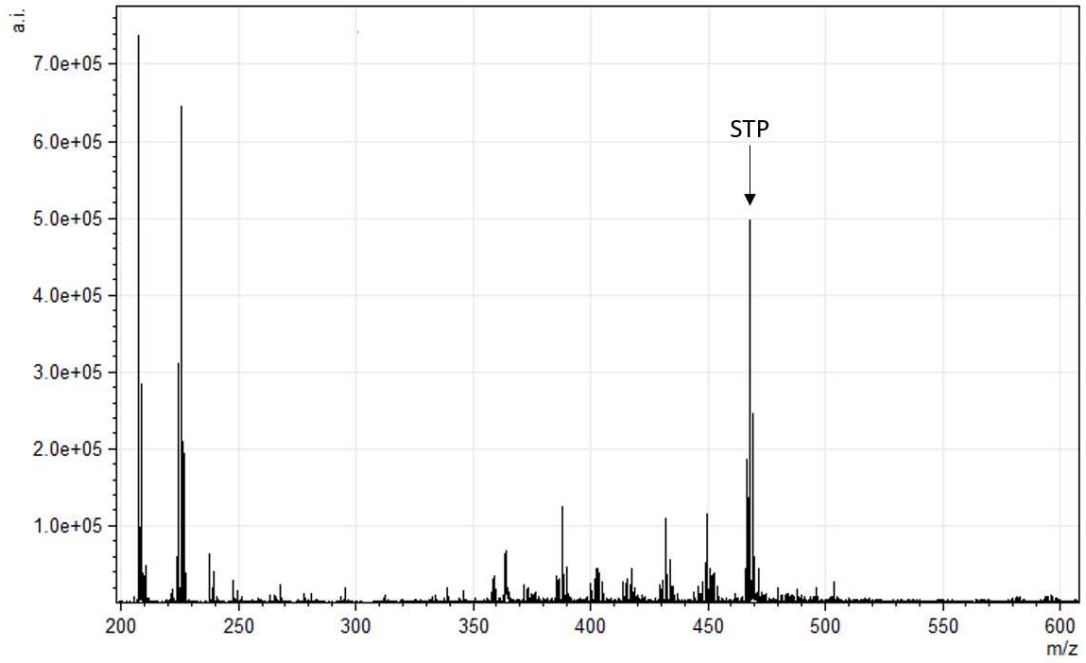


**Figure 4.23:** MALDI-TOF mass spectrum of an AMD-STP-transducer with the target plate created in-house in the low m/z region. The signal at 466.5 m/z belongs to intact STP. Further signals result from the matrix compounds.

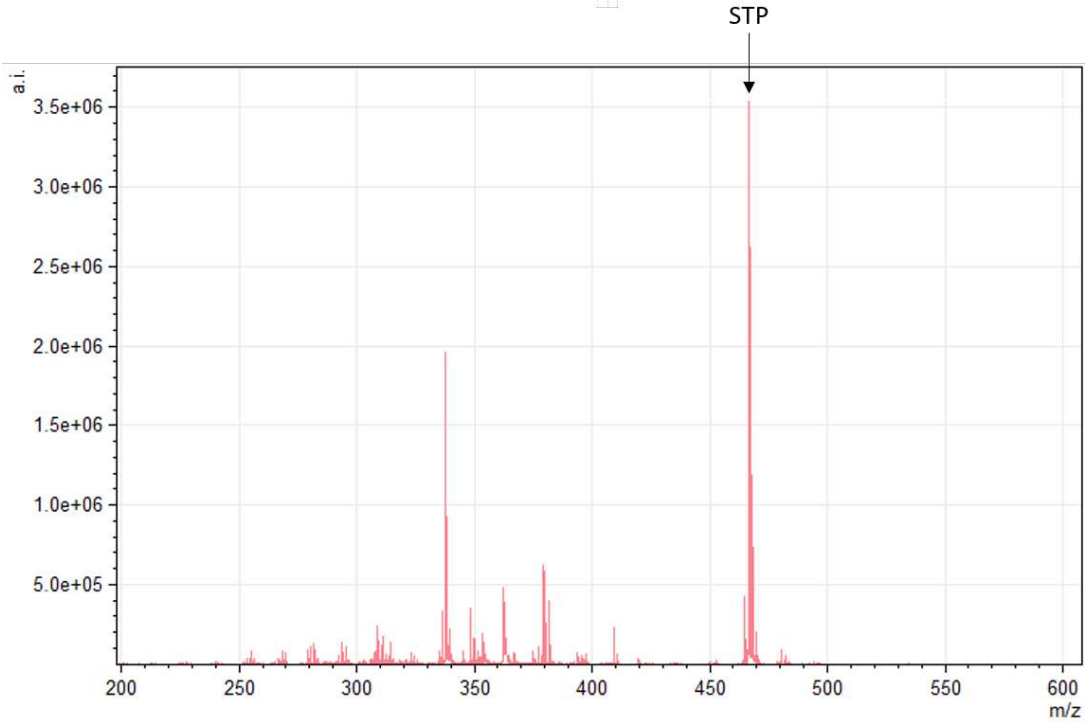


**Figure 4.24:** MALDI-TOF mass spectrum of STP without any matrix on a standard target plate. The intact STP molecule is observed at 466.5 m/z. Due to the ring systems in the molecular structure, a direct ionization with MALDI is possible without any matrix.

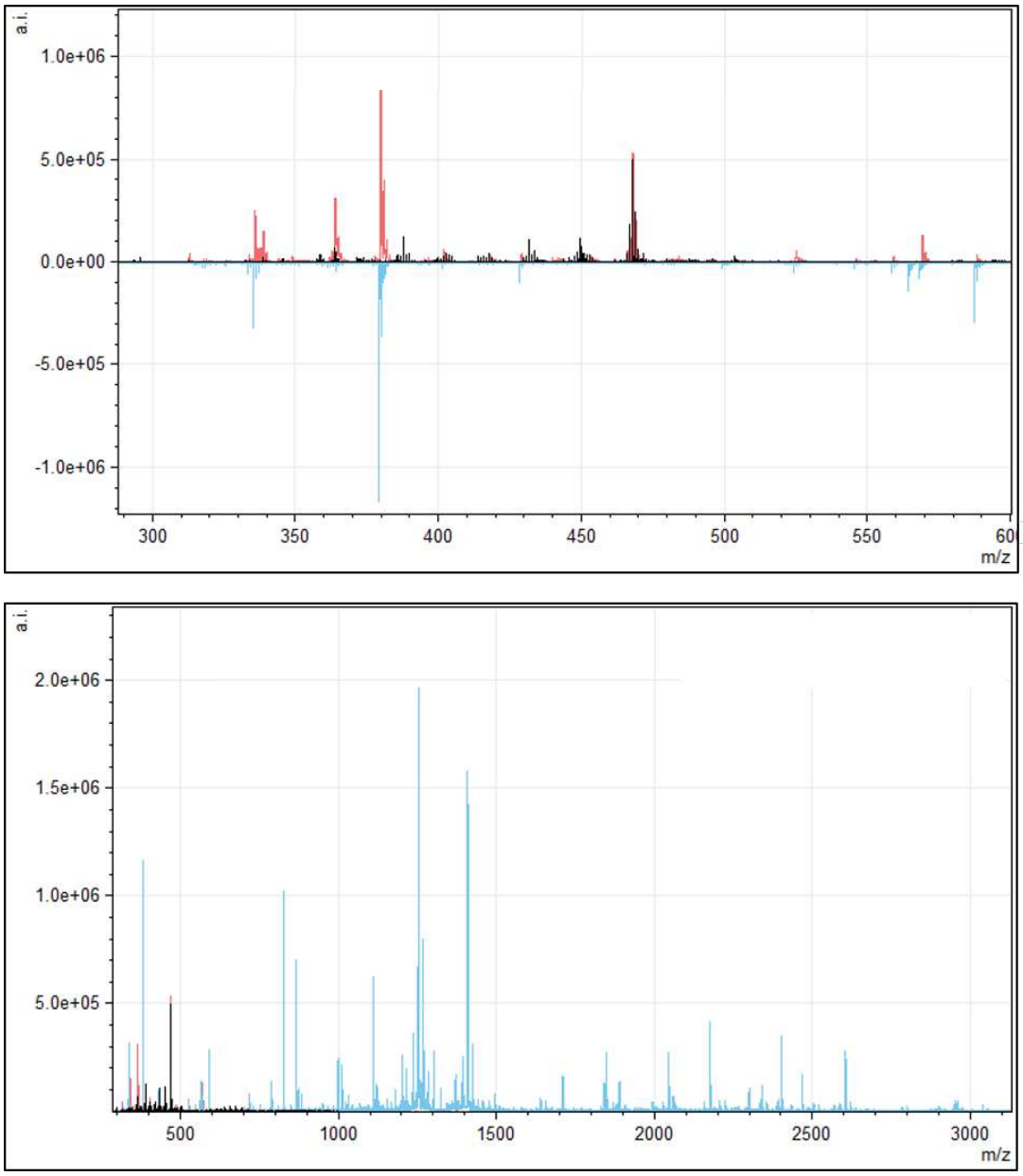


**Figure 4.25:** MALDI-TOF-MS spectra after the tryptic digestion of FAK on a transducer. Blue: Digestion of FAK in solution, measurement on a standard target plate with the matrix method described in Section 3.2.6. Red: Digestion of FAK dropped and dried on an AMD-STP-transducer and measured on the target plate constructed in-house. Black: Low mass spectrum of an AMD-STP-transducer, where signals generated by STP are present.

All MALDI-TOF-MS measurements are also performed with the system AMD-BisX-transducer and FAK as kinase. Further protein samples are investigated with the protein mix, on both the AMD-STP- and the AMD-BisX-transducers. Findings regarding the AMD-BisX-transducers are similar to those for AMD-STP-transducers and not further discussed here. The same holds true for the samples of the protein mix. While the inhibitor can be detected, the conductivity of the target plate constructed in-house is too weak to ionize and therefore detect any protein on the transducer surface after washing steps or the RIfS measurements.

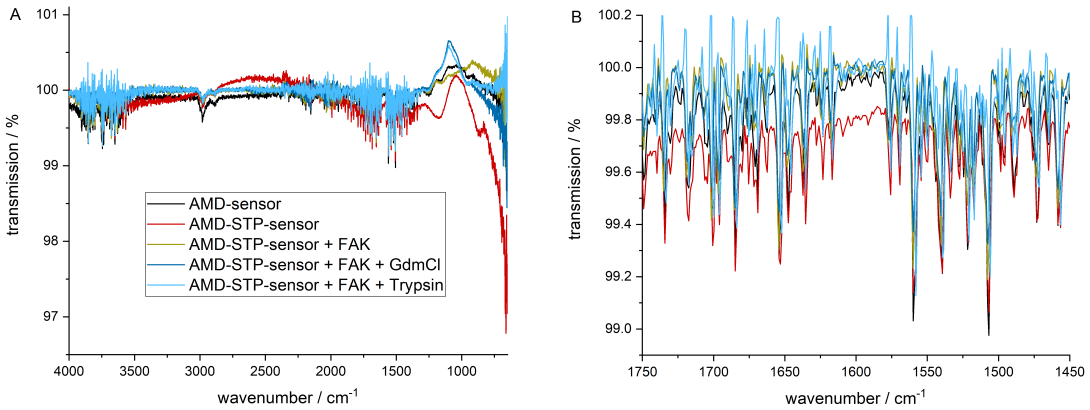


**Figure 4.26:** ATR-IR spectra of RIfS transducers in various steps of the RIfS measurement process: AMD-transducer, AMD-STP-transducer, AMD-STP-transducer with FAK association plain or followed by regeneration using GdmCl or trypsin-EDTA, cf. Section 3.2.6.

### 4.4.2 ATR-IR Measurements

As the MALDI-TOF-MS investigations of the transducers were challenged by the requirement of building a target plate in-house, a proof of the hypothesis, that a covalent bond might have been formed between the protein and the STP on the transducer surface, was not possible. Further surface analysis methods are required, to at least detect the protein on the transducer after its association.

To gain further insight into the transducer surface, ATR-IR spectroscopy is used by Leon Biesterfeld, as described in Section 3.2.6. Five different transducers are investigated to compare the surfaces: AMD-transducers, AMD-STP-transducers, AMD-STP-transducers measured in RIfS with FAK association, AMD-STP-transducers measured in RIfS with FAK association and regeneration with GdmCl or trypsin-EDTA. It is expected to see differences in the spectra at least between the original transducers and the transducers after RIfS measurements. For proteins, significant bands, especially for the amides, are in the region of 1450-1750 $cm^{-1}$ [188–192]. In principal, their detection is possible despite the presence of amino bonds between STP and the modified biopolymer on the transducer, as the IR signals should increase in the presence of proteins on the transducer. Another possible identification of protein in IR is a signal at 490 $cm^{-1}$ due to disulfide bonds. However, in the investigated FAK fragment only seven cysteine moieties are present, theoretically generating three disulfide bonds at maximum, which is too few amount to be detected with IR, assuming a protein monolayer on the transducer [193].
An overview over the five spectra for all experiments is given in Figure 4.26 A. Unfortunately, no significant differences between the spectra are observed. In Figure 4.26 B, spectra of the protein-specific region of 1450-1750 $cm^{-1}$ are enlarged, neither showing any significant differences. Obviously, only signals related to the AMD-surface are detected, but not covalent bonds between the FAK and the AMD-STP-transducers. IR-spectroscopy can detect amides and other specific functional groups, even if the molecule is covalently bound to the surface. As in the MALDI-TOF-MS investigations, a likely reason for the dissatisfying results is the insufficient

sensitivity of the ATR-IR spectroscopy, as protein is known to be present from RIfS assays. Here too, the method has to detect a monolayer of the protein on the transducer. Most methods, analyzing protein monolayers with IR useed surface enhanced systems to achieve a signal enhancement between two and five orders of magnitude, which is not applicable here. [194–196]

### 4.4.3 Raman Microscopy

In addition to MALDI-MS investigations and ATR-IR spectroscopy, Raman microscopy is used to gain insight into the chemistry on the transducer surface before and after FAK association. The measurements are performed by Prof. Natalia Ivleva at the TU München and the spectra are shown in Figure 4.27.

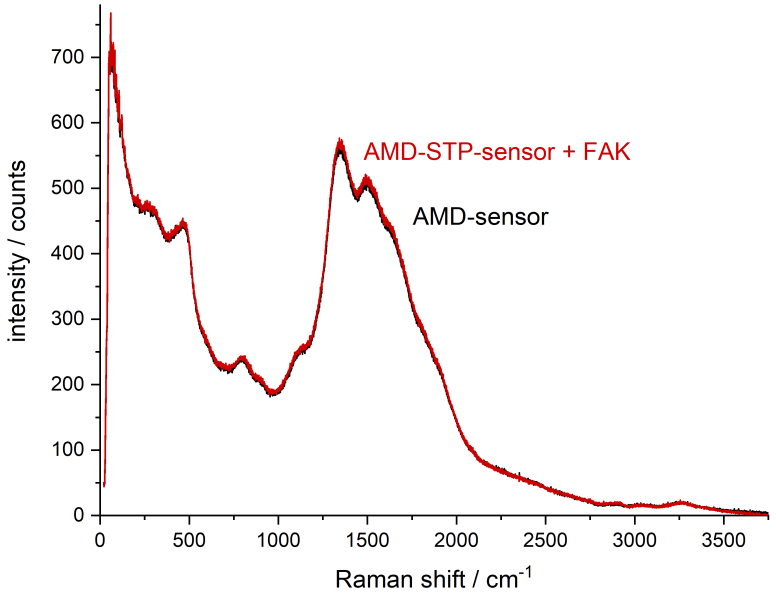


**Figure 4.27:** Raman spectra of a plain AMD-transducer (black) and an AMD-STP-transducer after association of FAK in RIfS (red). Amide bonds are expected in the range of 1200-1700 $cm^{-1}$.

By comparing the Raman spectrum of the AMD-transducer (Figure 4.27 black curve) with the AMD-STP-transducer after FAK association (Figure 4.27 red curve), no significant differences are present. Even in the wavenumber region of the Raman shift from 1200 to 1700 $cm^{-1}$, where the amide bands of the protein are expected, no differences in the spectra are visible. Disulfide bonds of proteins, located at 490-510 $cm^{-1}$, are also not found in the spectrum of the AMD-STP-transducer with associated FAK [192, 197–200]. Similar to the results of the ATR-IR spectroscopy, with Raman, no FAK was detected on the transducer.
It appears, that also for Raman LODs are too high to detect FAK in a monolayer on the transducer surface.
As in IR investigations, protein in monolayers can be detected with surface enhanced methods which can enhance the signal intensity up to six, in specific applications even up to eleven orders of magnitude. [195, 198, 201]

### 4.4.4 Discussion of the Results from Surface Analysis

None of the surface analytical methods (MALDI-MS, ATR-IR, Raman) is sensitive enough to show differences between a plain AMD-transducer and an AMD-STP-transducer with associated FAK. The limit of detection of these methods is not sufficient to detect the monolayer of protein present on the transducer surface. Nevertheless, in RIfS, all sensors analysed showed a change in optical thickness of approximately 1 nm generated by the association of FAK. This shows, that RIfS is a highly sensitive method, which detects less than a fraction of protein monolayers, while other methods fail. Both the direct assay as well as the binding inhibition assay show significant signals in RIfS and 1-λ reflectometry when injecting the protein mix as sample as well as for the purified kinases FAK and TGFβ. All signals are detected based on specific binding as non-specific interactions are successfully prevented, see Figure 4.6. The results regarding the signals of the RIfS measurements are highly comparable to similar experiments with selective association on the sensor: IgG antibodies (app. 150 kDa), Er α-LDB (63 kDa) and thrombin (70 kDa) showed changes in the optical thickness of 0.2-2.5 nM, dependent on the concentration (1-8 µg/mL), proving the limit of detection of the method [3, 4, 202].
The question on the type of interaction (physi- or chemisorption) between protein kinase and inhibitor on the sensor, explaining the strong binding and the failure of regeneration, remains open, yet.

## 4.5 Screening: The Power of the Developed Biosensor Assay

As the good limit of detection of the biosensor assays was proven, screening methods are investigated. Owing to the poor regeneration (cf. Section 4.3.2) each measurement is performed on a new, freshly produced transducer.

### 4.5.1 Spotting Methods

Inhibitor screenings on a sensor requires the immobilization of different inhibitors on one transducer. Therefore, the last surface modification step of 1-λ reflectometry transducers is modified to build array-based sensors, as described in Section 3.2.3. One of the advantages of 1-λ reflectometry over RIfS is the possibility for specifically resolved analysis of the surface which enables to simultaneously detect interaction of one kinase on different inhibitor spots for screening applications. Two spotting methods are tested in this work: manual spotting by hand and automatic spotting with a spotting machine (spotter). A comparison of the performance of these spotting methods uses TGFβ association on two AMD-STP-transducers. As seen in Figure 4.28 A, the spotting method strongly influences the spot size. While the minimum volume for one spot pipetted by hand is 0.03 µL, the capillary used for automatic spotting has an inner diameter of only 36 µm enabling drop volumes of approximately 1 nL per spot. Thus, the spot volume differs by four orders of magnitude and the regions of interest (ROI) largely differ (0.1 mm automatic spotting vs. 1.8 mm manual spotting) accordingly, see Figure 4.28 A.
Owing to the higher volume of inhibitor solution by the manual spotting method, a diffusional spreading of the drop occurs, which is seen in the image of the sensor in Figure 4.28 A2. The association signal of TGFβ on the automatically spotted inhibitor spots is twice the signal observed from the manually spotted inhibitor spots, see 4.28 B. The small size of the automatically spotted spots leads to a higher surface coverage of the inhibitor, responsible for the higher signal. However, Figure 4.28 B shows, that the noise in the signals recorded for the automatically spotted sensor is higher, than for the larger spots generated by hand.
For the evaluation of 1-λ reflectometry the images recorded of the sensor surface are used. In order to monitor the influence of the ROI size on the noise of the sensor signal, the noise of a baseline measurement on an AMD-STP-transducer evaluated with ROIs in different size, from only 1 evaluated pixel up to over 100 evaluted pixels, is compared. Figure 4.29 shows, that the noise in 1-λ reflectometry of a baseline depends on the number of pixels in the chosen ROI: With increasing number of pixels in the ROI, the noise decreases. The number of 10 to 30 pixels is the minimum of pixels required in order to reduce the noise to a minimum. A higher number of pixels does not provide further reduction in the signal quality. A larger ROI is thus advantageous. As already seen in Figure 3.5 A, the large size of the spots created manually on the transducer only tolerates three spots on one transducer.

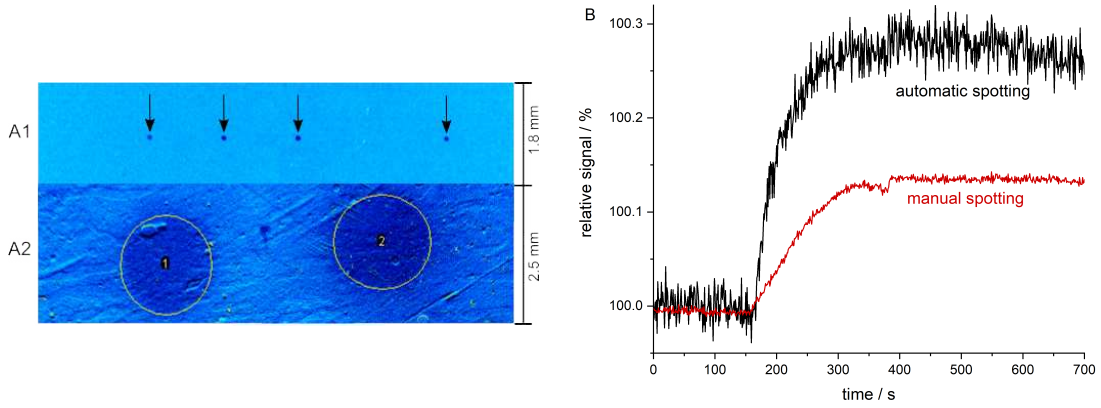


**Figure 4.28:** A: Images of a segment of two transducers. A1: Four spots automatically generated with the spotter, approximately covering 4 pixels in the image, A2: Spots manually generated via pipetting by hand, the regions of interest set for evaluation are marked with a circle of approximateley 121 pixels. B: 1-λ reflectometry binding curves of the direct assay of TGFβ (10 µg/mL) on an AMD-STP-transducer, where the signal of the two spotting methods (manually by hand or automatically with the spotter) are compared. For a better visualization and comparability to RIfS sensograms, the signals of the 1-λ reflectometry are inverted.

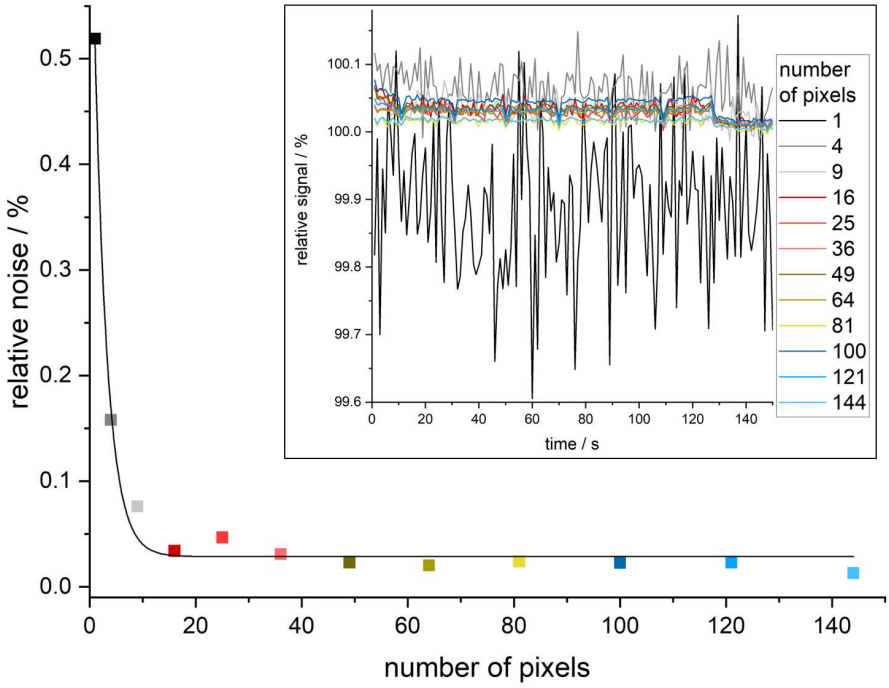


**Figure 4.29:** Graphical display of the dark noise of the 1-λ relectometry. The noise in the baseline curves depends on the number of pixels used in the ROI for the sensor evaluation. Reference for the noise is the averaged sensor signal for each measurements.

For the evaluation of 1-λ reflectometry, a sensor is required where a segment of the sensor surface is free from inhibitor, to define a reference ROI. Automatic spotting with the much smaller spots allows a much higher number of spots on one sensor, which is a great advantage with regard to a higher throughput for the screening. Moreover, comparing the sensor surface visible in Figure 4.28 A for the transducer spotted manually (A2), inhomogeneities of the sensor surface are visible, which is not the case for automatic spotting (A1), where the spots have a

much smoother surface. However, a compromise has to be found between the larger area of the ROI reducing the noise, the number of spots required for high-throughput screening, and the total surface coverage as reference spots ideally accompanying inhibitor spots. Even though a lower noise is expected for the manually spotted sensors, screening is performed with the sensors spotted automatically. Here, a larger variety of inhibitors as spots on the surface is reached, with a higher coverage of inhibitor on each spot resulting in better LODs.

As described in Section 3.2.3, the automatic spotting cannot be performed in a chamber filled with DMSO vapor, opposite to the manual method, which simplifies the immobilization process. The automatic spotting takes place under ambient conditions. Furthermore, the last cleaning step can be omitted. This leads to a higher homogeneously surface of the sensor. With the many advantages, the following screening is performed with sensors spotted automatically.

### 4.5.2 Inhibitor and Kinase Screening: Proof of Principle

For inhibitor screening, different inhibitors are spotted automatically onto AMD-transducers, which were refunctionalized with glutaric anhydride and activated. The arrays are made using fasudil, fragment1, fragment2, imatinib and STP. Each inhibitor is immobilized in four spots in one row, fasudil and STP with two rows each. Since the association of the protein is directly visible in the photographs of the sensor in 1-λ reflectometry, the spots can be seen in Figure 4.30. In each row of spots one place is free from inhibitor, and therefore free from kinase association, to control the spotting process and correct inhibitor immobilization, as well as to set the reference required for evaluation. Due to small changes in the pressure profile, generated by short stops of solution flow while changing the sample or pump direction (see Section 3.2.4), position of the reference ROI should be in the same region as the inhibitor spots on the sensor. To decrease the influence of the noise of the reference, the reference ROI is always chosen larger than the spots.
The visual control of the measurement by the images of the sensor surface, provides first hints on a successful inhibitor screening: Comparing the inhibitor rows with each other, different color changes are visible, due to differences in the strength of the protein association. More intense change of the color indicates a higher affinity, resulting in more proteins bound to the inhibitor spots on the sensor. In the image in Figure 4.30 A, the strongest signal change, strongest change in color, and thus highest protein association is obtained for fasudil, followed by imatinib > fragment2 > fragment1 > STP. Clearly, the signals are similar per row, for one type of inhibitor, pointing to a good reproducibility.
Quantitative information from the inhibitor screening is given by the binding signals of the arrays, see Figure 4.31. Here, all binding curves of the array measurements with the protein mix (Figure 4.31 A) and FAK (Figure 4.31 B) (each 50 µg/mL) are displayed. For the sample of the protein mix, shown in Figure 4.31 A, the spots of fasudil revealed the strongest association with an increase of the relative signal by 1.7% on average, whereas for STP, the relative signal increased only by 0.45% on average. The signals regarding the other inhibitors, fragment1,

fragment2 and imatinib show intermediate affinities. These differences show, that the binding strength of the protein mix is different among the inhibitors. This also holds true for the measurements with FAK as sample, proving that an inhibitor screening is reached with this method. For FAK as the kinase, a ranking for the amount bound on the particular spots of STP > imatinib > fragment2 > fasudil > fragment1 is found.

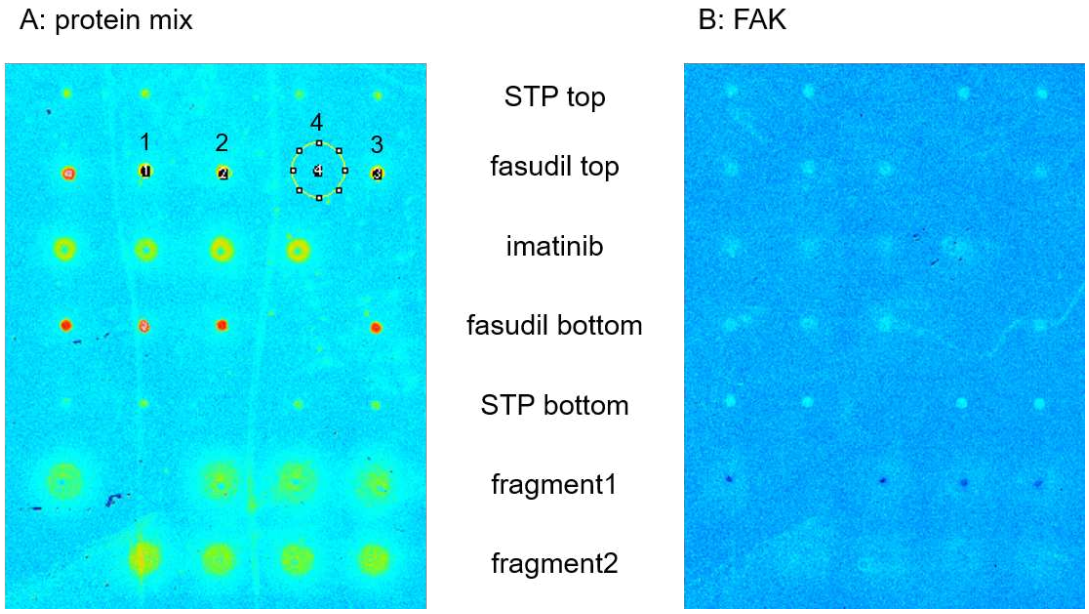


**Figure 4.30:** Images of the arrays for inhibitor screening, recorded with the CCD camera of the 1-λ reflectometry, settings are defined in Table 3.11: Inhibitors are spotted automatically on AMD-transducers in different rows, as defined in the middle. The images are taken after the association phase of the kinases. A: 50 µg/mL protein mix, ROIs for evaluating the signal on the fasudil spots are marked with circles 1-3 (approx. 16 pixels) plus the reference ROI 4 (approx. 100 pixels). ROI 1-3 are positioned directly on a spot, 4 is the reference ROI, positioned in a region of the sensor void of inhibitor. To decrease the influence of the noise of the reference, the reference ROI is chosen larger than the spots. B: 50 µg/mL FAK.

All sensor signals generated by the protein mix as samples are higher compared to the signals with FAK as the kinase sample, compare Figures 4.31 A and B. This finding is clearly seen in the bar chart in Figure 4.32. Exemplarily, imatinib shows an increase in the relative signal by 0.84% for the association of the protein mix, but only 0.13% for the association of FAK. A similar comparison can be made for all other inhibitor spots. The sensor signal thus not only depends on the inhibitor, but also on the kinase used as sample. With this comparison, the dependency on the specific binding strength by the kinase-inhibitor-pair is demonstrated.
The overall differences in binding signals for FAK and the protein mix, exemplary for the imatinib spots, where the signals show a 6.4-fold difference (0.84% for protein mix association vs. 0.13% for FAK association) are unlikely to be due to differences in the quality of the prepared transducers. Only changing the transducer while all other measurement conditions, including the sample kinases, were kept constant, is not responsible for such high signals differences. Both transducers were prepared in the same batch and stored for a similar time. Thus, the

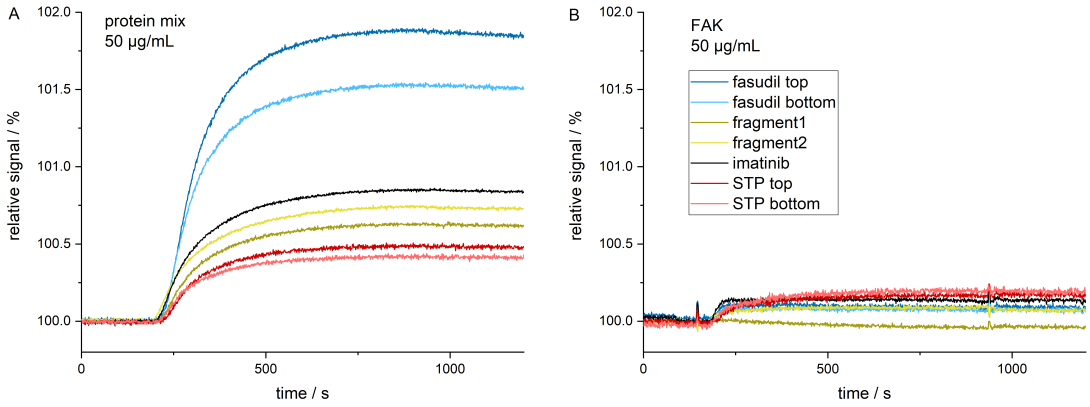


**Figure 4.31:** Proof of principle for inhibitor and kinase screening with 1-λ reflectometry on two sensor-arrays (AMD-transducers, spotted with different inhibitors). The association phases (200-1250 seconds) of A: the protein mix and B: FAK (both 50 µg/mL) are shown. A: The ROIs for the evaluation of fasudil and STP spots comprised 16 pixels, for the imatinib spots 36 pixels and for the fragment spots 49 pixels. B: The ROIs for the evaluation of all other spots comprised 16 pixels. The position of the inhibitor spots are displayed in Figure 4.30. A possible inhibitor screening as well as a kinase screening can be seen. For a better visualization and comparability to RIfS sensograms, the signals of the 1-λ reflectometry are inverted.

high significant difference are clearly expected to be mainly due to different affinities of different kinases to the inhibitor spots. These results declare the proof of principle for kinase screening with the developed sensor method.

Binding affinity trends from the screening investigations with FAK can mostly be compared to the results of the docking simulations and the MST measurements: FAK binding energies are simulated as STP > imatinib > fasudil > fragment1 = fragment2 over the full protein and imatinib > STP > fasudil > fragment1 = fragment2 in the binding pocket. With MST a trend of STP-Red > imatinib > fasudil is determined for FAK as kinase. However, for experiments with the protein mix, a comparison of the results of these three methods is difficult, due to the differences between the protein mix, which was investigated in the screening, the purified PKA, which was used in MST investigations, and the PKA structure in the simulations. For the PKA structure the trend STP > imatinib > fasudil > fragment1 > fragment2 was simulated over the full protein and similar inside the binding pocket, exept for fragment1 = fragment2. This can well be compared to the MST findings STP-Red > imatinib > fasudil. The difference, that STP showed the lowest affinity in the screening can be explained, as therefore, the protein mix was investigated and not the purified PKA, which seems to interact differently.
A full regeneration, tested here with trypsin-EDTA followed by GdmCl, was not reached, as discussed previously. Nevertheless, if a better regeneration would be reached and a reusability of the sensor arrays becomes possible, different kinases can be monitored sequentially on one array interacting with all inhibitors spotted. Without this, the reproducibility of the array manufacturing has to be investigated to ensure a good comparability between the arrays.
This array-based 1-λ reflectometry as introduced, is proven to be a promising tool for inhibitor and kinase screening in one method.

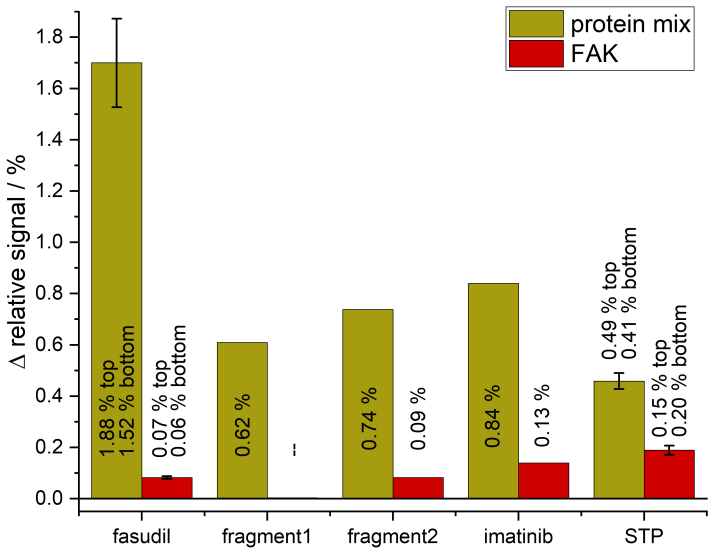


**Figure 4.32:** Quantitative analysis of the sensor signals of kinase and inhibitor screening as proof of principle in Figure 4.31. The protein mix and FAK (both 50 µg/mL) were allowed to associate on the spots of the sensor arrays from Figure 4.30.

## 4.6 Extending the Surface Chemistry: Kinase Extraction with Magnetic Nanoparticles

To make use of the strong affinity between the protein kinases and STP on the transducer surface, an additional strategy is followed to allow the identification of kinases binding on RIfS or 1-λ reflectometry sensors: kinase extraction is conducted with magnetic nanoparticles, which are modified on their dextran surface with carboxyl groups for further modification to covalently bind STP (NP-STP), similar to the transducer surfaces, see Figure 3.13. As in the direct assay on the sensor, a strong interaction between kinases and inhibitors is expected, when the modified nanoparticles are added to a solution containing protein kinases. This solution might be a bio sample or a cell culture. Kinases bound to the nanoparticles are extracted from the solution making use of the magnetic characteristics of the nanoparticles, see Figure 3.14.
In this work, investigations are performed with NP-STP and FAK or TGFβ as kinases. Quantitative evaluation is achieved via fluorescence measurements, owing to the tryptophan fluorescence of proteins with excitation at 280 nm and the detection of the emission at 300-400 nm. In Figure 4.33, the fluorescence intensity of several samples containing FAK are shown. Three FAK concentrations (5, 10 and 20 µg/mL) are chosen. The kinase concentration is quantified in samples before and after the kinase extraction with NP-STP, by fluorescence spectroscopy, as explained in Section 3.2.6. Comparing the maximum of the fluorescence intensity at 345 nm, it is clearly shown, that the fluorescence intensity of the supernatant decreases upon kinase extraction. For the sample with 5 µg/mL FAK, the fluorescence intensity of the unterated sample is 1.4-fold the fluorescence intensity of the supernatant after the kinase extraction. Considering the fluorescence intensities for the samples with 10 and 20 µg/mL FAK, these values are 1.9-fold and 1.6-fold, respectively.

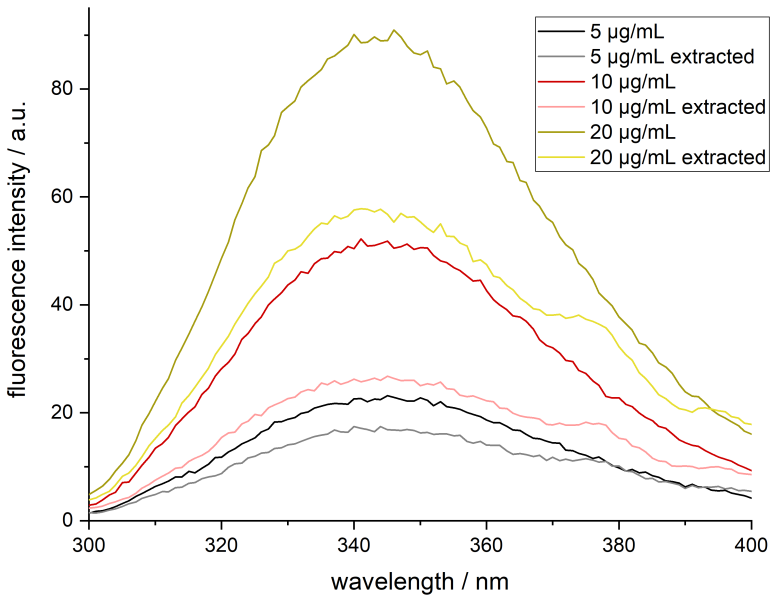


**Figure 4.33:** Tryptophan fluorescence intensity of samples containing FAK, before and after the extraction with NP-STP. The fluorescence intensity depends on the concentration of the protein. Fractions of the kinases are captured by the nanoparticles and therefore extracted from the solution.

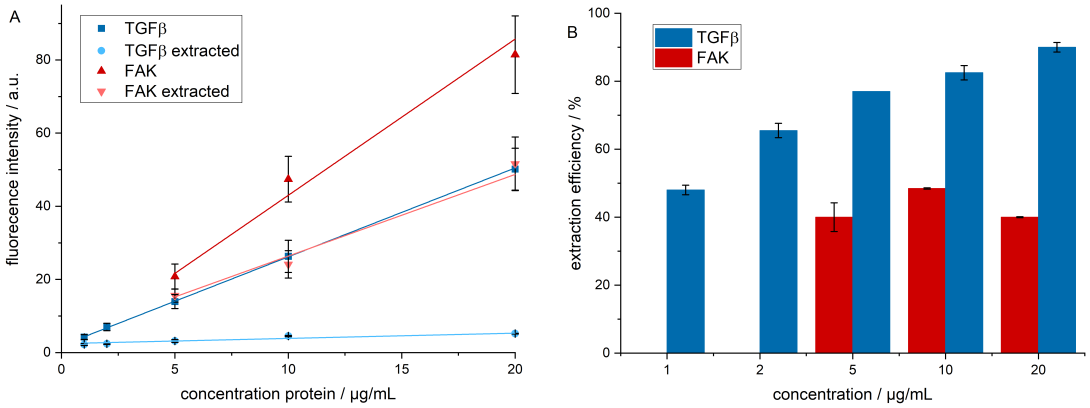


**Figure 4.34:** Quantitative analysis of the kinase extraction (FAK and TGFβ) with NP-STP from Figure 4.33. A: The protein kinase concentration is plotted against the fluorescence intensity of the maximum at 345 nm and the linear dependence of the fluorescence intensity on the kinase concentration is shown: dark red: FAK (coefficient of determination 0.962, slope 4.27 $\frac{a.u.}{\mu g/mL}$), bright red: supernatant of the FAK sample after extraction with NP-STP (coefficient of determination 0.956, slope 2.23 $\frac{a.u.}{\mu g/mL}$), dark blue: TGFβ (coefficient of determination 0.999, slope 2.43 $\frac{a.u.}{\mu g/mL}$), bright blue: supernatant of the TGFβ sample after extraction with NP-STP (coefficient of determination 0.872, slope 0.14 $\frac{a.u.}{\mu g/mL}$). B: The extraction efficiency depends on the protein concentration, with a constant ratio of protein to NP-STP.

The fluorescence intensity proves to linearly depend on the protein concentration investigated, see Figure 4.34 A, which allows to estimate the extraction efficiency. For FAK, approximately 40% of the proteins are captured by the nanoparticles, as seen in Figure 4.34 B. For TGFβ, a tendency to a higher extraction efficiency with increasing protein concentration is visible. While at a concentration of 1 µg/mL TGFβ approximately 50% are captured by the nanoparticles, in the solution of 20 µg/mL TGFβ nearly 90% of the kinases are bound to the particles. By comparing these slopes in Figure 4.34 A, two conclusions can be made: First, the slope of the fluorescence intensity of the untreated FAK sample is 1.8-fold the slope of the fluorescence intensity of the untreated TGFβ sample. Thus, FAK fluorescence is more sensitive to the kinase concentration than TGFβ. This perfectly correlates with the higher number of tryptophan molecules, in the proteins FAK and TGFβ used here, which are responsible for the protein fluorescence. The FAK investigated contains 14 tryptophan molecules, while the TGFβ investigated only contains eight. Thus, FAK has a 1.75-fold higher number of tryptophan molecules than TGFβ, well explaining the 1.8-fold higher sensitivity in fluoresence intensity of FAK in the untreated sample. Second, comparing the slopes of the FAK fluorescence intensity before and after the extraction of the kinases with the nanoparticles, the slope of the untreated FAK sample is 1.9-fold the slope of the fluorescence intensity of the FAK samples after the extraction with NP-STP. For TGFβ, this value is even 17.4. Therefore, the detected fluorescence of the TGFβ samples after the kinase extraction shows a higher dependency on the concentration of the protein, due to higher differences in the linear slopes.
The data show, that a kinase extraction of FAK and TGFβ with NP-STP is possible.

"I don’t know when theorists and experimentalists became rivals, but physics is not about competition - it’s about collaboration."

Love on the Brain

Ali Hazelwood

# 5 Overall Discussion and Summary

In this work a new method for kinase and inhibitor screening was developed and optimized, as schematically depicted in Figure 5.1. Using theoretical docking simulations and experimental methods, the interactions of the protein kinases and inhibitors, intended for this work, were shown and the energy of the interactions was investigated. Based on this information, a novel sensor method was developed, to detect and quantify the interactions between protein kinases and inhibitors. The method was further optimized to combine inhibitor and kinase screening. By transferring this analytical sensor method to applications with magnetic nanoparticles, a kinase extraction from solution was achieved, using the same surface chemistry as on the sensors.

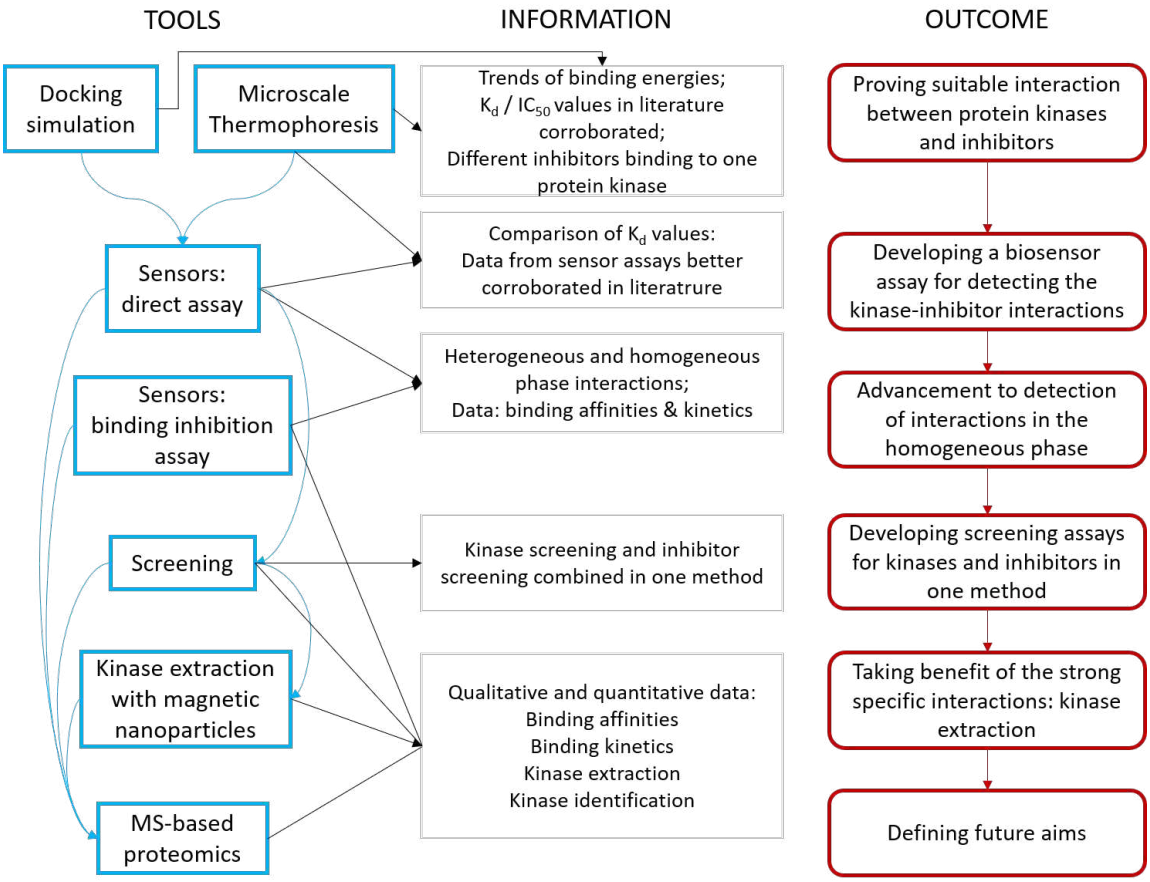


**Figure 5.1:** Schematic overview of the achievements of this thesis.

First, the interactions between protein kinases and inhibitors were investigated by docking simulations. They showed reasonable simulated binding energies for the kinase-inhibitor pairings between -11 to -5.5 kcal/mol, which corroborate the literature data [42, 43, 142, 203]. Docking simulations also showed, that all investigated inhibitors interact with the tested protein kinases in but also outside of the ATP-binding pocket. Even if the strongest binding of every observed kinase-inhibitor pair was simulated inside the binding pocket, the allosteric binding sites also showed strong affinities, which posed challenges in further experiments, where a defined binding

site is required.

Via MST, simulated data were corroborated by titrating various proteins against fluorescently labeled STP. The results demonstrated interactions depending on the kinase concentration but also provided quantitative data on the binding affinity by $IC_{50}$ values of 600-800 nM, well comparable to the literature, see Table 4.4. By competitive displacement assays in MST, fluorescently labeled STP complexed by a mix of proteins, was titrated with the inhibitors BisX, fasudil and imatinib. The slope of the resulting dose-response curve of the experiment with BisX was inverse to the dose-response curves of the direct assays and the competitive displacements assays with fasudil and imatinib. Depending on the binding sites of the small molecules over the whole proteins, which have been theoretically simulated before, the titrated inhibitors (fasudil and imatinib) formed a complex with STP and the kinases, whereas BisX replaced some of the STP-Red molecules from the complex, resulting in inverse slopes of the dose-response curves. The simulated binding sites of the kinases towards the inhibitors provided the basis to substantiate the different dose-response curves in the MST competitive displacement assays. Thus, docking simulations supported the understandings of experimental results.

Results of the docking simulations and MST investigations proved sufficient affinity between the pairs of protein kinases and inhibitors chosen for this work.
This was the basis to develop sensor methods for this set of molecules. Optical biosensor assays for kinase-inhibitor interactions were established successfully using direct assays and binding inhibition assays with RIfS and 1-λ reflectometry. Surface modification and assay conditions were optimized and allowed to gain a deeper understanding of the interaction processes. Direct assays on the sensors were quickly found to be successful, when protein kinases were flushed over the sensor surface and associated to the inhibitors immobilized on the transducer surface. The great advantage of the sensor measurements is their potential to evaluate the kinetics of the binding process, which is important considering further pharmaceutical applications, where the kinetics of drugs interacting with target molecules can influence the efficacy of the drug. Only a few other methods provide kinetic evaluation of bindings, see Table 5.1. Using exponential fits of the binding curves, the association and dissociation rate constants were calculated and the binding affinity determined using the dissociation and association constants, respectively. The calculated dissociation constants were well corroborated by other studies and could well be explained by the corresponding docking simulations and MST data, see Section 4.3.1.
With binding inhibition assays, where the protein kinases were pre-incubated with inhibitor in the homogeneous phase followed by the sensor measurement of this complex, it was also possible, to record the kinase-inhibitor interaction in the homogenoeus phase, using the same sensor setup. Interruptions in the sensograms, due to signals recording the association of the inhibitors in the sample to the sensor surface, were successfully eliminated using 1-λ reflectometry instead of RIfS. With this change of sensor system, successful binding inhibition assays were possible, performed with concentrations of the inhibitors up to a 100-fold molar excess relative to the kinases. The results of the docking simulations suggested, why such high excess of inhibitor was required for the pre-incubation with protein kinases: The simulations showed, that at minimum

nine binding sites for the inhibitors distributed over the whole kinase molecules exist, so there is a complex stoichiometry.
Incomplete regeneration of the kinases binding to the transducer surface was a major challenge of the sensor methods, which could not fully be resolved despite the high number of possible regeneration media tested, unfortunately unsuccessful. Either the regeneration efficiency was too low or the following kinase association on the same sensor for multiple measurement cycles was affected by the previous regeneration steps.
Thus, every sensor measurement required a newly prepared transducer, which reduced the robustness and reproducibility of the results of these developed sensor methods. To overcome these challenges, in a new approach a biotin-streptavidin system was introduced on the transducer, in order to determine the sensor capacity and thus to better compare the signal obtained using different transducers. However, the biotin-streptavidin system did not improve the comparability of the measurements as regeneration was also not achieved with this approach.
Three hypotheses were discussed to explain the failure of regeneration protocols:

1. Covalent bonds formed between the inhibitor on the transducer and the protein kinase.
2. Allosteric interactions were relevant at several parts of the kinases. This combination of interactions leads to several binding sites for each kinase on the transducer.
3. Changes in protein folding created a dense layer of proteins tightly attached to the transducer surface and not allowing any regeneration medium to enter the interfacial layer between the protein kinases and the inhibitor on the transducer.

With surface analytical methods (MALDI-TOF-MS, ATR-IR, Raman microscopy), these hypotheses were tested. Due to the insufficient conductivity of the transducers for MALDI-TOF-MS investigations and the monolayer of kinases on the transducer, which provided an insufficient amount of substance, limits of detection of ATR-IR or Raman microscopy were not met. Thus, it was not possible to gain insight into the nature of the interactions built on the surface during the sensor measurements. However, these findings clearly highlighted the high sensitivity of the sensor measurements, where significant changes in the optical thickness of 1 nm and more, were recorded. A deeper knowledge on the type of interaction might aid in a better regeneration of the surface in the future.

By combining the spotting of the inhibitors on the transducer surface with the internal reference system of the 1-λ reflectometry, the power of this methods was demonstrated with the implementation of an array-based screening. Different inhibitors were spotted in rows on a transducer, generating an array-based sensor. This enabled an inhibitor screening when flushing a specific kinase over the transducer. Different sensor signals on the different inhibitor spots were detected, when kinases in the protein mix were investigated as sample. This clearly confirmed the successful inhibitor screening. Flushing different kinases over the sensor array, as exemplified for the protein mix and purified FAK, showed, that the signals also depended on the

kinases investigated. Not only higher signals for association of the protein mix were detected, but also a different ranking of inhibitor-affinities. These findings clearly show the possibility for a kinase screening with the sensor arrays developed in this work.
With this proof of principle this study showed, that both inhibitor as well as kinase screening were successfully performed with a single setup providing kinetic data.

The strong binding of the kinases to the surfaces with immobilized inhibitors was advantageously used to extract the protein kinases from solutions by magnetic nanoparticles modified with the same surface chemistry as the transducers. STP, covalently bound to the nanoparticles similar to the transducers, was found to capture protein kinases such as FAK or TGFβ in solution. By magnetic separation, these protein kinases were extracted from the solution. The extraction is monitored by the intrinsic protein fluorescence of the tryptophan moieties. The estimate calculation shows, that the particle surface present in one experiment was three to four orders of magnitude higher than the sensor surface covered in the flow cell in RIfS analysis, providing sufficient capacity for the extraction.
The recovery of the kinases from the nanoparticles and sensor surfaces faced challenges, see Section 4.3.2. However, using a tryptic digestion or a successful regeneration, the following scenario could be anticipated: NP-STP are added to a solution containing ATP-dependent protein kinases. The kinases are captured by the nanoparticles and can then be magnetically separated from the solution. Upon a tryptic digestion or a successful regeneration, some peptides or the whole kinases are released to be identified by mass spectrometry. If the regeneration process includes a digestion of the protein, peptide fingerprinting is directly possible. This downstream analysis can provide a complete identification of all kinases captured. More strategies combining these methods to provide comprehensive information on the kinase-inhibitor interactions are given in Section 6. Using the same surface chemistry on transducers and nanoparticles is ideal to directly combine kinase screening of purified kinases, with an identification and a kinetic evaluation from the biosensors.

With regard to future pharmaceutical drug design, the label-free method developed in this thesis provides significant advantages: In the direct assay, the inhibitor is covalently bound to the sensor surface, which is comparable to a labeling in other methods such as luminescent assays or most MST methods. The part of the small molecule involved in the chemical linkage to the surface/to the labeling cannot take part in the interaction with the kinases. In the binding inhibition assay, the interaction of the protein kinases with a free and unbound inhibitor is analyzed, however, via detection of the free kinases interacting with the inhibitors bound to the transducer surface. The possibility to record interactions in the homogeneous phase, is a great advantage of the binding inhibition assay over the direct assay, regarding the unaltered molecular structure of the inhibitor. Furthermore, binding inhibition assays provide investigations on kinases interacting with inhibitors, that do not provide suitable functional groups for the immobilization to the transducer surface. For this, an inhibitor with low selectivity but high affinity to a broad range of kinases, such as STP, can be immobilized on the sensor surface, detecting binding inhibitions with different inhibitors in the homogeneous phase.

The analytical method developed in this work provides a label-free and time-resolved characterization of protein kinase-inhibitor interactions. Sensor investigations provide kinetic data, in contrast to nearly all classical methods such as radiometric and luminescent assays, assays with separation techniques and mass spectrometry or electochemical sensors. Binding rates, important to understand the kinetic of the binding process between protein kinases and possible drug candidates, can be evaluated. Furthermore, interactions can be observed directly in the heterogeneous phase but also indirectly in the homogeneous phase (direct assay vs. binding inhibition assay). Another important advantage of the biosensor method developed here, is the possibility for screening both kinases and inhibitors with only one method, as proven exemplarily in this thesis. This is a great advancement over most commonly known analysis methods, where, if at all, only one binding partner can be screened, see Table 5.1.
As often discussed, see Section 2, docking simulations provide a virtual screening of both, kinases and inhibitors, but only calculate theoretical data, which have to be verified by experiments. Some methods allowing kinase and inhibitor screening, such as capillary electrophoresis or thermal stability shift assay, are only described for the screening of one target group alone [9, 55–59, 72]. MST is able to screen kinases or inhibitors, but does not provide kinetic data compared to the sensor measurements, see Table 5.1. With SPR, as a competitive sensor to the reflective biosensors of this work, kinase screening is difficult to be implemented given that the kinase is immobilized on the sensor surface. In the homogeneous phase, only the method KiNativ might provide both inhibitor and kinase screening, but this has not yet been discussed in the literature [65, 66]. In the heterogeneous phase, electrochemical sensors might provide a simultaneous screening of protein kinases and inhibitors, when the recognition elements can be monitored specifically in an array-based sensor, similar to the array-based 1-λ reflectometry as displayed in Section 4.5. This is already published as single screening of kinases or inhibitors [74, 76–78]. Only biolayer interferometry, which is also based on reflectometry, such as RIfS, can currently provide inhibitor and kinase screening with one setup, as well as evaluating kinetic data [85–88].

Table 5.1 clearly shows, that all requirements for a comprehensive analysis of protein kinases interacting with inhibitors, combined with screening for both binding partners, are achieved with the biosensor assays, developed in this work. The sensor and nanoparticle applications developed here, bring highly applicable systems for a comprehensive analysis, when combined with other methods, as further discussed in Section 6 on the basis of the Figures 6.2 and 6.3. In the current development status of the sensor investigations, a coupling to further MS-based protein identification is only possible with MALDI-MS and classical proteomics should be possible, as outlined in Figure 5.1.

**Table 5.1:** Comparison of classic screening methods for protein kinase interactions with the methods developed in this work. Identification of kinases is only possible with methods combined with a mass spectrometric analysis. The methods of optical sensors, developed in this work, are in bold. References are given more detailed in Table 2.1 from in the Introduction (Section 2).

| **Method** | **Labeling** | **Screening** | **HTS** | **Cell-based** | **Affinity** | **Kinetic** |
|---|---|---|---|---|---|---|
| Docking Simulation | - | kinases and inhibitors | yes | - | - | - |
| Radiometric | yes | kinases or inhibitors | no | no | (yes) | no |
| Luminescent | yes | kinases or inhibitors | yes | (yes) | (yes) | no |
| Separation techniques (-MS) | (yes) | kinases and/or inhibitors | (yes) | (yes) | (yes) | no |
| MST | (yes) | kinases or inhibitors | no | yes (cell lysate) | yes | no |
| Electrochemical sensors | no | kinases and/or inhibitors | no | (yes) | (yes) | no |
| **Optical sensors (deveolped in this work)** | **no** | **kinases and/or inhibitors** | **yes** | **yes** | **yes** | **yes** |

"The science of today is the technology of tomorrow."
Edward Teller

# 6 Outlook

On the basis of the results of this thesis, further optimization and investigations are engaged in order to deepen the knowledge gained on the binding processes or to further advance the analytical methods.

## 6.1 Data Improvement by Further Investigation of Standard Methods

Simulations in the ATP-binding pocket can be improved by more detailed definitions of the GridBox used in order to better define the area of interest. In order to generate further theoretical data, binding affinities can be simulated with protein kinase structures, that are calculated using artificial intelligence (AI). A comparison of the data simulated by protein structures which were obtained by crystallographic data and the AI-based ones, can optimize the results by using information from different sources.
MST experiments can be extended, for instance by reversing the competitive assay: another inhibitor than STP is fluorescently labeled and in complex with the protein kinases and presented at a constant concentration, while non-labeled STP is titrated. With regard to the different directions of the dose-response curves of this work, it would be interesting to see the competitive behavior and resulting dose-response curves of these inverted assays. As an alternative, both the protein kinases and STP could be labeled with different fluorophores to simultaneously and more accurately monitor the molecular diffusion and interaction of each compound in the capillaries.
Investigations on further protein kinases and inhibitor interactions can be broadened by comparing the MST data with the improved docking simulations. However, with regard to the results of this work, it must always be considered that the affinity data from MST can only provide trends for affinities, but the dissociation constants, determined in this thesis, are higher than previously published data.

## 6.2 Analyzing Allosteric Binding

The relevance of the knowledge on the presence of allosteric binding became visible in this thesis in the binding inhibition assays conducted with 1-λ reflectometry as well as in the docking simulations and MST investigations. E.g. inhibition of the kinases in the homogeneous phase was only reached, when the inhibitor was added in a large excess, which was explained by a complex stoichiometry with multiple binding sites, see Section 4.3.4. A strategy to better quantify the specific and allosteric bindings is proposed here, based on the assumption, that all allosteric interactions can be detected with the sensor in the heterogeneous phase.
To shed light on allosteric interactions a combination of a binding inhibition assay on a sensor with the covalent labeling approach of the method KiNativ [65, 66] can be conducted. The

experiments need streptavidin to be immobilized on the transducer surface as recognition element, expected to bind the biotin-label from the KiNativ method. This biotin-tag is previously linked to ATP. By the specific interaction of ATP in the ATP-binding pocket of a protein, the biotin-tag changes its binding partner from ATP to the protein: A lysine moiety of the kinase in the binding pocket reacts with the biotin-tag to covalently label the protein with the biotin label. As in the KiNativ approach, ATP then leaves the binding pocket. This labeling process can be prevented by inhibitors successfully competing with ATP for the binding pocket. Combined with RIfS, the following experiment is possible:

1. Recording a sensor signal of a normal binding inhibition assay on a streptavidin-transducer, as in Section 4.3.4: As the sample only includes protein kinases and inhibitors and due to the lack of biotin, the sensor signal obtained here serves as a baseline, as it is expected to remain constant, as displayed in Figure 6.1 in Curve 1.

2. Recording a sensor signal of biotin-labeled kinases on the streptavidin-transducer: While the biotin, covalently linked to the protein binding pocket, binds to the streptavidin on the sensor, an increase in the signal is expected, see Figure 6.1, Curve 2.

3. Recording a sensor signal of a kinase solution, that was pre-incubated with an inhibitor and then biotin-labeled, on a streptavidin-transducer: In the pre-incubation a fraction of protein kinases is inhibited by the inhibitors specifically in the binding pocket. Adding biotin-tagged ATP to the pre-incubated solution, all binding pockets blocked by the inhibitor are expected to remain unlabeled by the biotin-tag. Hence, for all inhibitors interacting specifically in the ATP-binding pocket of the kinases, which prevents the biotin labeling, no binding to the streptavidin-transducer is expected. If a signal is recorded, labeling was possible in the binding pocket and interactions of the inhibitors with the kinases in the pre-incubation are only allosteric. Thus, it is expected to detect a lower amount of kinases interacting with the streptaviding-transducer via the biotin-label, as shown in Figure 6.1, Curve 3. Then, the difference in the sensor signal of Curves 2 and 3 in Figure 6.1 reveals of direct interactions of the inhibitor in the binding pocket. Titration experiments can provide information on the stoichiometry of the binding between protein kinases and inhibitors in the homogeneous phase and the equilibrium between inhibitor and ATP.

These experiments can also be adapted to direct assays on an AMD-inhibitor sensor, when the ATP-binding pocket becomes blocked by the KiNativ labeling, only by the covalent bond formation of the linker with the lysine in the binding pocket. The labeling with biotin on the tag is not necessary. Performing direct assays, the covalent labeling in the binding pocket might prevent the specific interaction of the protein in its binding pocket with the inhibitor on the transducer surface. Again, sensograms only show allosteric interactions, if the binding pocket is saturated with the KiNativ tag. Comparing the sensograms of the investigations with labeled and non-labeled proteins might provide information on the specific interaction inside the

binding pocket. Upon a titration of the tag, information on the binding stoichiometry between protein kinases and their inhibitors on the sensor surface might be determined. A similar set of sensograms should be observed as in Figure 6.1, where Curve 2 shows the signal of the label-free and Curve 3 of the labeled protein, interacting with the sensor surface. The difference in these signals indicates the specific interactions of the protein kinases in the binding pocket with the inhibitors on the transducer surface.

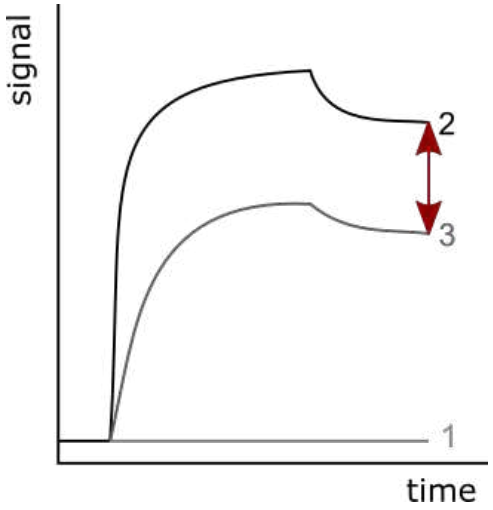


**Figure 6.1:** Possible sensogram of RIfS investigations on a streptavidin-transducer to record the allosteric interactions between protein kinases and inhibitors. 1: Normal binding inhibition assay without any compounds interacting with streptavidin. 2: Biotin-labeled kinases (compare the KiNativ method by Patricelli et al. [65, 66]) interacting with the streptavidin immobilized on the transducer surface, creating a RIfS signal. 3: Inhibited kinases were labeled with biotin as in 2. Only ATP-binding pockets void of inhibitors can be labeled and thus interact with streptavidin, evolving changes in the optical thickness. Specific inhibition in the ATP-binding pocket is thus visible by the difference in the binding curves 2 and 3.

A combination of these strategies including biosensor investigations and KiNativ labeling can be expanded using magnetic nanoparticles immobilized with streptavidin. In the binding inhibition assay, all protein kinases that were not inhibited in the homogeneous phase during the pre-incubation, and were therefore labeled with the biotin-tag, can be extracted from the sample solution with the streptavidin nanoparticles. The remaining protein kinases with inhibitors interacting in the ATP-binding pocket can then be detected, when these complexes interact allosterically with the inhibitor immobilized to the transducer. As the biotin-labeled kinases are removed from the sample, the sensor signal will decrease, compared to the sensor signal of the same experiment without prior nanoparticle-based kinase extraction, compare Figure 6.1, Curve 3 and 2. The difference of these sensograms provides information on the specific binding of the inhibitor to the binding pocket of the kinases and again, titration experiments can improve the understanding of relevant processes.

## 6.3 Achieving a Better Understanding of the Binding Processes

**Surface Analysis**

Further analysis techniques to better understand the processes on the transducer surface are discussed shortly: As shown in Section 4.6, the intrinsic tryptophan fluorescence can be used for protein kinase detection. A fluorescence signal might thus be recorded also for kinases associated to the transducer, albeit the sensitivity of a monolayer of kinases in combination with the development of a suitable setup will be challenging. Protein monolayers were detected after fluorescence-labeling or indirectly via fluorescence correlation spectroscopy [204, 205]. In contrast, direct detection via the native fluorescence of tryptophan was not found in other studies. Classical analysis via the light absorption of proteins with UV-Vis spectroscopy might be impaired by the absorption of STP itself, which is bound to the transducer surface. As seen in Figure 4.12, the absorption of STP (250-400 nm) overlays the absorption bands of proteins at 290 nm. Also here, the monolayer of kinases on the transducer might challenge the limits of detection of this spectroscopic technique.

The spectroscopic methods (ATR-IR and Raman) used in this thesis, were not successful in providing information on the type of binding between protein kinases and the inhibitors on the transducer surface. It is open, if surface enhancement in IR- or Raman investigations would improve the results, see Section 4.4.2 and 4.4.3. These enhanced methods use a metal layer in the sensing basis. On the one hand, this is difficult to be implemented into the transducer and on the other hand, a metal layer would impair RIfS. Microscopy methods, such as atomic force microscopy or scanning electron microscopy should be able to detect the differences of a transducer without and with associated kinases on its surface. It might even be possible to monitor the tertiary structure of the protein on the surface to a certain extent, if there is a flat dense layer generated by the straddling of the protein or rather a cluster building of proteins on the surface [206–211]. However, further analysis of the processes on the transducer surface for RIfS investigations require an intense research and a high operating expense in order to gain further information.

**Other Studies**

As the influence of the light on the interaction between protein kinases and inhibitors on the transducer was not fully understood from the results and the overall discussion, see Section 4.3.2 and 5, further experiments are planned. By the assumption that the kinases covalently bind to STP immobilized on the transducer surface, a MALDI-TOF-MS investigation in solution might provide the intended information: Irradiating a solution of protein kinases and STP by the RIfS light source can simulate the possible photochemical processes on the transducer surface in the homogeneous phase. The kinase-inhibitor-linked product generated can be analyzed by MALDIT-TOF-MS. If free STP signals are detected in this sample, with the same intensity as the reference sample without protein kinases, a covalent bond between the STP and the protein kinases can be ruled out. If there are only small or even no signals found for free STP, but instead kinase signals differing in the mass related to the covalently linked STP, a covalent bond between the molecules is proven.

Since STP or fragments thereof were found to be ionized and detected by MALDI-TOF-MS investigations without matrix, this complete experiment can even be performed without matrix. Only unbound STP or STP involved in intermolecular interactions (but not covalently bound) with the kinases should then be detected. If these experiments result in a conformation of the covalent bond hypothesis, a comparison of these tests with experiments using green light as irradiated during the 1-λ reflectometry, and with the laboratory light, present during sample preparation, are required, in order to find the cause for the covalent bond formation.

## 6.4 Optimization of the Reproducibility in Producing the Sensor Surface

A major focus for future research is the search for another auxilliary-system to enhance repeatability of the sensor measurements by providing a clear reference and ideally a possibility for a successful regeneration. For example, DNA hybridization can be investigated. For the hybridization, only small DNA/RNA fragments are required, as shown for SPR and RIfS measurements with oligonucleotides in the scale of 15 bases [181–184]. Instead of the biotin-streptavidin system already tested in this thesis in Section 4.3.3, a single DNA or RNA strand is covalently bound to the transducer surface as the last step of the transducer modification. This process can be monitored in a first step in the measurement protocol. Flushing a solution of the complementary strand linked to an inhibitor over the sensor, the two strands hybridize and by that, the inhibitor becomes laterally bound to the transducer. The changes in optical thickness can be used as a reference indicating the capacity of the inhibitor on the sensor surface. Now, analysis of the association of protein kinases, as performed in direct or binding inhibition assays, is possible. All auxiliary-systems can also be implemented into the modification of the nanoparticles to enhance kinase extraction from solutions. This referencing strategy guarantees a high comparability between single measurements, each on a new transducer.
Regeneration may now be achieved separating the hybridized double strand by HCl, which enables the reuse of the sensor [212, 213]. With the option to use the capacity of the sensor surface as a reference and the re-use of sensors after successful regeneration, high throughput analysis becomes possible at low costs.
This improvement is further combined with an expected higher reproducibility and comparability of assays and precision of thermodynamic and kinetic data. With multiple measurements using the same transducer and with the introduction of flow channels into the flow cell of 1-λ reflectometry, the development of a high throughput method seems possible. With these channels, different kinases or different kinase concentrations as samples can be monitored in parallel measurements on the same sensor. This development would lead to a high-throughput method to simultaneously conduct inhibitor and kinase screening, combined with an evaluation of the binding affinities as well as kinetic data of the kinase-inhibitor interactions.

## 6.5 Structure Modification of Drug Targets

Binding inhibition assays on the sensors can be performed by two strategies, depending on the inhibitor bound to the transducer surface. In one strategy, the inhibitors immobilized to the surface and the inhibitors for the pre-incubation in the homogeneous phase are the same. This provides a comparison of the binding process of this specific kinase-inhibitor pair in the homogeneous vs. the heterogeneous phase. In another strategy, a non-specific inhibitor with high affinity, such as STP, is immobilized to the transducer surface and different inhibitors are chosen in the homogeneous phase for the binding inhibition assay. Thus, the structure of the small molecules as drug targets can be varied slightly, e.g. by changing single functional groups. This method provides the screening of highly promising inhibitor structures and thus enhances drug design.

## 6.6 Towards Comprehensive Analytical Information: Strategies to Combine Different Methods

As discussed in Section 2 and summarized in Table 5.1, methods providing information on protein kinases interacting with inhibitors should meet following requirements:

- label-free methods to monitor the binding in unaltered molecular structures of the binding partners
- evaluating affinity data to define the binding strength
- evaluating kinetic data to define the binding process
- screening of both, kinases and inhibitors to define the specificity of possible drugs and identify new relevant drug candidates
- cell-based applications to evaluate all data in pharmaceutically relevant biological environments
- high throughput to save time and quickly provide larger datasets

To meet these requirements, different methods have to be combined.
Regarding the successful proof of principle of a screening method with the array-based 1-λ reflectometry presented in this thesis, a broader screening for a high number of protein kinases and inhibitors becomes possible now. Not only the search for new small molecules acting as inhibitors is possible, including drug design, but also the screening of protein kinases, binding to specific inhibitors. Finally, the evaluation of the kinetics of the binding can be obtained.
In order to improve this highly promising methods, a coupling with MS analysis can enhance the interpretation of all data. Coupling applications of biosensor measurements with MS analysis have already been investigated for SPR or RIfS in combination with MALDI-MS. MS-based

identification of bound proteins, glycoproteins, antibodies or enzyme inhibitors was shown. Mostly, MALDI was applied directly to the transducer surface after matrix addition. For SPR, the gold-layer on the transducer aids in the ionization process, while for RIfS a special transducer basis with an ITO-layer was produced [214–218].
The kinetic data from the sensor evaluations, developed in this work, can be amplified with qualitative data of the kinases, such as amino acid sequences, depending on the MS application. As MS analysis is destructive, it should always be the last step in the analytical process. Connecting the sensor methods or nanoparticle applications with an MS-approach is possible in three combinations:

1. Biosensor transducers are used as MALDI targets (as already tried in this thesis). By finding a construct to improve the conductivity of the transducer, intact proteins might be detected with MS. Screening investigations, e.g. on array-based transducers for 1-λ reflectometry, can be continued since the spatial resolution of MALDI can accurately ionize specific spots. However, after the MALDI application, the transducer surface is destroyed and cannot be reused. Advantageously, MALDI investigations from this thesis are possible without a regeneration step.

2. Considering a successful regeneration, kinases eluted from the transducer surface can be identified with mass spectrometry. For this scenario, RIfS or 1-λ reflectometry are the sensor methods of choice, as the regeneration process does not distinguish between proteins. Thus, only one protein should be associated to the transducer surface and regenerated for further analysis. Furthermore, the LOD of the mass spectrometric approach is more likely to be reached with a higher amount of kinases interacting with a larger area of the sensor surface. Regeneration with a tryptic digestion provides downstream analysis of the proteins via peptide mapping.

3. The unsuccessful regeneration of the protein kinases from the transducer surfaces limits the amount of kinases eluted, so the LOD of MS analysis may not be met. Thus, nanoparticles can be used, instead of the biosensor applications. The modified nanoparticles reach a higher coverage, thus a higher amount of kinases associated to the particles and thus a higher amount of kinases can be captured and possibly be eluted. Hence, protein identification is more likely than in strategy 2. Auxiliary-systems, such as described for the transducer, can be adapted to the nanoparticles, improving the regeneration process.

### 6.6.1 From Simulations to Sensor Arrays Developed in this Thesis: Broad Screening

Combining simulation methods with experimental assays can reduce costs and time. Using this strategy with the biosensors, developed in this work, broad analytical information is obtained, displayed in the scheme in Figure 6.2.
With docking simulations a larger number of protein kinases and inhibitors can theoretically be

screened for their binding energies. The best pairs of kinases interacting with inhibitors can be chosen for further experimental studies, hence, the number of compounds to be further investigated is reduced. With biosensor assays, introduced as screening with 1-λ reflectometry and inhibitors spotted on the transducer surface, the interactions of these specific kinase-inhibitor pairs can be determined. The sensor assays provide additional data on the binding affinity (thermodynamic) and on the binding kinetics and defines the specificity of the tested kinases and inhibitors, finding the matches with the highest binding affinity.

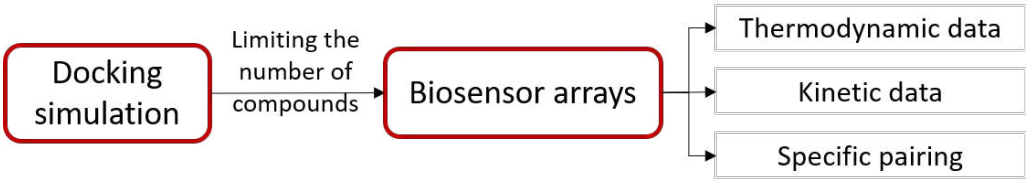


**Figure 6.2:** Docking simulations are combined with the biosensor assay from 1-λ reflectometry, developed in this thesis. Via docking simulations, protein kinases and inhibitors with best binding energy can be determined and then further analyzed with biosensor assays in a screening with an evaluation of thermodynamic and kinetic data.

### 6.6.2 Generating Comprehensive Analytical Information from Biological Samples

To become fully comprehensive, kinases (or inhibitors) have to be identified, which can only be accomplished using mass spectrometry. A strategy including kinase identification is shown in Figure 6.3. The single steps of this strategy are highlighted in color. Combining all of these combinations provides a comprehensive analytical platform for the screening of kinase-inhibitor interactions including kinase identification.

1. (green box) Purified kinases are investigated with regard to their binding behavior with inhibitors via an array-based biosensor assay, similar to Figure 6.2. This screening method provides first information on the types of kinases and their interactions with inhibitors, as well as thermodynamic and kinetic information on the binding process. Regarding the inhibitors immobilized on the transducer surface, a general affinity towards a non-specific inhibitor, such as STP, or the affinity to specific inhibitors can be determined. As discussed in Section 6.5, different binding inhibition assays provide different information regarding the interaction in the homogeneous or heterogeneous phase. This method provides thermodynamic and kinetic data of the binding process and aids in defining the specificity of the binding pairs.

2. (green and blue box) The screening method from Step 1 can also be performed with a biological sample, such as a cell lysate. Here, a comparison of the thermodynamic and kinetic data from purified kinases vs. kinases in the cell lysate provides information on influences on the kinase-inhibitor interactions by compounds in the cell lysate.

3. (green, blue and yellow box) Due to the similarity of the transducer surface and the surface of the magnetic nanoparticles, promising inhibitors can be immobilized on the particle

surface. This enables the extraction of kinases interacting with a specific inhibitor in a biological sample, such as a cell lysate. Using nanoparticles, this step provides a purification of these kinases from the cell lysate, possibly aided by chromatographic fractionation. Then, in-depth characterization of their binding kinetics and thermodynamic with the sensor array in Step 1 is possible.

4. (dark red box) Extracted kinases can be identified with MS application on a molecular level.

These combinations consider all advantages of the sensor measurements and thus provide a complete thermodynamic, kinetic and proteomic investigation of protein kinases interacting with inhibitors.

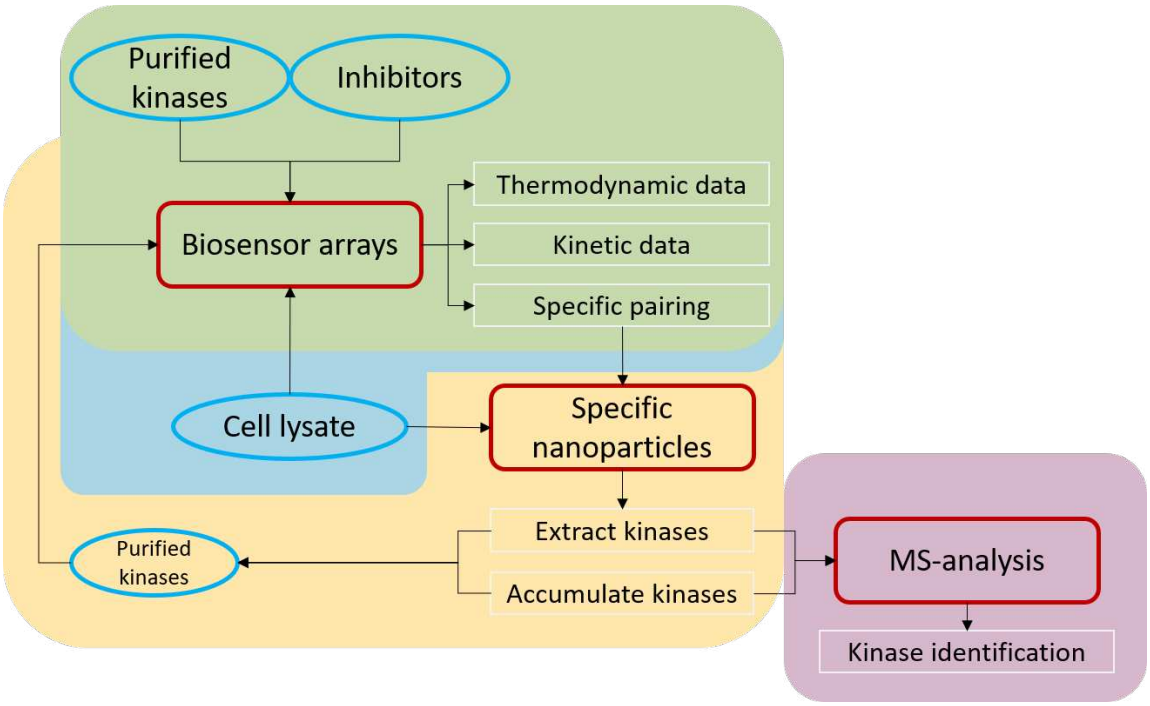


**Figure 6.3:** Scheme of a comprehensive platform for protein kinases interacting with inhibitors, also in biological samples. With the array-based screening, thermodynamic and kinetic data and the specific binding of the kinase-inhibitor pairs is determined from purified kinases (green box) and kinases in a cell lysate (green and blue box). Different binding inhibition assays can be performed. With this knowledge, all kinases, binding to a specific inhibitor immobilized on the nanoparticles, can be extracted from biological samples (e.g. cell lysate). Kinase-inhibitor interactions of these purified kinases can be further investigated with the biosensor array (green, blue and yellow box) and additionally, a kinase identification is provided by proteomics using MS analysis (wine red box).

# References

[1] R. Siegel, A. Giaquinto, and A. Jemal. Cancer statistics, 2024. *CA-Cancer J Clin*, 74:12–49, 2024.

[2] R. Roskoski. Properties of FDA-approved small molecule protein kinase inhibitors: A 2021 update. *Pharmacol Res*, 165:105463, 2021.

[3] O. Birkert and G. Gauglitz. Development of an assay for label-free high-throughput screening of thrombin inhibitors by use of reflectometric interference spectroscopy. *Anal Bioanal Chem*, 372:141–147, 2002.

[4] M. Rothmund, A. Schütz, A. Brecht, G. Gauglitz, G. Berthel, and D. Gräfe. Label free binding assay with spectroscopic detection for pharmaceutical screening. *Fresenius J Anal Chem*, 359:15–22, 1997.

[5] M. Ewald, A.Le Blanc, G. Gauglitz, and G. Proll. A robust sensor platform for label-free detection of anti-salmonella antibodies using undiluted animal sera. *Anal Bioanal Chem*, 405:6461–6469, 2013.

[6] BS. Chhikara and K. Parang. Chemical biology global cancer statistics 2022: The trends projection analysis. *Chem Biol Lett*, 10:1–16, 2023.

[7] R. Siegel, K. Miller, N. Wagle, and A. Jemal. Cancer statistics, 2023. *CA-Cancer J Clin*, 73:17–48, 2023.

[8] S. Klaeger, S. Heinzlmeir, M. Wilhelm, H. Polzer, B. Vick, P. Koenig, M. Reinecke, B. Ruprecht, S. Petzoldt, C. Meng, J. Zecha, K. Reiter, H. Qiao, D. Helm, H. Koch, M. Schoof, G. Canevari, E. Casale, S. Depaolini, A. Feuchtinger, Z. Wu, T. Schmidt, L. Rueckert, W. Becker, J. Huenges, A. Garz, B. Gohlke, D. Zolg, G. Kayser, T. Vooder, R. Preissner, H. Hahne, N. Tõnisson, K. Kramer, K. Goetze, F. Bassermann, J. Schlegl, H. Ehrlich, S. Aiche, A. Walch, P. Greif, S. Schneider, E. Felder, J. Ruland, G. Médard, I. Jeremias, K. Spiekermann, and B. Kuster. The target landscape of clinical kinase drugs. *Science*, 358:1148–1165, 2017.

[9] O. Fedorov, B. Marsden, V. Pogacic, P. Rellos, S. Mueller, A. Bullock, J. Schwaller, M. Sundstroem, and S. Knapp. A systematic interaction map of validated kinase inhibitors with Ser/Thr kinases. *PNAS*, 104:20523–20528, 2007.

[10] HJ. Boehm and G. Klebe. What can we learn from molecular recognition in protein–ligand complexes for the design of new drugs? *Angew Chem Int Edit*, 35:2588–2614, 1996.

[11] X. Du, Y. Li, Y. Xia, S.Ai, J. Liang, P. Sang, X. Ji, and S. Liu. Insights into protein–ligand interactions: Mechanisms, models, and methods. *Int J Mol Sci*, 17:144, 2016.

[12] K. van der Saal. *Biochemie*. Springer-Verlag GmbH Deutschland, 2020.

[13] J. Slon-Usakiewicz, J. Dai, W. Ng, J. Foster, E. Deretey, L. Toledo-Sherman, P. Redden, A. Pasternak, and N. Reid. Global kinase screening. applications of frontal affinity chromatography coupled to mass spectrometry in drug discovery. *Anal Chem*, 77:1268–1274, 2005.

[14] K. Coan, J. Ottl, and M. Klumpp. Non-stoichiometric inhibition in biochemical high-throughput screening. *Expert Opin Drug Discov*, 6:405–417, 2011.

[15] G. Hamilton, H. Chen, G. Deshmukh, C. Eigenbrot, R. Fong, A. Johnson, P.r Kohli, P.. Lupardus, B. Liederer, S. Ramaswamy, H. Wang, J. Wang, Z. Xu, Y. Zhu, D. Vucic, and S. Patel. Potent and selective inhibitors of receptor-interacting protein kinase 1 that lack an aromatic back pocket group. *Bioorganic Med Chem Lett*, 29:1497–1501, 2019.

[16] P. Singh and W. Ward. Alternative assay formats to identify diverse inhibitors of protein kinases. *Expert Opin Drug Discov*, 3:819–831, 2008.

[17] M. Williams. *Protein-ligand interactions*, chapter 1, pages 3–34. Humana Press Springer, Methods in Molecular, second edition, 2013.

[18] S. Omura, Y. Iwai, A. Hirano, A. Nakagawa, J. Awaya, H. Tsuchiya, Y. Takahashi, and R. Asuma. A new alkaloid AM-2282 of streptomyces origin taxonomy, fermentation, isolation and preliminary characterization. *J Antibiotics*, 30:275–282, 1977.

[19] S. Omura, Y. Sasaki, Y. Iwai, and H. Takeshima. Staurosporine, a potentially important gift from a microorganism. *J Antibiotics*, 48:535–548, 1995.

[20] H. Nakano, E. Kobayashi, I. Takahashi, T. Tamaoki, Y. Kuzuu, and H. Iba. Staurosporine inhibits tyrosine-specific protein kinase activity of Rous sarcoma virus transforming protein p60. *J Antibiotics*, 40:706–708, 1987.

[21] A. Disney, B.Kellam, and L. Dekker. Alkylation of staurosporine to derive a kinase probe for fluorescence applications. *Chem Med Chem*, 11:972–979, 2016.

[22] D. Treiber C. Atteridge M. Azimioara Michael G Benedetti T. Carter P. Ciceri P. Edeen M. Fabian, W. Biggs and M. Floyd. A small molecule–kinase interaction map for clinical kinase inhibitors. *Nat Biotechnol*, 23:329–336, 2005.

[23] P. Radhika, M. Kumar, and K. Nagasree. Protein kinase inhibitors from microorganisms. *Stud Nat Prod Chem*, 44:403–445, 2015.

[24] A. Gescher. Staurosporine analogues — pharmacological toys or useful antitumour agents? *Crit Rev Oncology/Hematology*, 34:127–135, 2000.

[25] A. Dar and K. Shokat. The evolution of protein kinase inhibitors from antagonists to agonists of cellular signaling. *Annu Rev Biochem*, 80:769–795, 2011.

[26] P. Cohen, D. Cross, and P. Jaenne. Kinase drug discovery 20 years after imatinib: Progress and future directions. *Nat Rev Drug Discov*, 20:551–569, 2021.

[27] R. Lorenz, J. Wu, F. Herberg, S. Taylor, and R. Engh. Drugging the undruggable: How isoquinolines and PKA initiated the era of designed protein kinase inhibitor therapeutics. *Biochem*, 60:3470–3484, 2021.

[28] M. Attwood, D. Fabbro, A. Sokolov, S. Knapp, and H. Schioeth. Trends in kinase drug discovery: Targets, indications and inhibitor design. *Nat Rev Drug Discov*, 20:839–861, 2021.

[29] S. Laufer, J. Bajorath, M. Gehringer, N. Gray, S. Frye, and C. Lindsley. Publication criteria and requirements for studies on protein kinase inhibitors - What is expected? *J Med Chem*, 65:6973–6974, 2022.

[30] J. Gao, J. Jian, Z. Jiang, and A. van Schepdael. Screening assays for tyrosine kinase inhibitors: A review. *J Pharm Biomed Anal*, 223:115166, 2023.

[31] J. Landro, I. Taylor, W. Stirtan, D. Osterman, J. Kristie, E. Hunnicutt, P. Rae, and P. Sweetnam. HTS in the new millennium: The role of pharmacology and flexibility. *J Pharmacol Toxicol Methods*, 44:273–289, 2000.

[32] N. Fathi, A. Saadati, M. Alimohammadi, H. Abolhassani, S. Sharifi, N. Rezaei, and M. Hasanzadeh. Biosensors for the detection of protein kinases: Recent progress and challenges. *Microchem J*, 182:107961, 2022.

[33] Y. Wang and H. Ma. Protein kinase profiling assays: A technology review. *Drug Discov Today Technol*, 18:1–8, 2015.

[34] S. Lemeer, C. Zoergiebel, B. Ruprecht, K. Kohl, and B. Kuster. Comparing immobilized kinase inhibitors and covalent ATP probes for proteomic profiling of kinase expression and drug selectivity. *J Proteome Res*, 12:1723–1731, 2013.

[35] P. Czodrowski, G. Hoelzemann, G. Barnickel, H. Greiner, and D. Musil. Selection of fragments for kinase inhibitor design: Decoration is key. *J Med Chem*, 58:457–465, 2015.

[36] U. Danielson. *Interaction kinetic data generated by surface plasmon resonance biosensors and the use of kinetic rate constants in lead generation and optimization.* WILEY-VCH, Weilheim, Germany, 2012.

[37] D. Duran, P. Hermosilla, T. Ropinski, B. Kozlikova, A. Vinacua, and P.Vazquez. Visualization of large molecular trajectories. *IEEE Trans Vis Comput Graph*, 25:987–996, 2019.

[38] S. Davies, H. Reddy, M. Caivano, and P. Cohen. Specificity and mechanism of action of some commonly used protein kinase inhibitors. *Biochem J*, 351:95–105, 2000.

[39] H. Nordin, M. Jungnelius, R. Karlsson, and O. Karlsson. Kinetic studies of small molecule interactions with protein kinases using biosensor technology. *Anal Biochem*, 340:359–368, 2005.

[40] Y. Jia, C. Quinn, A. Gagnon, and R. Talanian. Homogeneous time-resolved fluorescence and its applications for kinase assays in drug discovery. *Anal Biochem*, 356:273–281, 2006.

[41] Y. Hu and J. Bajorath. Exploring the scaffold universe of kinase inhibitors. *J Med Chem*, 58:315–332, 2015.

[42] O. Trott and A. Olson. AutoDock Vina: Improving the speed and accuracy of docking with a new scoring function, efficient optimization, and multithreading. *J Comput Chem*, 31:455–461, 2010.

[43] H. Guterres and W. Im. Improving protein-ligand docking results with high-throughput molecular dynamics simulations. *J Chem Inf Model*, 60:2189–2198, 2020.

[44] J. Herbert, E. Seban, and J. Maffrand. Characterization of specific binding sites for [3H]-staurosporine on various protein kinases. *BBRC*, 171:189–195, 1990.

[45] F. Meggio, A. Deana, M. Ruzzene, A. Brunati, L. Cesaro, B. Guerra, T. Meyer, H. Mett, D. Fabbro, P. Furet, G. Dobrowolska, and L. Pinna. Different susceptibility of protein kinases to staurosporine inhibition. *Eur J Biochem*, 234:317–322, 1995.

[46] T. Tamaoki and H. Nakano. Potent and specific inhibitors of protein kinase C of microbial origin. *Biotech*, 8:732–735, 1990.

[47] J. Oishi, X. Han, J. Kang, Y. Asami, T. Mori, T. Niidome, and Y. Katayama. High-throughput colorimetric detection of tyrosine kinase inhibitors based on the aggregation of gold nanoparticles. *Anal Biochem*, 373:161–163, 2008.

[48] D. Lavogina, M. Lust, I. Viil, N. Koenig, G. Raidaru, J. Rogozina, E. Enkvist, A. Uri, and D. Bossemeyer. Structural analysis of ARC-type inhibitor (ARC-1034) binding to protein kinase A catalytic subunit and rational design of bisubstrate analogue inhibitors of basophilic protein kinases. *J Med Chem*, 52:308–321, 2009.

[49] Y. Li, W. Xie, and G. Fang. Fluorescence detection techniques for protein kinase assay. *Anal Bioanal Chem*, 390:2049–2057, 2008.

[50] H. Zegzouti, J. Alves, T. Worzella, G. Vidugiris, G. Cameron, J. Vidugiriene, and S. Goueli. *Screening and profiling kinase inhibitors with a luminsecenz ADP detection platform*. Promega Corporation, 2011.

[51] M. Davis, J. Hunt, S. Herrgard, P. Ciceri, L. Wodicka, G. Pallares, M. Hocker, D. Treiber, and P. Zarrinkar. Comprehensive analysis of kinase inhibitor selectivity. *Nat Biotechnol*, 29:1046–1051, 2011.

[52] E. Varkondi, E. Schäfer, Györgyi Bökönyi, Tibor Gyökeres, Laszlo Örfi, Istvan Petak, Akos Pap, Orsolya Szokoloczi, and R. Keri, G.and Schwab. Comparison of ELISA-based tyrosine kinase assays for screening EGFR inhibitors. *J Recept Signal Transduct*, 25:45–56, 2005.

[53] S. Bauer, M. Gehringer, and S. Laufer. A direct enzyme-linked immunosorbent assay(ELISA) for the quantitative evaluation of JanusKinase 3 (JAK3) inhibitors. *Anal Methods*, 6:8817–8822, 2014.

[54] M. Goetterta, S. Luika, R. Graeserb, and S. Laufera. A direct ELISA assay for quantitative determination of the inhibitory potency ofsmall molecules inhibitors for JNK3. *J Pharm Biomed Anal*, 55:236–240, 2011.

[55] H. Nehmé, R. Nehmé, P. Lafite, S. Routier, and P. Morin. Human protein kinase inhibitor screening by capillary electrophoresis using transverse diffusion of laminar flow profiles for reactant mixing. *J Chromatogr A*, 1314:298–305, 2013.

[56] J. Han and Z. Chen. Cathepsin B inhibitor screening in traditional chinese medicines by electrophoretically mediated microanalysis. *Anal Methods*, 8:8528–8533, 2016.

[57] R. Řemínek, M. Zeisbergerová, M. Langmajerová, and Z. Glatz. New capillary electrophoretic method for on-line screenings of drug metabolism mediated by Cytochrome P450 enzymes. *Electrophoresis*, 34:2705–2711, 2013.

[58] B. Nguyen, M. Park, J. Pyun, Y. Yoo, and M. Kang. Efficient PKC inhibitor screening achieved using a quantitative CE-LIF assay. *Electrophoresis*, 37:3146–3153, 2016.

[59] Y. Zhang, F. Li, and J. Kang. Screening of histone deacetylase 1 inhibitors in natural products by capillary electrophoresis. *Anal Methods*, 9:5502–5508, 2017.

[60] J. Slon-Usakiewic, W. Ng, J. Dai, A. Pasternak, and P. Redden. Frontal affinity chromatography with MS detection (FAC-MS) in drug discovery. *Drug Discov Today*, 10:409–416, 2005.

[61] M. Bantscheff, D. Eberhard, Y. Abraham, S. Bastuck, M. Boesche, S. Hobson, T. Mathieson, J. Perrin, M. Raida, C. Rau, V. Reader, G. Sweetman, A. Bauer, T. Bouwmeester, C. Hopf, U. Kruse, G. Neubauer, N.Ramsden, J. Rick, B. Kuster, and G. Drewes. Quantitative chemical proteomics reveals mechanisms of action of clinical ABL kinase inhibitors. *Nat Biotechnol*, 25:1035–1044, 2007.

[62] E. Ng, F. Yang, A. Kameyama, M. Palcic, O. Hindsgaul, and D. Schriemer. High-throughput screening for enzyme inhibitors using frontal affinity chromatography with liquid chromatography and mass spectrometry. *Analytical chemistry*, 77:6125–6133, 2005.

[63] M. Winter, R. Ries, C. Kleiner, D. Bischoff, A. Luippold, T. Bretschneider, and F. Buettner. Automated MALDI target preparation concept: Providing ultra-high-throughput mass spectrometry–based screening for drug discovery. *SLAS Technol*, 24:209–221, 2019.

[64] D. Min, J. Su, and M. Mrksich. Profiling kinase activities by using a peptide chip and mass spectrometry. *Angew Chem*, 116:6099–6103, 2004.

[65] M. Patricelli, A. Szardenings, M.Liyanage, T. Nomanbhoy, M. Wu, H. Weissig, A. Aban, D. Chun, S. Tanner, and J. Kozarich. Functional interrogation of the kinome using nucleotide acyl phosphates. *Biochem*, 46:350–358, 2007.

[66] M. Patricelli, T. Nomanbhoy, J. Wu, H. Brown, D. Zhou, J. Zhang, S. Jagannathan, A. Aban, E. Okerberg, C. Herring, B. Nordin, H. Weissig, Q. Yang, J. Lee, N. Gray, and J. Kozarich. In situ kinase profiling reveals functionally relevant properties of native kinases. *Chem Biol*, 18:699–710, 2011.

[67] C. Wienken, P. Baaske, U. Rothbauer, D. Braun, and S. Duhr. Protein-binding assays in biological liquids using microscale thermophoresis. *Nat Commun*, 1:1–7, 2010.

[68] C. Entzian and T. Schubert. Studying small molecule–aptamer interactions using microscale thermophoresis (MST). *Methods*, 97:27–34, 2016.

[69] P. Linke, K. Amaning, M. Maschberger, F. Vallee, V. Steier, P. Baaske, S. Duhr, D. Breitsprecher, and A. Rak. An automated microscale thermophoresis screening approach for fragment-based lead discovery. *J Biomol Screen*, 21:414–421, 2016.

[70] S. Seidel, C. Wienken, S. Geissler, M.Jerabek-Willemsen, S. Duhr, A. Reiter, D. Trauner, D. Braun, and P. Baaske. Label-free microscale thermophoresis discriminates sites and affinity of protein–ligand binding. *Angew Chem Int Ed*, 51:10656–10659, 2012.

[71] A. Chramiec-Głąbik, M. Rawski, S. Glatt, and T. Lin. *RNA-protein complexes and interactions*, chapter 3, pages 29–53. Springer Protocols, Duarte, USA, 2023.

[72] F. Soon, K. Suino-Powell, J. Li, E. Yong, H. Xu, and K. Melcher. Abscisic acid signaling: Thermal stability shift assays as tool to analyze hormone perception and signal transduction. *PLOS ONE*, 7:e47857, 2012.

[73] X. Xu, Z. Nie, J. Chen, Y. Fu, W. Li, Q. Shen, and S. Yao. A DNA-based electrochemical strategy for label-free monitoring the activity and inhibition of protein kinase. *Chem Commun*, pages 6946–6948, 2009.

[74] J. Ji, H. Yang, Y. Liu, H. Chen, J. Kong, and B. Liu. $TiO_2$-assisted silver enhanced biosensor for kinase activity profiling. *Chem Commun*, pages 1508–1510, 2009.

[75] S. Martić, M. Labib, and H.-B. Kraatz. Electrochemical investigations of sarcoma-related protein kinase inhibition. *Electrochim Acta*, 56:10676–10682, 2011.

[76] S. Martić, S. Tackenburg, Y. Bilokin, A. Golub, V. Bdzhola, S. Yarmoluk, and H. Kraatz. Electrochemical screening of the indole/quinolone derivatives as potential protein kinase CK2 inhibitors. *Anal Biochem*, 421:617–621, 2012.

[77] B. Li, X. Shi, W. Gu, K. Zhao, N. Chen, and Y. Xian. Graphene based electrochemical biosensor for label-free measurement of the activity and inhibition of protein tyrosine kinase. *Analyst*, 138:7212–7217, 2013.

[78] A. Wieckowska, D. Li, R. Gill, and I. Willner. Following protein kinase acivity by electrochemical means and contact angle measurements. *Chem Commun*, pages 2376–2378, 2008.

[79] S. Rauf, J. Luo, H. Qazi, M. Sohail, R. Tao, C. Fu, S. Rauf, I. Ahmad, H. Iqbal, and H. Li. A novel leaky surface acoustic wave biosensor for detection of PKA activity in cell lysates based on peptide biomineralized metal nanoclusters. *Sens Actuator A Phys*, 351:114107, 2023.

[80] A. Salehi-Reyhani, F. Gesellchen, D. Mampallil, R. Wilson, J. Reboud, O. Ces, K. Willison, J. Cooper, and D. Klug. Chemical-free lysis and fractionation of cells by use of surface acoustic waves for sensitive protein assays. *Anal Chem*, 87:2161–2169, 2015.

[81] K. Viht, S. Schweinsberg, M. Lust, A. Vaasa, G. Raidaru, D. Lavogina, A. Uri, and F. Herberg. Surface-plasmon-resonance-based biosensor with immobilized bisubstrate analog inhibitor for the determination of affinities of ATP- and protein-competitive ligands of cAMP-dependent protein kinase. *Anal Biochem*, 362:268–277, 2007.

[82] T. Mori, K. Inamori, Y. Inoue, X. Han, G. Yamanouchi, T. Niidome, and Y. Katayama. Evaluation of protein kinase activities of cell lysates using peptide microarrays based on surface plasmon resonance imaging. *Anal Biochem*, 375:223–231, 2008.

[83] N. Willemsen-Seegers, J. Uitdehaag, M. Prinsen, J.. de Vetter, J. de Man, M. Sawa, Y. Kawase, R. Buijsman, and G. Zaman. Compound selectivity and target residence time of kinase inhibitors studied with surface plasmon resonance. *J Mol Biol*, 429:574–586, 2017.

[84] Y. Inoue, T. Mori, G. Yamanouchi, X. Han, T. Sonoda, T. Niidome, and Y. Katayama. Surface plasmon resonance imaging measurements of caspase reactions on peptide microarrays. *Anal Biochem*, 375:147–149, 2008.

[85] J. Concepcion, K. Witte, C. Wartchow, S. Choo, D. Yao, H. Persson, J. Wei, P. Li, B. Heidecker, W. Ma, R. Varma, L. Zhao, D. Perillat, G. Carricato, M. Recknor, K. Du, H. Ho, T. Ellis, J. Gamez, M. Howes, J. Phi-Wilson, S. Lockard, R. Zuk, and H. Tan. Label-free detection of biomolecular interactions using biolayer interferometry for kinetic characterization. *CCHTS*, 12:791–800, 2009.

[86] R. Petersen. Strategies using bio-layer interferometry biosensor technology for vaccine research and development. *Biosens*, 7:49–64, 2017.

[87] N. Shah and T. Duncan. Bio-layer interferometry for measuring kinetics of protein-protein interactions and allosteric ligand effects. *JoVE*, 84:e51383, 2014.

[88] A. Sultana and J. Lee. Measuring protein-protein and protein-nucleic acid interactions by biolayer interferometry. *Curr Protoc Protein Sci*, 79:19.25.1–19.25.26, 2015.

[89] K. Huynh and C. Partch. Analysis of protein stability and ligand interactions by thermal shift assay. *Curr Protoc Protein Sci*, 79:28.9.1–28.9.14, 2015.

[90] R. Jafari, H. Almqvist, H. Axelsson, M. Ignatushchenko, T. Lundbaeck, P. Nordlund, and D. Molina. The cellular thermal shift assay for evaluating drug target interactions in cells. *Nat Prot*, 9:2100–2122, 2014.

[91] P. Iliev, D. Hanke, and B. Page. STAT protein thermal shift assays to monitor protein-inhibitor interactions. *Chem Bio Chem*, 23:e202200039, 2022.

[92] S. Attarha, A. Reithmeier, S. Busker, M. Desroses, and B. Page. Validating signal transducer and activator of transcription (stat) protein–inhibitor interactions using biochemical and cellular thermal shift assays. *ACS Chem Biol*, 15:1842–1851, 2020.

[93] M. Gal, I. Bloch, N. Shechter, O. Romanenko, and O. Shir. Efficient isothermal titration calorimetry technique identifies direct interaction of small molecule inhibitors with the target protein. *CCHTS*, 19:4–13, 2016.

[94] G. Iyer, P. Taslimi, and S. Pazhanisamy. Staurosporine-based binding assay for testing the affinity of compounds to protein kinases. *Anal Biochem*, 373:197–206, 2008.

[95] J. di Trani, S. de Cesco, R. O'Leary, J. Plescia, C. do Nascimento, N. Moitessier, and A. Mittermaier. Rapid measurement of inhibitor binding kinetics by isothermal titration calorimetry. *Nat Commun*, 9(893), 2018.

[96] S. Myers and A. Baker. Drug discovery - An operating model for a new era. *Nat Biotechnol*, 19:727–730, 2001.

[97] H. Moses, R. Dorsey, D. Matheson, and S. Thier. Financial anatomy of biomedical research. *JAMA*, 294:1333–1342, 2005.

[98] I. Muegge, I.and Enyedy. Virtual screening for kinase targets. *Curr Med Chem*, 11:693–707, 2004.

[99] P. Fechner, O. Bleher, M. Ewald, K. Freudenberger, D. Furin, U. Hilbig, F. Kolarov, K. Krieg, L. Leidner, G. Markovic, G. Proll, F. Proell, S. Rau, J. Riedt, B. Schwarz, P. Weber, and Julia Widmaier. Size does matter! Label-free detection of small molecule–protein interaction. *Anal Bioanal Chem*, 406:4033–4051, 2014.

[100] M. Gilson and H. Zhou. Calculation of protein-ligand binding affinities. *Annu Rev Biophys Biomol Struct*, 36:21–42, 2007.

[101] W. Janzen. Screening technologies for small molecule discovery: The state of the art. *Chem Biol*, 21:1162–1170, 2014.

[102] S. Agarwal and R. Mehrotra. An overview of molecular docking. *JSM Chem*, 4:1024–1029, 2016.

[103] S. Srinivasan, R. Batra, H. Chan, G. Kamath, M. Cherukara, and S. Sankaranarayanan. Artificial intelligence guided de novo molecular design targeting COVID-19. *ACS Omega*, 6:12557–12566, 2021.

[104] R. Nussinov, M. Zhang, Y. Liu, and H. Jang. AlphaFold, artificial antelligence (AI), and allostery. *J Phys Chem B*, 126:6372–6383, 2022.

[105] G. Poli, A. Martinelli, and T. Tuccinardi. Reliability analysis and optimization of the consensus docking approach for the development of virtual screening studies. *J Enzyme Inhib Med Chem*, 31:167–173, 2016.

[106] K. Vogel, Z. Zhong, K. Bi, and B. Pollok. Developing assays for kinase drug discovery – Where have the advances come from? *Expert Opin Drug Discov*, 3:115–129, 2008.

[107] R. Fratti. *SNAREs methods and protocols*, chapter 11, pages 191–198. Humana Press, Urbana, USA, 2019.

[108] M. Jerabek-Willemsen, C. Wienken, D. Braun, P. Baaske, and S. Duhr. Molecular interaction studies using microscale thermophoresis. *Assay Drug Dev Technol*, 9:342–353, 2011.

[109] S. Seidel, P. Dijkman, W. Lea, G. van den Bogaart, Moran Jerabek-Willemsen, Ana Lazic, Jeremiah S. Joseph, Prakash Srinivasan, Philipp Baaske, Anton Simeonov, Ilia Katritch, Fernando A. Melo, John E. Ladbury, G. Schreiber, A. Watts, D. Braun, and S. Duhr. Microscale thermophoresis quantifies biomolecular interactions under previously challenging conditions. *Methods*, 59:301–315, 2013.

[110] I. van den Broek, W. Niessen, and W. van Dongen. Bioanalytical LC–MS/MS of protein-based biopharmaceuticals. *J Chromatogr B*, 929:161–179, 2013.

[111] J. Watson and O. Sparkman. *Introduction to mass spectrometry - instrumentation, application and strategies for data interpretation*, chapter 9. John Wiley & Sons, 4th edition, 2007.

[112] J. Gross. *Mass spectrometry - A textbook - Matrix-assisted laser desorption/ionization*, chapter 10. Springer-Verlag Berlin Heidelberg, 1st edition, 2004.

[113] C. Haslam, J. Hellicar, A. Dunn, A. Fuetterer, N. Hardy, P. Marshall, R. Paape, M. Pemberton, A. Resemannand, and M. Leveridge. The evolution of MALDI-TOF mass spectrometry toward ultra-high-throughput screening: 1536-well format and beyond. *J Biomol Screen*, 21:176–186, 2016.

[114] Y. Cho, H. Su, W. Wu, D. Wu, M. Hou, C. Kou, and J. Shiea. Biomarker charactization by MALDI-TOF/MS. *Adv Clin Chem*, 69:209–254, 2015.

[115] B. Mamyrin. Time-of-flight mass spectrometry (concepts, achievements, and prospects). *Internat J Mass Spectrom*, 206:251–266, 2001.

[116] A. Kettenbach, T. Wang, B. Faherty, D. Madden, S. Knapp, C. Bailey-Kellogg, and S. Gerber. Rapid determination of multiple linear kinase substrate motifs by mass spectrometry. *Chem Biol*, 19:608–618, 2012.

[117] K. Cammann, U. Lemke, A. Rohen, J. Sander, H. Wilken, and B. Winter. Chemical sensors and biosensors - principles and applications. *Angew Chem*, 30:516–539, 1991.

[118] A. Brecht and G. Gauglitz. Recent developments in optical transducers for chemical or biochemical applications. *Sens Actuators B Chem*, 38:1–7, 1997.

[119] G. Gauglitz. Analytical evaluation of sensor measurements. *Anal Bioanal Chem*, 410:5–13, 2018.

[120] P. Damborský, J. Švitel, and J. Katrlík. Optical biosensors. *Essays Biochem*, 60:91–100, 2016.

[121] T. Mir and H. Shinohara. 2D-SPR biosensor detects the intracellular signal transduction in PC 12 cells at single cell level. pages 677–681. ICST, 2012.

[122] K. Cali, E. Tuccori, and K. Persaud. Gravimetric biosensors. *Meth Enzymol*, 642:435–468, 2020.

[123] P. Fechner, F. Proell, C. Albrecht, and G. Gauglitz. Kinetic analysis of the estrogen receptor alpha using RIfS. *Anal Bioanal Chem*, 400:729–735, 2011.

[124] C. Haenel and G. Gauglitz. Comparison of reflectometric interference spectroscopy with other instruments for label-free optical detection. *Anal Bioanal Chem*, 372:91–100, 2002.

[125] M. Murphy, L. Jason-Moller, and J. Bruno. Using biacore to measure the binding kinetics of an antibody-antigen interaction. *Curr Prot Protein Sci*, 45:19.14.1–19.14.17, 2006.

[126] A. Kortt, G. Oddie, P. Iliades, L. Gruen, and P. Hudson. Nonspecific amine immobilization of ligand can be a potential source of error in biacore binding experiments and may reduce binding affinities. *Anal Biochem*, 253:103–111, 1997.

[127] G. Gauglitz. Direct optical sensors: Principles and selected applications. *Anal Bioanal Chem*, 381:141–155, 2005.

[128] M. Fischer. *Surface plasmon resonance*, chapter 3, pages 55–74. Humana Press, Utrecht, The Netherlands, 2010.

[129] H. Takeda, N. Osima, and N. Nomura. *Surface plasmon resonance*, chapter 8, pages 131–146. Humana Press, 2010.

[130] A. DeLean, P. Munson, and D. Rodbard. Simultaneous analysis of families of sigmoidal curves: Application to bioassay, radioligand assay, and physiological dose-response curves. *Am J Physiol*, 235:E97, 1978.

[131] J. Siegel, M. Berner, J. Werner, G. Proll, P. Fechner, and M. Schubert. Fourier spotting: A novel setup for single-color reflectometry. *Anal Bioanal Chem*, 414:1787–1796, 2022.

[132] D. Verzijl, T. Riedl, P. W. H. I. Parren, and A. F. Gerritsen. A novel label-free cell-based assay technology using biolayer interferometry. *Biosens Bioelecton*, 87:388–395, 2017.

[133] L. Lu, T. Suscovich, S. Fortune, and G. Alter. Beyond binding: Antibody effector functions in infectious diseases. *Curr Opin Virol*, 18:46–61, 2018.

[134] S. Selvarajah, N. Sexton, K. Kahle, R. Fong, Kimberly-Anne Mattia, Joy Gardner, Kai Lu, Nathan M. Liss, Beatriz Salvador, David F. Tucker, Trevor Barnes, Manu Mabila, Xiangdong Zhou, Giada Rossini, Joseph B. Rucker, D. Sanders, A. Suhrbier, V. Sambri, A. Michault, M. Muench, B. Doranz, and G. Simmons. A neutralizing monoclonal antibody targeting the acid-sensitive region in chikungunya virus E2 protects from disease. *PLoS Negl Trop Dis*, 7:e2423, 2013.

[135] X. Xiong, S. Martin, L. Haire, S. Wharton, R. Daniels, M. Bennett, J. McCauley, P. Collins, P. Walker, J.Skehel, and S. Gamblin. Receptor binding by an H7N9 influenza virus from humans. *Nature*, 499:496–499, 2013.

[136] R. Huey, G. Morris, A. Olson, and D. Goodsell. A semiempirical free energy force field with charge-based desolvation. *J Comput Chem*, 28:1145–1152, 2007.

[137] S. Cosconati, S. Forli, A. Perryman, R. Harris, D. Goodsell, and A. Olson. Virtual screening with AutoDock: Theory and practice. *Expert Opin Drug Discov*, 5:597–607, 2010.

[138] G. Anderson, M. Jacoby, F. Ligler, and K.. King. Effectiveness of protein A for antibody immobilization for a fiber optic biosensor. *Biosens Bioelectron*, 12:329–336, 1997.

[139] K. Andersson, M. Haemaelaeinen, and M. Malmqvist. Identification and optimization of regeneration conditions for affinity-based biosensor assays. A multivariate cocktail approach. *Anal Chem*, 71:2475–2481, 1999.

[140] T. Kenakin. The mass action equation in pharmacology. *Br J Clin Pharmacol*, 81:41–51, 2016.

[141] G. M. Raab. Comparison of a logistic and a mass-action curve for radioimmunoassay data. *Clin Chem*, 29:1757–1761, 1983.

[142] D. Santiago, Y. Pevzner, A. Durand, M. Tran, R. Scheerer, K. Daniel, S. Sung, H. Woodcock, W. Guida, and W. Brooks. Virtual target screening: Validation using kinase inhibitors. *J Chem Inf Model*, 52:2192–2203, 2012.

[143] A. Ciulli and C. Abell. Fragment-based approaches to enzyme inhibition. *Curr Opin Biotechnol*, 18:489–496, 2007.

[144] Q. Li. Application of fragment-based drug discovery to versatile targets. *Front Mol Biosci*, 7:180, 2020.

[145] P. Mortenson, V. Berdini, and M. O'Reilly. Fragment-based approaches to the discovery of kinase inhibitors. *Methods Enzymol*, 548:69–92, 2014.

[146] K. Babaoglu and B. Shoichet. Deconstructing fragment-based inhibitor discovery. *Nat Chem Biol*, 2:720–723, 2006.

[147] M. Mondal, N. Radeva, H. Fanlo-Virgós, S. Otto, G. Klebe, and A. Hirsch. Fragment linking and optimization of inhibitors of the aspartic protease endothiapepsin: Fragment-based drug design facilitated by dynamic combinatorial chemistry. *Angew Chem Int Ed*, 55:9422–9426, 2016.

[148] P. Hillertz. *A study of methods in fragment-based drug discovery*. PhD thesis, University of Heidelberg, Heidelberg, 2009.

[149] B. Burlingham and T. Widlanski. An intuitive look at the relationship of Ki and IC50: A more general use for the dixon plot. *J Chem Ed*, 80:214–218, 2003.

[150] C. Chang and Y. Cheng. Ribonucleotide reductase isolated from human cells. *Biochem Pharmacol*, 27:2297–2300, 1978.

[151] S. Lippok, S. Seidel, S. Duhr, K. Uhland, H. Holthoff, D. Jenne, and D. Braun. Direct detection of antibody concentration and affinity in human serum using microscale thermophoresis. *Anal Chem*, 84:3523–3530, 2012.

[152] S. Patnaik, W. Zheng, J. Choi, O. Motabar, N. Southall, W. Westbroek, W. Lea, A. Velayati, E. Goldin, E. Sidransky, W. Leister, and J. Marugan. Discovery, structure–activity relationship, and biological evaluation of noninhibitory small molecule chaperones of glucocerebrosidase. *J Med Chem*, 55:5734–5748, 2012.

[153] C. Breitenlechner, M. Gaßel, H. Hidaka, V. Kinzel, R. Huber, R. Engh, and D. Bossemeyer. Protein kinase A in complex with Rho-kinase inhibitors Y-27632, fasudil, and H-1152P. *Struct*, 11:1595–1607, 2003.

[154] J. Kabir, M. Lobo, and I. Zachary. Staurosporine induces endothelial cell apoptosis via focal adhesion kinase dephosphorylation and focal adhesion disassembly independent of focal adhesion kinase proteolysis. *Biochem J*, 367:145–155, 2002.

[155] J. Bjorge, J. Kudlow, G. Mills, and A. Paterson. Inhibition of stimulus-dependent epidermal growth factor receptor and transforming growth factor-α mRNA accumulation by the protein kinase C inhibitor staurosporine. *FEBS Lett*, 243:404–408, 1989.

[156] A. Chauhan and T. Khan. Focal adhesion kinase - an emerging viable target in cancer and development of focal adhesion kinase inhibitors. *Chem Biol Drug Des*, 97:774–794, 2021.

[157] E. Shanthi, M. Krishna, G. Arunesh, K. Reddy, J. Kumar, and V. Viswanadhan. Focal adhesion kinase inhibitors in the treatment of metastatic cancer: A patent review. *Expert Opin Ther Patents*, 24:1077–1100, 2014.

[158] Y. Lu and H. Sun. Progress in the development of small molecular inhibitors of focal adhesion kinase (FAK). *J Med Chem*, 63:14382–14403, 2020.

[159] D. Glass, H. Cheng, B. Kemp, and D. Walsh. Differential and common recognition of the catalytic sites of the cGMP-dependent and cAMP-dependent protein kinases by inhibitory peptides derived from the heat-stable inhibitor protein. *J Biol Chem*, 261:12166–12171, 1986.

[160] J. Demaille, K. Peters, and E. Fischer. Isolation and properties of the rabbit skeletal muscle protein inhibitor of adenosine 3',5'-monophosphate dependent protein kinases. *Biochem*, 16:3080–3086, 1977.

[161] H. Haake, A. Schuetz, and G. Gauglitz. Label-free detection of biomolecular interaction by optical sensors. *Fresenius J Anal Chem*, 366:576–585, 2000.

[162] R. Dinis-Oliveira. Heterogeneous and homogeneous immunoassays for drug analysis. *Bioanal*, 6:2877–2896, 2014.

[163] R. Williams, J. Phillips, and K. Mysels. The critical micelle concentration of sodium lauryl sulphate at 25° C. *Trans Faraday Soc*, 51:728–737, 1955.

[164] E. Fuguet, C. Ràfols, M. Rosés, and E. Bosch. Critical micelle concentration of surfactants in aqueous buffered and unbuffered systems. *Anal Chim Acta 5*, 548:95–100, 2005.

[165] M. Mahmood and D. Al-Koofee. Effect of temperature changes on critical micelle concentrationfor tween series surfactant. *GJSFR*, 13:1–5, 2013.

[166] A. Dominguez, A. Fernandez, N. Gonzalez, E. Iglesias, and L. Montenegro. Determination of critical micelle concentration of some surfactants by three techniques. *J Chem Educ*, 74:1227–1231, 1997.

[167] Y. Esaka, K. Tanaka, B. Uno, M. Goto, and K. Kano. Sodium dodecyl sulfate-Tween 20 mixed micellar electrokinetic chromatography for separation of hydrophobic cations: Application to adrenaline and its precursors. *Anal Chem*, 69:1332–1338, 1997.

[168] M. Johnson. Detergents: Triton X-100, Tween-20, and more. *Mater Methods*, 3:163, 2013.

[169] M. Feng, A. Morales, A. Poot, T. Beugeling, and A. Bantjes. Effects of Tween 20 on the desorption of proteins from polymer surfaces. *J Biomater Sci Polym Ed*, 7:415–424, 2012.

[170] E. Sahin, A. Grillo, M. Perkins, and C. Roberts. Comparative effects of pH and ionic strength on protein–protein interactions, unfolding, and aggregation for IgG1 antibodies. *J PHarm Sci*, 99:4830–4848, 2010.

[171] J. Novotny and K. Sharp. Electrostatic fields in antibodies and antibody/antigen complexes. *Prog Biophys Mol Biol*, 58:203–224, 1992.

[172] G. Blanchard, C. Taylor, B. Busey, and M. Willamson. Regeneration of immunosorbent surfaces used in clinical, industrial and environmental biosensors. *J Immunol Methods*, 130:263–275, 1990.

[173] J. Goode, J. Rushworth, and P. Millner. Biosensor regeneration: A review of common techniques and outcomes. *Langmuir*, 31:6267–6276, 2015.

[174] K. Alam, O.. Gani, and R.. Engh. Inhibitor binding to mutants of protein kinase A with GGGxxG and GxGxxA glycine-rich loop motifs. *JMR*, 34:e2882, 2021.

[175] L. Puumala, S. Grist, J. Morales, J. Bickford, L. Chrostowski, S. Shekhar, and K. Cheung. Biofunctionalization of multiplexed silicon photonic biosensors. *Biosensors*, 13:53, 2023.

[176] J. Tan, B. Yoon, G. Ma, T. Sut, N. Cho, and J. Jackman. Unraveling how ethanol-induced conformational changes affect BSA protein adsorption onto silica surfaces. *Langmuir*, 36:9215–9224, 2020.

[177] M. Haun and S. Wasi. Biotinylated antibodies bound to streptavidin beads: A versatile solid matrix for immunoassays. *Anal Biochem*, 191:337–342, 1990.

[178] L. Chaiet and F. Wolf. The properties of streptavidin, a biotin-binding protein produced by streptomycetes. *Arch Biochem Biophys*, 106:1–5, 1964.

[179] C. Dundas, D. Demonte, and S. Park. Streptavidin–biotin technology: Improvements and innovations in chemical and biological applications. *Appl Microbiol Biotechnol*, 97:9343–9353, 2013.

[180] P. Weber, D. Ohlendorf, J. Wendoloski, and F. Salemme. Structural origins of high-affinity biotin binding to streptavidin. *Sci Rep*, 243:85–88, 1989.

[181] I. Vikholm-Lundin, R. Piskonen, and W. Albers. Hybridisation of surface-immobilised single-stranded oligonucleotides and polymer monitored by surface plasmon resonance. *Biosens Bioelectron*, 22:1323–1329, 2007.

[182] B. Moehrle, M. Kumpf, and G. Gauglitz. Determination of affinity constants of locked nucleic acid (LNA) and DNA duplex formation using label free sensor technology. *Analyst*, 130:1634–1638, 2005.

[183] G. Marincovic. *Einsatz von Nanopartikeln und optimierten Schichtsystemen für die Signalverstärkung inreflektometrischen Biosensoren*. PhD thesis, Eberhard Karls Universität Tübingen, 2008.

[184] F. Proell. *iRIfS-imaging reflectometric interference sensor*. PhD thesis, Eberhard Karls Universität Tübingen, 2010.

[185] H. Griesser, P. Kingshott, S. McArthur, K. McLean, G. Kinsel, and R. Timmons. Surface-MALDI mass spectrometry in biomaterials research. *Biomater*, 25:4861–4875, 2004.

[186] S. Forest, J. Breault-Turcot, P. Chaurand, and J. Masson. Surface plasmon resonance imaging-MALDI-TOF imaging mass spectrometry of thin tissue sections. *Anal Chem*, 88:2072–2079, 2016.

[187] S. Patrie and M. Mrksich. Self-assembled monolayers for MALDI-TOF mass spectrometry for immunoassays of human protein antigens. *Anal Chem*, 79:5878–5887, 2007.

[188] J. Andrade, C. Pereira, J. de Almeida Junior, C. Viana, L. de Oliveira Neves, P. da Silva, M. Bell, and V. de Carvalho dos Anjos. FTIR-ATR determination of protein content to evaluate whey protein concentrate adulteration. *LWT Food Sci Technol*, 99:166–172, 2019.

[189] A. Bouhekka and T. Buergi. In situ ATR-IR spectroscopy study of adsorbed protein: Visible light denaturation of bovine serum albumin on $TiO_2$. *Appl Surf Sci*, 261:369–374, 2012.

[190] S. Olsztyńska-Janus, Z. Kiełbowicz, and M. A. Czarnecki. ATR-IR study of skin components: Lipids, proteins and water. Part II: Near infrared radiation effect. *SAA*, 202:93–101, 2018.

[191] C. Vigano, L. Manciu, F. Buyse, E. Goormaghtigh, and J.-M. Ruysschaert. Attenuated total reflection IR spectroscopy as a tool to investigate the structure, orientation and tertiary structure changes in peptides and membrane proteins. *Polymers*, 55:373–380, 2000.

[192] S. Oladepo, K. Xiong, Z. Hong, S. Asher, J. Handen, and I. Lednev. UV resonance Raman investigations of peptide and protein structure and dynamics. *Chem Rev*, 112:2604–2628, 2012.

[193] P. Sihota, R. Yadav, V. Dhiman, S. Bhadada, V. Mehandia, and N. Kumar. Investigation of diabetic patient's fingernail quality to monitor type 2 diabetes induced tissue damage. *Sci Rep*, 9:3193, 2019.

[194] K. Ataka and J. Heberle. Use of surface enhanced infrared absorption spectroscopy (SEIRA) to probe the functionality of a protein monolayer. *Polymers*, 82:415–419, 2006.

[195] K. Ataka, S. Stripp, and J. Heberle. Surface-enhanced infrared absorption spectroscopy (SEIRAS) to probe monolayers of membrane proteins. *BBA*, 1828:2283–2293, 2013.

[196] A. Seiça, M. Iqbal, A. Carvalho, J. Choe, F. Boulmedais, and P. Hellwig. Study of membrane protein monolayers using surface-enhanced infrared absorption spectroscopy (SEIRAS): critical dependence of nanostructured gold surface morphology. *ACS Sens*, 6:2875–2882, 2021.

[197] G. Thomas. Raman spectroscopy of protein and nucleic acid assemblies. *Annu Rev Biophys Biomol Struct*, 28:1–27, 1999.

[198] N. Ivleva, M. Wagner, H. Horn, R. Niessner, and C. Haisch. Raman microscopy and surface-enhanced Raman scattering (SERS) for in situ analysis of biofilms. *J Biophoton*, 3:548–556, 2010.

[199] S. Signorelli, S. Cannistraro, and A. Bizzarri. Structural characterization of the intrinsically disordered protein p53 using Raman spectroscopy. *Appl Spectrosc*, 71:823–832, 2017.

[200] N. Biswas, A. Waring, F. Walther, and R. Dluhy. Structure and conformation of the disulfide bond in dimeric lung surfactant peptides SP-B1–25 and SP-B8–25. *BBA*, 1768:1070–1082, 2007.

[201] B. Sharma, R. Frontiera, A. Henry, E. Ringe, and R. van Duyne. SERS: Materials, applications, and the future. *Mater Today*, 15:16–25, 2012.

[202] G. Gauglitz, A. Brecht, G. Kraus, and W. Mahm. Chemical and biochemical sensors based on interferometry at thin (multi-)layers. *Sens Actuators B*, 11:21–27, 1993.

[203] C. Cavasotto and R. Abagyan. Protein flexibility in ligand docking and virtual screening to protein kinases. *J Mol Biol*, 337:209–225, 2004.

[204] C. Roecker, M. Poetzl, F. Zhang, W. Parak, and G. Nienhaus. A quantitative fluorescence study of protein monolayer formation on colloidal nanoparticles. *Nat Nanotechnol*, 4:577–580, 2009.

[205] M. Sekar, P. Hampton, T. Buranda, and G. López. Multifunctional monolayer assemblies for reversible direct fluorescence transduction of protein-ligand interactions at surfaces. *J Am Chem Soc*, 121:5135–5141, 1999.

[206] M. Coen, R. Lehmann, P. Groening, M. Bielmann, C. Galli, and L. Schlapbach. Adsorption and bioactivity of protein A on silicon surfaces studied by AFM and XPS. *J Colloid Interface Sci*, 233:180–189, 2001.

[207] Z. Zhou, X. Wang, L. Birch, T. Rayment, and C. Abell. AFM study on protein immobilization on charged surfaces at the nanoscale: toward the fabrication of three-dimensional protein nanostructures. *Langmuir*, 19:10557–10562, 2003.

[208] N. Barinov, V. Prokhorov, E. Dubrovin, and D. Klinov. AFM visualization at a single-molecule level of denaturated states of proteins on graphite. *Colloids Surf B Bioniterfaces*, 146:777–784, 2016.

[209] M. Verheul and S. P. F. M. Roefs. Structure of whey protein gels, studied by permeability, scanning electron microscopy and rheology. *Food Hydrocoll*, 12:17–24, 1998.

[210] Y. Tan, J. Schallom, N. Ganesh, K. Fujikawa, A. Demchenko, and K. Stine. Characterization of protein immobilization on nanoporous gold using atomic force microscopy and scanning electron microscopy. *Nanoscale*, 3:3395–3407, 2011.

[211] S. Gorinstein, E. Pawelzik, E. Delgado-Licon, K. Yamamoto, S. Kobayashi, H. Taniguchi, R. Haruenkit, Y. Park, S. Jung, J. Drzewiecki, and S. Trakhtenberg. Use of scanning electron microscopy to indicate the similarities and differences in pseudocereal and cereal proteins. *IJFST*, 39:183–189, 2004.

[212] R. Wang. Immobilisation of DNA probes for the development of SPR-based sensing. *Biosens Bioelecton*, 20:967–974, 2004.

[213] W. Chen, W. Hu, Y. Su, A. Taylor, S. Jiang, and G. Chang. A multispot DNA chip fabricated with mixed ssDNA/oligo (ethylene glycol) self-assembled monolayers for detecting the effect of secondary structures on hybridization by SPR imaging. *Sens Actuators B Chem*, 125:607–614, 2007.

[214] E. Stigter, G. de Jong, and W. van Bennekom. Coupling surface-plasmon resonance and mass spectrometry to quantify and to identify ligands. *TRAC*, 45:107–120, 2013.

[215] J. Xue, Y. Bai, and H. Liu. Hybrid methods of surface plasmon resonance coupled to mass spectrometry for biomolecular interaction analysis. *Anal Bioanal Chem*, 411:3721–3729, 2019.

[216] U. Anders, J. Schaefer, F. Hibti, C. Frydman, D. Suckau, A. Plückthun, and R. Zenobi. SPRi-MALDI-MS: Characterization and identification of a kinase from cell lysate by specific interaction with different designed ankyrin repeat proteins. *Anal Bioanal Chem*, 409:1827–1836, 2017.

[217] M. Mehlmann, A. Garvin, M. Steinwand, and G. Gauglitz. Reflectometric interference spectroscopy combined with MALDI-TOF mass spectrometry to determine quantitative and qualitative binding of mixtures of vancomycin derivatives. *Anal Bioanal Chem*, 382:1942–1948, 2005.

[218] G. Proll, L. Steinle, F. Proell, M. Kumpf, B. Moehrle, M. Mehlmann, and G. Gauglitz. Potential of label-free detection in high-content-screening applications. *J Chromatogr A*, 1161:2–8, 2007.